ABSTRACT

SHEN, ZHAN. Centralized and Decentralized Volt/Var Control Schemes for FREEDM System. (Under the direction of Dr. Mesut E. Baran).

This study first investigates the impact of high-penetration residential photovoltaics (PV) on power distribution systems, both Green Hub-type and Future Renewable Electric Energy Delivery and Management (FREEDM)-type power distribution systems. Voltage varies during daily operation as the load and PV profile changes. In order to meet the requirement of system normal operation, Volt/Var Control (VVC) schemes are proposed in both centralized and decentralized fashion. The objective of VVC is formulated as minimizing system power loss while regulating voltage profile within acceptable limits. The centralized VVC scheme is a two-phase control scheme where gradient based Phase I control targets at regulating voltages and linear programming (LP)-based Phase II optimization aims at minimizing power loss. Compared with the heavy computational burden and dependence on communications infrastructure, decentralized control can achieve a system-wide optimization goal as well as parallel computation and a weaker requirement for communications. The proposed Dantzig Wolfe (DW)-based decentralized VVC partitions the original large-scale optimization problem into smaller subproblems.

The proposed centralized and decentralized VVC schemes are tested on the FREEDM IEEE 34 node test feeder and the FREEDM Notional System, respectively. Improvements have been made for each control scheme. Based on the simulation result, it is clear that both proposed schemes can achieve the optimization goal of minimizing power loss while maintaining voltages within the feasible region. When comparing the control effect between

centralized and decentralized VVC schemes, although the control effect of DW-based decentralized VVC is not as good as centralized VVC, it can still provide acceptable results.

Centralized and Decentralized Volt/Var Control Schemes for the FREEDM System

by
Zhan Shen

A dissertation submitted to the Graduate Faculty of
North Carolina State University
in partial fulfillment of the
requirements for the degree of
Doctor of Philosophy

Electrical Engineering

Raleigh, North Carolina

2013

APPROVED BY:

Dr. Mesut E. Baran
Committee Chair

Dr. Subhashish Bhattacharya

Dr. Aranya Chakrabortty

Dr. Fen Wu

DEDICATION

TO MY PARENTS
CHUNLIN SHEN AND BAILU DU

BIOGRAPHY

Zhan Shen was born in Henan, China in 1987. She received a B.S. in Electrical Engineering from North China Electric Power University in 2008 and a Ph.D. in Electrical Engineering from North Carolina State University (NCSU) in 2013. She started to pursue the Ph.D. degree at NCSU at the Future Renewable Electric Energy Delivery and Management (FREEDM) System Center in the same year. She interned at ABB's US Corporate Research Center during the summer of 2011 and joined Southern Electric Power Research Institute, a subsidiary of China Southern Power Grid Company, in 2013. Her research interests include: power system analysis and control, smart grid and renewable energy, Volt/Var control (VVC), and distributed control.

ACKNOWLEDGMENTS

My sincere gratitude goes to the people who made this work possible.

To my advisor, Dr. Mesut Baran, for his continued guidance, encouragement, and support throughout my research.

To my committee members, Dr. Subhashish Bhattacharya, Dr. Aranya Chakrabortty, and Dr. Fen Wu, for their valuable suggestions and help.

To my research fellows at the FREEDM System Center. It's been a great pleasure to work with and learn from all of you. You are like brothers and sisters to me.

To the faculty and staff at the FREEDM System Center for providing such a great research environment.

To all my friends, for the time we've spent together, for the joy and pain we've shared, and for the bright future we are heading to.

To my dearest sister and best friend, Cheng Wang, who has accompanied me for whatever I've been through.

And last and foremost, to my parents, Chunlin Shen and Bailu Du, for the love and support they have given me since birth, and for providing me with the opportunity to study and be the person I want to be.

TABLE OF CONTENTS

LIST OF TABLES

LIST OF FIGURES

CHAPTER 1. Introduction

1.1 Background

With the appearance of Distributed Renewable Energy Resources (DRER) in power distribution systems, the conventional system operating and control schemes are facing new challenges. In order to resolve the new issues, it is necessary to do an in-depth impact study to determine all potential problems during daily systems operations.

As a critical application in distribution automation, Volt/Var Control (VVC) provides voltage regulation within specified tolerances and achieves a system-wide optimization goal. In the conventional distribution system, since the substation is assumed to be the only source of the whole feeder, voltage will drop gradually from the substation toward the end of the feeder. Voltage-regulating devices are needed to boost the voltage throughout the system. However, in the distribution system where high-penetration DRERs are presented, the VVC scheme will deal with unforeseeable system conditions and responses. Therefore, it is necessary to design new control schemes to meet the needs of the new circumstances.

In addition, by employing smart devices, it is possible to implement the traditional centralized VVC scheme in a decentralized manner. By partitioning the original large-scale optimization problem into smaller subproblems, local slave control will be able to process its own subproblem in parallel, which can reduce the computational burden and save time. Instead of collecting information from the whole system and sending it to the central controller, the requirements of information exchange and the dependency of control applications on the communications infrastructure will be greatly reduced, thus saving capital investment on communications, too.

1.2 Outline

Chapter II gives the definition of a smart distribution system, a Green Hub system, and a FREEDM system, as well as new enabling technologies that make smart distribution systems possible. The testbeds that have been developed at the FREEDM System Center are introduced. Then, a literature survey is conducted on the topic of the impact of renewables on distribution systems. Potential steady state impacts are mentioned, and standard investigation approaches are followed. Then, the steady state impact of a high penetration of residential photovoltaics (PV) on the Green Hub-type and FREEDM-type of both testbeds is demonstrated. Simulation results are presented and analyzed. Because of daily voltage variation and emerging new devices, it is necessary to develop a new VVC strategy for FREEDM-type distribution systems.

Chapter III proposes a two-phase centralized VVC scheme after investigating the potential centralized control strategies for a power distribution system. The objective of VVC is formulated as: to minimize system power loss while regulating the voltage profile within acceptable limits. Gradient-based phase I control targets regulating voltages when a voltage violation exists. Then, starting with a feasible operating condition, linear programming (LP) -based phase II optimization aims to minimize the power loss within the feasible region. Improvements have been proposed together to guarantee the accuracy of linearization and check its optimality. The proposed centralized VVC scheme is then tested on the FREEDM IEEE 34 node test feeder.

Chapter IV proposes a Dantzig Wolfe (DW) -based decentralized VVC scheme after comparing the pros and cons of centralized and decentralized control. The DW decomposition scheme shows its advantage in partitioning large-scale LP problems that are in “block angular” form into smaller subproblems. After DW decomposition, the new formation of problems can be solved in an iterative process where at each step the subproblems are solved separately. The master problem, which consists of the coupling constraints, will be solved by the revised simplex method. Two test feeders are used to check the effectiveness of the proposed decentralized control scheme. Improvements in accuracy are also presented.

Chapter V summarizes the present work and proposes future work regarding the improvements and an application-decentralized VVC scheme.

CHAPTER 2. Impact of High Penetration PV on a Smart Distribution System

This chapter introduces the concept of smart distribution systems, Green Hub systems, and FREEDM systems. The structure of the main enabling components, such as a solid-state transformer (SST) and distributed PV systems, are also presented briefly in this chapter. After defining the broader picture, the two test systems that will be used later are presented. The Residential Notional System and the IEEE 34 System are modified to be the Green Hub system and the FREEDM system in the PSCAD.

A high-penetration PV impact study will also be evaluated on the Green Hub-type distribution system and the FREEDM-type distribution system in this chapter. In order to evaluate the capability of accommodating renewable energy in both conventional and smart distribution systems, the actual daily load and PV profiles are obtained and simulated on the test systems. The Cloud passage scenario is also considered to show how system voltage responds to the sudden change in real power generation. By analyzing the daily voltage variation, the necessity of developing a VVC strategy for FREEDM-type smart distribution systems becomes obvious.

2.1 Basic Concept of Smart Distribution Systems

The electric power system has been undergoing substantial changes by adopting more types and a higher penetration of DRER. Many emerging technologies, such as PV systems, microturbines and distributed energy storage devices (DESD), have an inverter interface with the distribution systems, and provide possibilities for “smarter” intelligent operations of the power system. In the past several years, the idea of the smart grid has gained increasing visibility. Lots of works on investigating the structure, capability, and features of the smart grid have been presented [1]-[4]. Then, the U.S. government has mandated the transformation of the existing electric grid into a smart grid through the Energy Independence and Security Act of 2007 (EISA07) and the American Recovery and Reinvestment Act of 2009 (ARRA09). The smart grid is then defined as an electric system that uses information, two-way, cyber-secure communications technologies, and computational intelligence in an integrated fashion across the entire spectrum of the energy systems from generation to consumption of the electricity [1]. In order to make it clear, a comparison is made between a conventional power distribution system and a smart distribution system [1], [2].

1) The substation is the only source in the conventional distribution system, while the smart distribution system can use power from renewable distributed generation (DG), as well as DESD.

2) A unidirectional flow of energy from the source to the customers is used in the conventional distribution system, while a bidirectional power flow may occur in a smart distribution system.

3) The conventional system structure is not flexible, while plug-and-play devices, such as electric vehicles (EVs) and islanding operation of a certain part of the distribution system are enabled in the smart distribution system.

4) Customers have limited information and no opportunity to contribute to the conventional system, while they are informed and encouraged to actively enable better energy conservation in the smart distribution system.
5) Real-time monitoring and control are limited in the conventional distribution system. However, with the application of smart meters and inverter-based devices, utilization of instant measurement could optimize energy flow to reduce losses and lower cost. The integration of secure communications and control across the smart distribution system promotes interoperability and open systems and increases safety and operational flexibility.

The basic objectives of a smart grid are to improve reliability, promote the high-penetration of renewable resources, create dynamic islanding, and improve generation efficiencies [4]. In order to qualify as a smart grid, some new features need to be implemented. EISA07 defines eight philosophies of the smart grid: distribution energy resources (DER) and peak-shaving, demand response, self-healing, sensing, consumer devices, optimizing distributed assets, islanding and advanced tools, as shown in Figure 2-1.

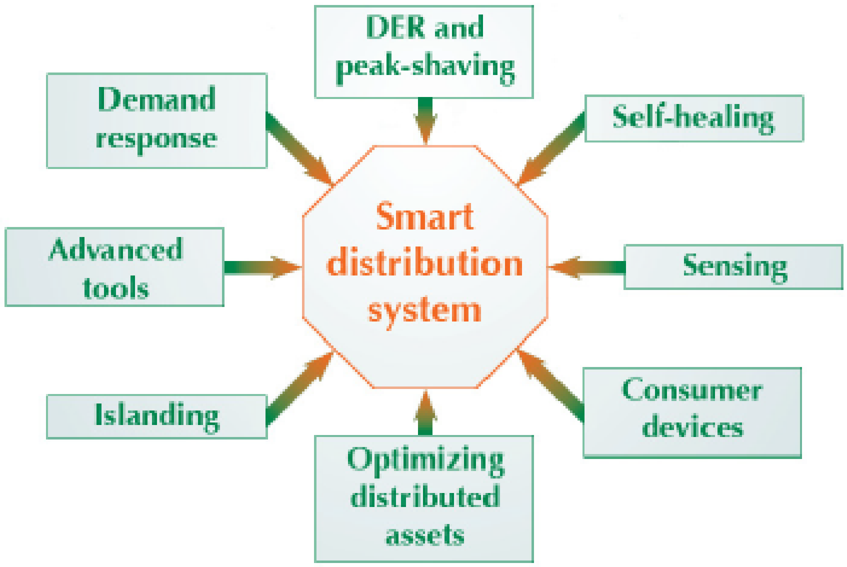

Figure 2-1 Eight philosophies of the smart distribution system

2.1.1 Enabling Technologies and New Devices

Compared with conventional systems, there are several new electronics-based devices introduced in the FREEDM system. PV is the renewable energy resource that is utilized, and SST is an inverter-based transformer used to connect the DGs to the main distribution feeder.

2.1.1.1 Solid-State Transformer (SST)

As discussed previously, an inverter-based transformer is required to accommodate the large number of DESDs and DRERs. SST is a power-electronics device that does much more than a step-down transformer. An important objective of using STTs in the FREEDM system is to achieve compatibility and flexibility [5]. The use of SSTs separates the grid side parameters from the secondary side, so that the system stability is strengthened because the low-voltage side is strongly decoupled from the grid.

In the FREEDM system, all the loads on phase A are supplied through 200 kilovolt-amperes (kVA) SSTs. These SSTs are modeled based on the new prototype SST being developed at the FREEDM System center [5]. The topology of the SST is shown in Figure 2-2.

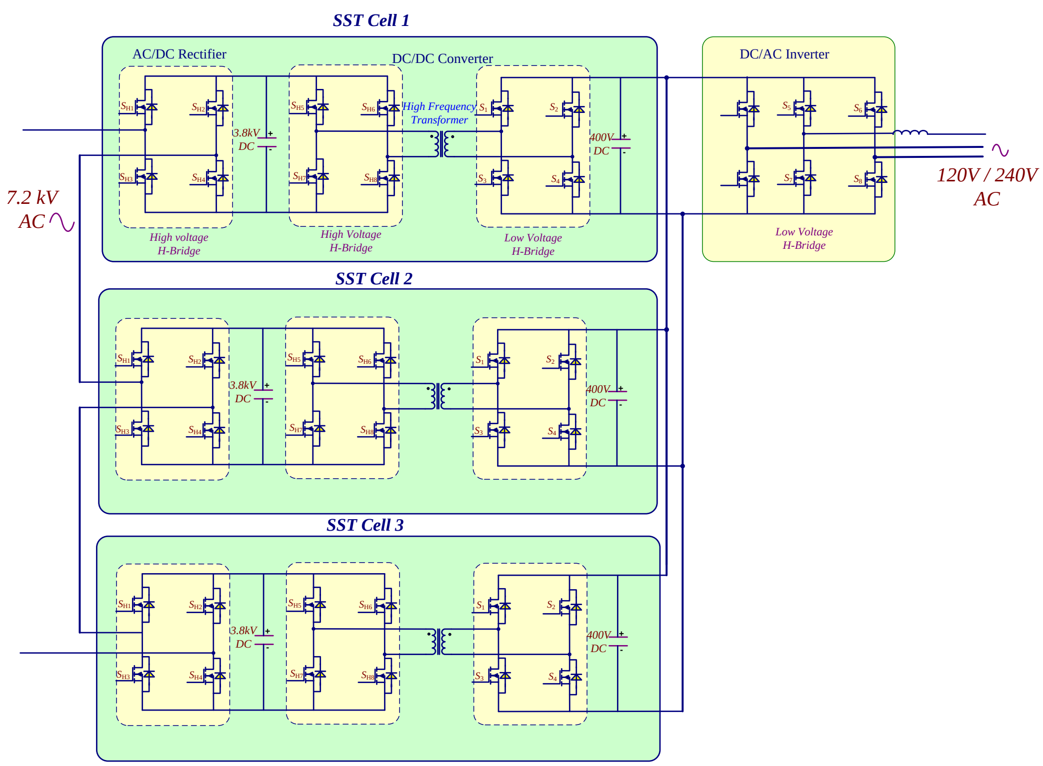

Figure 2-2 Topology of the Solid State Transformer [6]

The model structure of the SST is shown in Figure 2-3. The SST is rated as single-phase input voltage 60 hertz (Hz), 7.2 kilovolts (kV), output voltage 60Hz, 240/120 volts (V), 1 phase/3 wires. The SST consists of: a high-voltage high-frequency cascaded H-Bridge alternating current/direct current (AC/DC) rectifier that converts 60Hz, 7.2kV AC to three cascaded 3.8kV DC buses; three high-voltage high-frequency DC-to-DC converters that convert 3.8kV to 400V DC bus and a voltage source inverter (VSI) that inverts 400V DC to 60Hz, 240/120V, 1 phase/3 wires. An SST has the features of load voltage regulation, voltage sag compensation, fault isolation, power factor correction, harmonic isolation, and DC output. Each SST can manage the fault currents on both the low voltage and high voltage sides. Its large control bandwidth provides the plug-and-play feature for distributed resources to rapidly identify and respond to changes in the system [7]. Besides, another main feature of an SST is that it can automatically work under a per-unit power factor without receiving any control commands. Therefore, all the reactive load inquires on the secondary side will be provided by the corresponding SSTs. When receiving reactive power injection commands from the control center, SSTs can also perform as Var compensation devices and inject reactive power based on needs. Therefore, in the FREEDM system, there is no need to use conventional voltage regulation devices, such as voltage regulators (VR), Load Tap Changers (LTCs), or capacitor banks (CAPs).

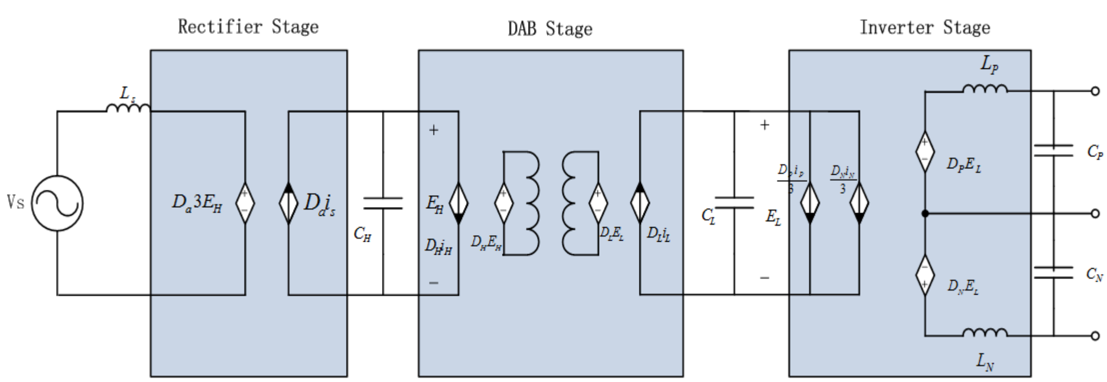

Figure 2-3 SST average model structure

In order to have a three-phase 69/12kV substation SST, three single-phase SST models have been used in delta/wye connection, as shown in Figure 2-4. These single-phase SST models are basically the same models as the original SST model except that the voltages measured at the power stage have been scaled down from 69/12kV to 12/7.2kV and the voltage signals calculated by the controllers have been scaled up from 12/7.2kV to 69/12kV in order to make the original design usable.

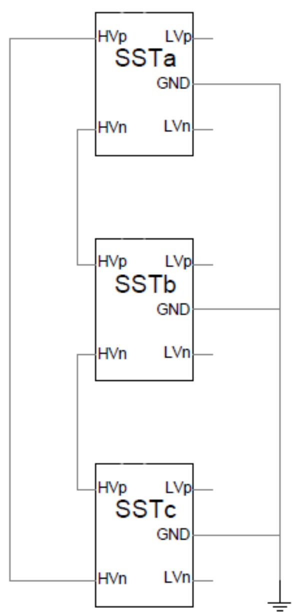

Figure 2-4 Three-phase substation SST

2.1.1.2 PV System

In the smart distribution system, DRER is one of the key components. Here, PV systems are connected to the distribution feeder via SSTs to minimize the disturbances generated when connecting or disconnecting PV systems. Figure 2-5 shows the topology of the PV system. A boost DC/DC converter is used to increase the output voltage of the PV array to 500V. Then, the PV system is connected to the grid through a single-phase DC-to-AC inverter. A simple proportional-integral (PI) controller is used to regulate the DC bus voltage. A PV array is operated at the maximum power point (MPP) under all conditions, and it can generate AC output current in phase with the AC utility grid voltage since PV has a power-electronics interface [8]. Also, we assume that the power conversion efficiency is close to 100%.

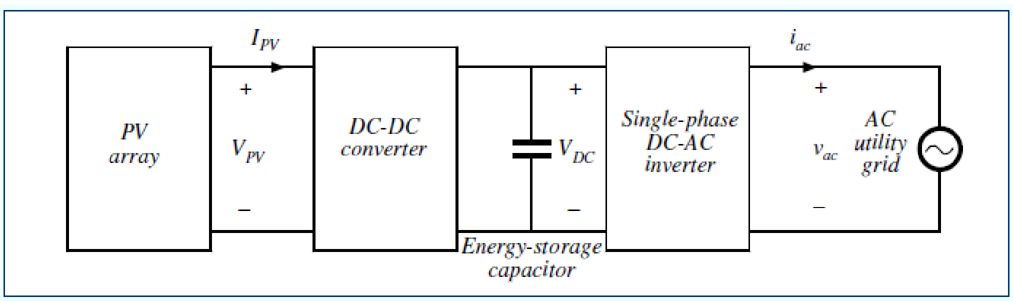

Figure 2-5 Topology of the PV array

The PV units simulated are residential grid-connected-type and provide about 100% of the residential load in this simulation. PVs are non-dispatchable and designed to deliver the maximum available power. An average model-based PV model has been adopted to represent these PVs.

2.1.2 Concept of the Green Hub System

In a conventional distribution system, magnetic transformers are used to connect DRERs to the distribution feeder, as shown in Figure 2-6. Traditionally, distribution systems are designed by assuming that the substation is the only energy source. With the presence of DRERs, unexpected problems, which will be explained later in this chapter, may occur. As the penetration level of the DRERs gets higher, the problems become more severe. Therefore, it is necessary to find a better approach to accommodating and utilizing the DRERs with high penetration.

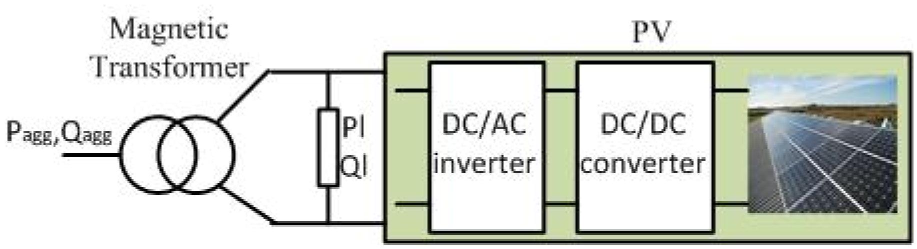

Figure 2-6 Single-phase customer load and DRER connection in Green Hub System

2.1.3 Concept of the FREEDM System

The FREEDM system is a new smart distribution system that facilitates seamless integration of high-penetration DRERs and DESDs with the existing power grid. Motivated by the success of the Internet, the architecture of the FREEDM system is proposed as a roadmap for a future automated and flexible electric-power system in Figure 2-7 [5], [9]-[11]. As explained in [11], residential class DRER, DESD, and loads are connected to the system through a revolutionary, highly efficient power-electronics-based intelligent energy management (IEM) subsystem. Each IEM will have bidirectional energy flow control capability allowing it to provide key plug-and-play features and isolate the system from faults on the user side. An intelligent fault management (IFM) subsystem will be used to isolate potential faults in the 12kV primary circuit and provide the reconfiguration capability and unprecedented power quality to the users. The brain of the FREEDM system will be provided by the Distributed Grid Intelligence (DGI) software embedded in each IEM and IFM. The FREEDM system will be connected to the traditional grid through a higher power IEM.

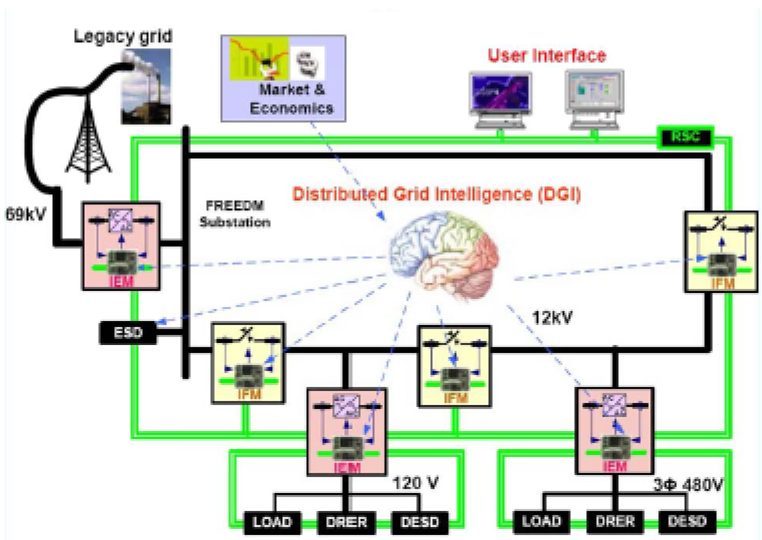

Figure 2-7 Architecture of the FREEDM system [6]

As presented in [5], three key technologies are critical in the information Internet: the plug-and-play interface, an information router that directs information to the right place, and an open-standard operating system. However, none of these is available in today's power grid. The proposed FREEDM system is a power distribution system that interfaces with residential customers and industrial customers with the following features:

1) The first key feature is a plug-and-play interface that includes both a 400V DC bus and a conventional 240V AC bus, as shown in Figure 2-8. This plug-and-play interface also contains an open-standard-based communications interface so that any device coupled to the grid will be recognized as soon as it is connected.
2) The second feature is an energy router or an IEM device that connects to the 12kV AC distribution bus and supports the regulated 120V AC or 400V DC bus. In the FREEDM system, SST plays the role of the energy router.
3) The third key feature is an open-standard-based operating system, called DGI. This feature is embedded into the IEM device.

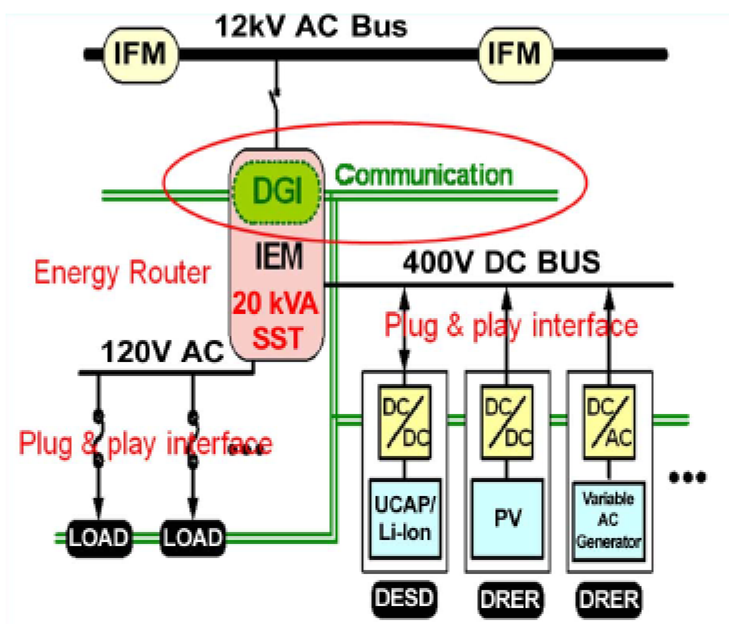

Figure 2-8 Interface of a future customer in the FREEDM system [9]

By merging advanced power-electronics technology and information technology to form a future distribution power grid, the proposed FREEDM system should be able to [11]:

- Have a new delivery interface that allows plug-and-play of any DRER or DESD, at anytime and anywhere;
- Have a communications infrastructure backbone that allows the real-time management of Load, DRER, and DESD through DGI software;
- Have the capability of being isolated from the main grid and operate in islanded mode;
- Have high power quality and reliability;
- Have improved overall system efficiency and power factor correction.

The connection of a single-phase customer load and PV with the presence of SST in the FREEDM system is shown in Figure 2-9. Since SSTs are single-phase, all customer loads, regardless of whether they are originally delta or Y connections, will be connected ground to phase via SST.

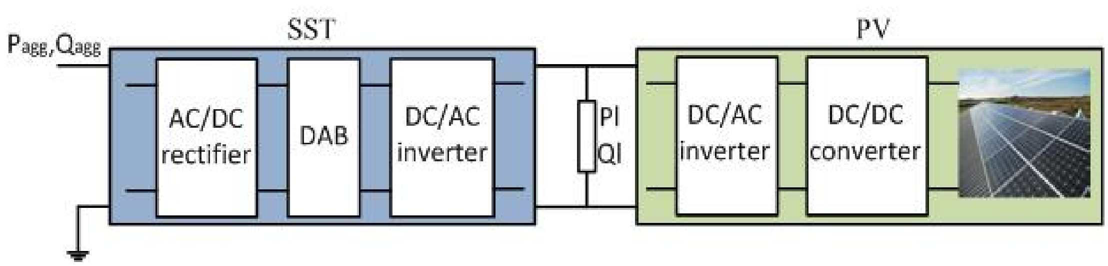

Figure 2-9 Single-phase customer load and DRER connection with the presence of SST in the FREEDM system

To make it clear, the differences between a conventional distribution system, a Green Hub-type distribution system, and a FREEDM-type distribution system are summarized in Table 2-1.

1) A substation is designed as the only source in conventional distribution systems and no DRERs are connected at the residential level. However, DRERs are available in both the Green Hub-type distribution system and the FREEDM-type distribution system. Therefore, transformers are needed in order to accommodate the DRERs.
2) Traditional magnetic transformers are utilized as distribution transformers in the Green Hub-type distribution system, while SSTs are used in the FREEDM-type distribution system. As described above, SSTs can inject reactive power according to the commands received from the control center. So, there is no need for conventional control devices, such as CAPs, VRs, and LTCs, in the FREEDM-type distribution system.
3) The control and regulation devices in conventional and Green Hub-type distribution systems are the same, but they differ from the FREEDM-type distribution system.

Table 2-1 Differences between conventional, Green Hub-type, and FREEDM-type distribution systems

	Conventional	Green Hub	FREEDM
Trans	No	Magnetic	SST
PV	No	Yes	Yes
Conv Control	Yes	Yes	No

2.2 Testbeds Developed at the FREEDM System Center

In the following text, the Residential Notional System and the IEEE 34 node test feeder testbeds, which were developed at the FREEDM System Center for research purposes, will be presented. The nature of these two feeders is the same, both are distribution feeders. By adding the DRERs—in our case, PV—to the conventional system, the two feeders will become Green Hub system. By replacing the conventional magnetic transformers with SSTs, the backbone of these systems will be basically FREEDM system, where the functionality of IEM, IFM and DGI will be embedded.

The most common type of distribution system for serving residential loads is the radial-type. Therefore, our focus in this study is radial-type distribution systems. In these test systems, high-penetration PV systems are considered as DRERs. The installation capacity of PV is 100% of the peak local load at each customer end. Due to the daily load and PV generation variation, voltages along the feeder also vary and may cause problems in normal operations of the distribution system. Therefore, the impact of high-penetration PV systems on the smart distribution system is investigated below, and the necessity for VVC strategy development will be discussed, too.

2.2.1 Residential Notional System

The Residential Notional System is developed based on the actual residential distribution circuit in Progress Energy's service area. The original system has two 15kV class feeders that operate at 12.47kV nominal voltage. Each feeder has about 200 line segments. To facilitate the development of a notional system that can be simulated easily without the loss of detail, a compromise has been made by lumping together the loads connected to sections of the feeders. In order to investigate the issues being brought up by the high penetration of PV systems, each customer has a roof-top PV system. It is assumed that each PV system can generate up to the maximum load of the residential unit. The Residential Notional System is modeled in PSCAD.

Generation I of the Residential Notional System utilizes a magnetic transformer to accommodate PV systems, which is a so-called Green Hub-type Residential Notional System. Later, SSTs will be used to replace the magnetic transformer and make the Residential Notional System a FREEDM-type system, which is called the Residential Notional System II in the text below. Figures 10 and 11 show the single-line diagram of the implemented system. Detailed data for the Residential Notional System is given in Appendix A.

1) Base value: Base voltage along the main distribution feeder is 12kV, so the per-phase base voltage is 6.9282kV. Set the base capacity to be 10 megavolt-amperes (MVA), Table A-1 shows all of the base values that are used in the Residential Notional System.

2) Loads: The Residential Notional System is a three-phase unbalanced distribution feeder. Table A-2 contains the load data for the Residential Notional System.

3) Line sections: The original system's line data is provided in Table A-3. If we divide all the resistance and inductance by its corresponding line length, it becomes clear that all the lines are of the same type. The line's positive/zero resistance and inductance per kilometer is shown in Table A-4.

4) Substation transformer: The substation transformer data of the Residential Notional System is shown in Table A-5. The rated voltage of the substation transformer is 69kV/12kV.

5) Capacitor banks: There are four fixed CAPs in the Residential Notional System, and the detailed data is shown in Table A-6.

Then, the one-line diagram of the Green Hub-type Residential Notional System, named Residential Notional System I, is shown in Figure 2-10, where the substation and distribution transformers are all conventional magnetic transformers.

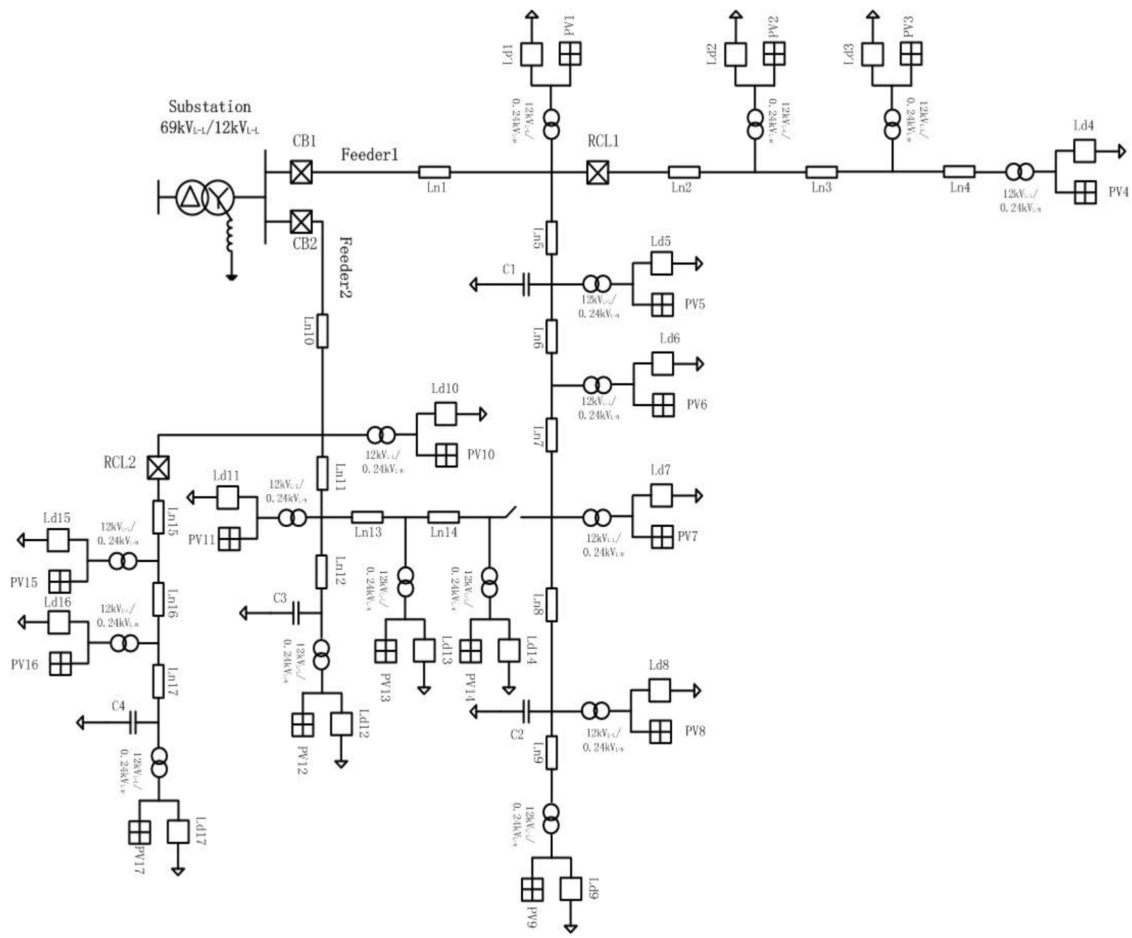

Figure 2-10 One-line diagram of Residential Notional System I

In order to make Residential Notional System I into a FREEDM system, the distribution transformers are all replaced by SSTs and the substation transformer is still a conventional magnetic transformer. With the presence of SSTs, there is no need for conventional control devices, so all the CAPs are removed from the system. The one-line diagram of Residential Notional System II is shown in Figure 2-11.

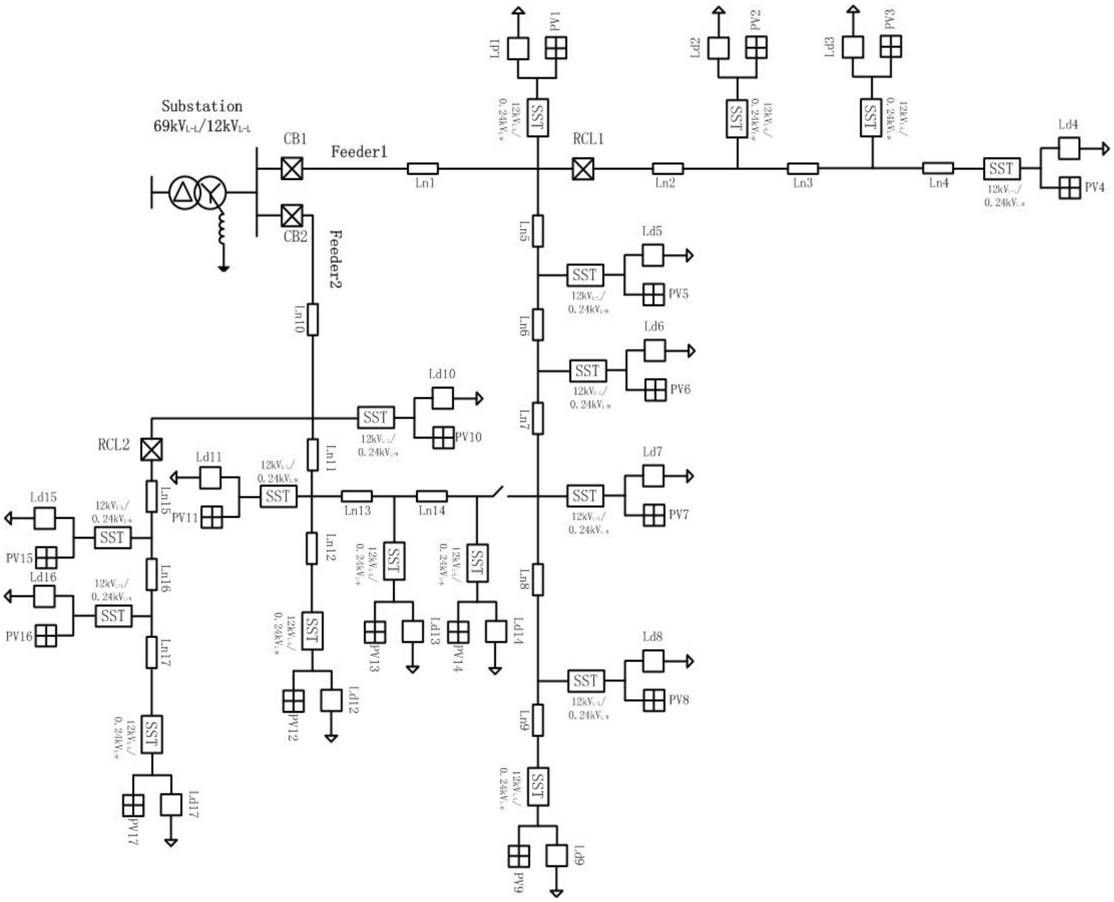

Figure 2-11 Single-line diagram of Residential Notional System II

2.2.2 IEEE 34 Node System

IEEE 34 node test feeder is an actual feeder located in Arizona with nominal voltage of 24.9kV. It is characterized by its long line length and heavy peak load. An in-line distribution transformer, between node 832 and 888, steps down the voltage to 4.16kV for a short section of the feeder. There are two VRs connected between node 814-850 and node 852-832, and two CAPs connected at node 844 and 848 individually. These Var compensation and voltage regulation devices are needed to maintain a good voltage profile.

IEEE 34 system is an unbalanced system with both "spot" and "distributed" loads. However, since single-phase conventional transformers or SSTs are going to be used to connect loads and PVs to the primary feeder, all the loads are modified to be the Y connection.

Similarly, as a Residential Notional System, Generation I of the IEEE 34 system utilize magnetic transformers to accommodate PV systems, which is a so-called Green Hub-type IEEE 34 system. Later, SSTs will be used to replace the magnetic transformer and make the IEEE 34 system a FREEDM-type system, which is called IEEE 34 Gen II in the following text. Figures 12 and 13 show the single-line diagram of the implemented IEEE 34 system. Detailed data for the IEEE 34 system is given in [12], [13].

Several changes have been made to the original IEEE 34 node system:

1) Instead of connecting directly to the primary feeder, all the loads are now connected via conventional transformers (24.9kV L-L/240V L-N rating) or SSTs (7.2kV L-L/240V L-L rating).
2) PVs, with installation capacity the same as local peak loads, are connected at the secondary side of the distribution transformer.
3) Conventional control devices (VRs and CAPs) are removed in the IEEE 34 node system II

Detailed data for the IEEE 34 Node System is given in Appendix B, which includes:

1) Base value: Base voltage along the main distribution feeder is 24.9kV, so per-phase base voltage is 14.2760kV. Set base capacity to be 10MVA, and Table A-7 shows all the base values that are used.

2) Loads: As stated before, instead of using “spot” loads and “distributed” loads, all the loads are represented as Y connections at the corresponding nodes. Table A-8 is the aggregated load data in the IEEE 34 node system.

3) Line sections: There are six types of lines in the IEEE 34 node system: 300, 301, 302, 303, 304, and 200. Table A-9 shows the line impedance and susceptance for each type. Line types 300, 301, 302, 303, and 304 work under the 24.9kV voltage level, and type 200 works under 4.16kV voltage level. Types 300, 301, and 200 are three-phase distribution lines, but types 302, 303, and 304 are single-phase conductors, where type 302 is connected to phase A and types 303 and 304 are connected to phase B. Table A-10 gives the sending and receiving node to which each line is connected, the line length, and the line type.

4) Voltage Regulator and Transformer: There are two VRs in the system, connected between nodes 814 and 850 and between nodes 852 and 832. They are modeled as LTC transformers with three different taps that can work independently for three phases. The impedance of VR is chosen to be the same as shown in Table A-11. There are two types of transformers in the original IEEE 34 node system. The rated voltage of substation transformer is 69kV/24.9kV and for transformer 832 is 24.9kV/4.16 kV. The impedances of these two transformers are shown in Table A-12.

5) Capacitor Banks: There are two fixed CAPs in the IEEE 34 system, with the detailed data shown in Table A-13.

For the Green Hub-type IEEE 34 node system, which is named IEEE 34 system I, substation and distribution transformers are all conventional magnetic transformers. All conventional control devices, two VRs, and two CAPs, are still kept in the system. The one-line diagram of IEEE 34 System II is shown in Figure 2-12.

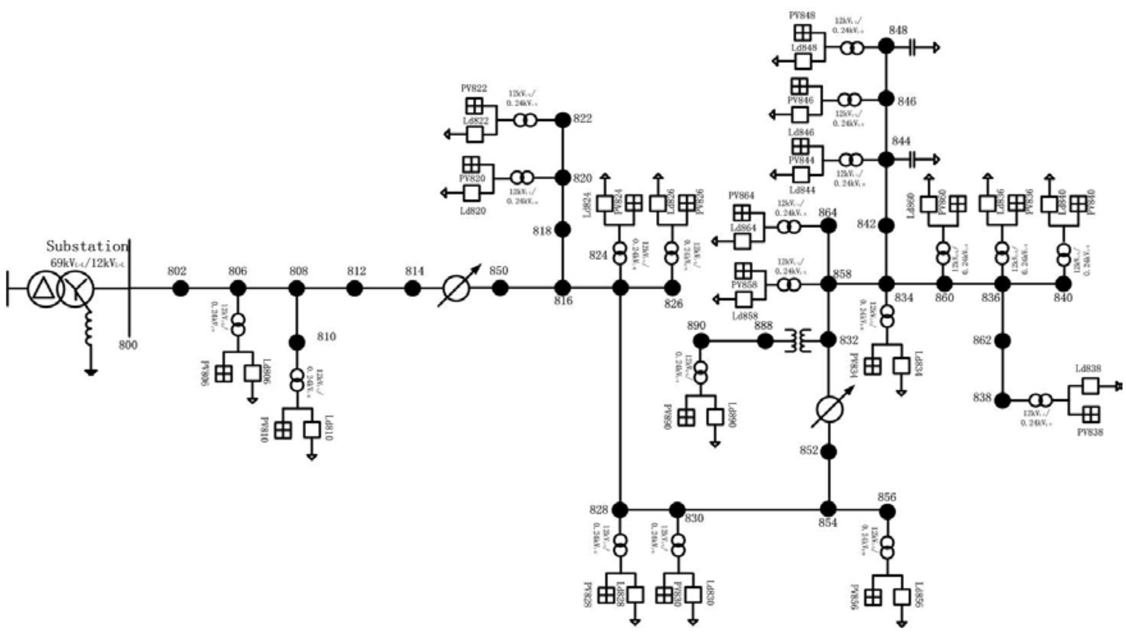

Figure 2-12 One-line diagram of IEEE 34 System I

In order to make the IEEE 34 I system into a FREEDM system, distribution transformers are all replaced by SSTs. CAPs and VRs are all removed. The substation transformer is still a conventional magnetic transformer. The distribution transformer that is connected between 852 and 832 is removed. The one-line diagram of IEEE 34 system II is shown in Figure 2-13.

One may notice that the primary feeder line to line voltage in the IEEE 34 II system is 12kV instead of 24.9kV. The reason is that the physical SST developed in the FREEDM system center is with fixed rating (7.2kV L-L/240V L-L). So all the customer loads are resized accordingly to guarantee that the real and reactive power consumed is the same as in original

IEEE 34 system. The substation transformer is therefore changed from 69kV L-L/24.9kV L-L to 69kV L-L/12kV L-L, and the distribution transformer between node 832 to 888 with a rating of 24.9kV L-L/4.16kV L-L is removed. Therefore, the primary feeder voltage of node 888 and 890 is now 12kV L-L instead of 4.16kV L-L. Finally, all the feeder lengths are modified based on the new voltage level so that the per-unit impedance of each line section remains the same.

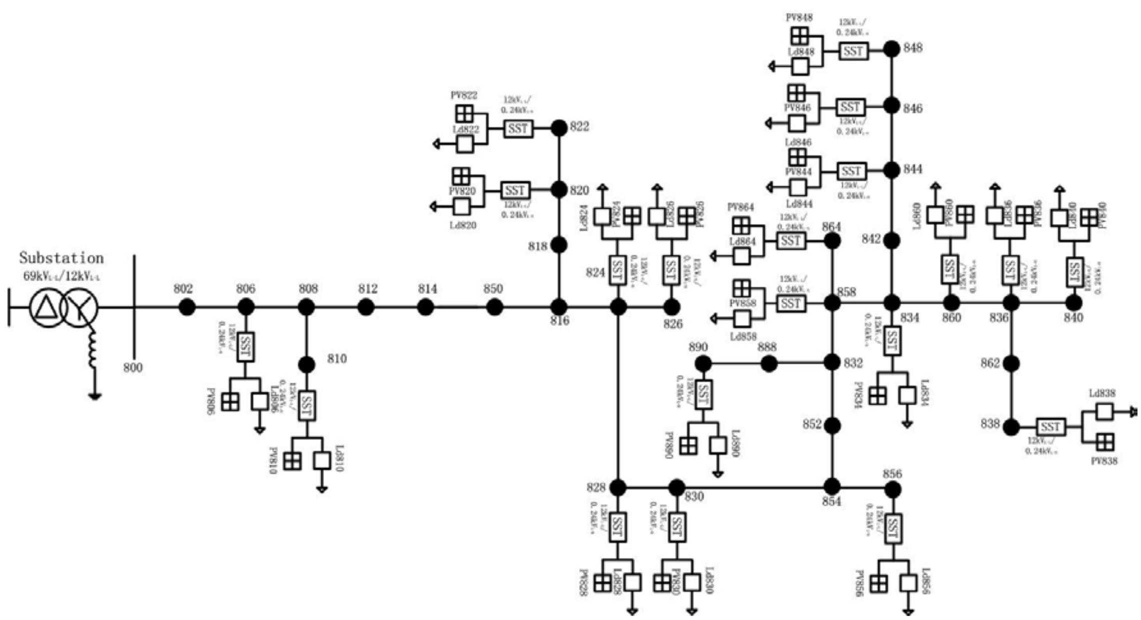

Figure 2-13 One-line diagram of IEEE 34 System II

2.2.3 Conventional Voltage Regulation Rules in the Distribution System

Voltage regulation is an important subject in electrical distribution engineering. It is the utility's responsibility to keep the customer's voltage within specified tolerances. In the conventional distribution system, since substation is assumed to be the only source of the whole feeder, voltage will drop gradually from the substation toward the end of the feeder. Therefore, additional voltage-regulating devices are needed to boost the voltage throughout the system. The devices provide voltage supports that can be classified as follows [14]:

1) Source or sinks of reactive power, such as shunt capacitors, shunt reactors, and static Var compensators (SVC)
2) Line-reactant compensators, such as series capacitors
3) Regulating transformers, such as LTC transformers and boosts

Usually, distribution substations are equipped with LTC transformers that operate automatically under load or with separate VRs that provide bus regulation [15]. As loads increase, the regulating apparatus boosts the voltage at the substation to compensate for the voltage drop in the distribution feeder. In the case where customers are far from the substation or where the voltage drop along the primary circuit is excessive, additional regulators or capacitors located at selected points provide supplementary regulation. Conventional control schemes of VRs and CAPs are simple local measurement-based schemes. Figure 2-14 illustrates the typical application of these two kinds of devices.

Figure 2-14 Voltage regulators and capacitor banks used on a distribution feeder

2.2.3.1 Voltage Regulator

Feeder VRs are used extensively to regulate the voltage at each feeder separately to maintain a reasonably constant voltage at the point of utilization. They are either induction-type or step-type VRs.

Step-type VRs can be either station-type or distribution-type. A station-type VR can be single-phase or three-phase and can be used in substations for bus voltage regulation or individual feeder voltage regulation. Distribution-type VRs can be only single-phase and is pole-mounted on overhead primary feeders. Step-type VRs are autotransformers with many taps in the series winding. Most regulators are designed to correct the line voltage from a 10% boost to a 10% buck.

In addition to its autotransformer component, a step-type regulator also has two other major components: the tap-changing mechanism and the control mechanism. Ordinarily, each VR is equipped with the necessary controls and accessories so that the taps are changed automatically under load by a tap changer, which responds to a voltage-sensing control to maintain a predetermined output voltage. It also provides the ability to adjust the line drop compensation by selecting the resistance and reactance settings.

VRs located in the substation or on a feeder are used to keep the voltage constant at a fictitious regulation or regulating point without regard to the magnitude or power factor of the load. The regulation point is usually selected to be somewhere between the regulator and the end of the feeder. A VR uses local measurements (current and voltage) to adjust the voltage at its terminals by varying its taps. A VR is controlled by a VR relay and has two control options:

1) Regulate the voltage at its terminals, or
2) Regulate the voltage at a remote point down the feeder.

This is achieved through a "line-drop compensation" scheme, which involves estimating the voltage at the remote target point by using the current measurement. Figure 2-15 illustrates this scheme [15].

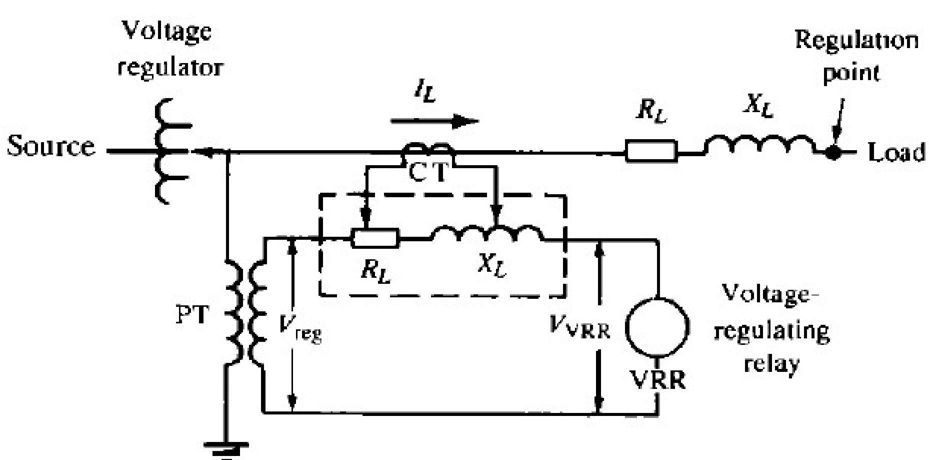

Figure 2-15 Voltage regulator mechanism [15]

LTC measures the local voltage and current and then transfers to a relatively low voltage-level circuit to calculate the voltage at regulating point (V_{VRR}). The voltage-regulating relay (VRR) is used to control tap changes. As illustrated in Figure 2-16, this relay has the following three basic settings that control tap changes:

- Set voltage (SV): It is the desired output of the regulator. It is also called the set point or band center.
- Bandwidth (BW): The VR controls monitor the difference between the measured and the set voltages. Only when the difference exceeds one-half of the BW will a tap change start.
- Time delay (TD): It is the waiting time between the time when the voltage goes out of the band and when the controller initiates the tap change. Longer TDs reduce the number of tap changes. Typical TDs are 10 to 120 seconds.

VRR compares the voltage V_{VRR} with the set point, if the difference between V_{VRR} and the set voltage exceeds half of the BW, the timer starts counting. When the timer reaches the TD, it sends commands to move the taps up or down.

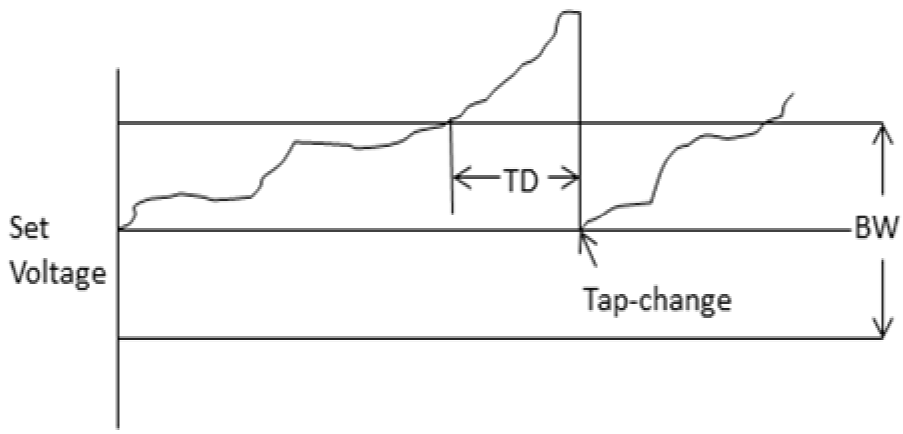

Figure 2-16 VR controls TDs with respect to set voltage and bandwidth

The VR typically has 32 tap positions (±16), which correspond to a range of ±10% of the transformer-rated voltage. In other words, each step is 0.625% of the rated voltage. The LTC is a mechanical device. Typically, the amount of time needed to move from one position to the next is 1 to 2 seconds. In a large power system, especially for long-feeder systems, more than one VR is installed. An improper TD setting will result in unnecessary tap changes, which may shorten the lifetime of the VRs. The most common way to coordinate them is to set a longer TD for the VRs that are further from the substation or in lower-voltage networks. The first VR's TD should be between 30 and 60 seconds [16]. The further VRs could range from 30 to 120 seconds.

In the two testbeds introduced above, there are two VRs in the IEEE 34 node system and no VRs in the Residential Notional System. The VRs in the IEEE 34 node system are connected separately between 814-850 (VR1) and 852-832 (VR2). According to the control setting discussed above, the VR control scheme in the IEEE 34 system is designed as shown in Table 2-2. Both VRs have the same setting voltage (122V) and bandwidth (+/-1V). The time costs for the tap to move from one position to the next position is set to be 1 second, which is called "time per step" (T/S). The philosophy of the operating sequence is that VR2 will wait until the operation of VR1 finishes. Since each step costs 1 second and the maximum steps needed for a VR to move from flat start to extreme setting is 16 steps, the difference between the TDs of VR1 and VR2 should be longer than 16 seconds. Therefore, the TDs of VR1 and VR2 are set to be 30 seconds and 60 seconds, respectively.

Table 2-2 Voltage regulator control scheme adopted in the IEEE 34 System

	VR1	VR2
SV(V)	122	122
BW(V)	+/-1	+/-1
TD(s)	30	60
T/S(s)	1	1

2.2.3.2 Capacitor Banks

The reactive power of the load could be supplied by substation or by capacitors in the conventional distribution system without DRERs. Installed capacitors could offset the reactive power demand of the load and, thus, reduce the current and boost the voltage at the points where they are installed. CAPs can be either series or shunt into the circuit. A series capacitor directly offsets the inductive reactance of the circuit, while a shunt capacitor can change the power factor of the load [15].

There are two ways for CAPs to be connected to the system: fixed or switched. Fixed capacitors are placed to provide the minimum voltage boost needed during normal loading. The limit of a fixed capacitor is an excessive leading power factor and a voltage rise in case of a light load, as shown in Figure 2-17. Therefore, fixed capacitors are sized to meet the minimum reactive load.

Switched capacitors provide the extra voltage boost needed during heavy load conditions. They can be switched as a block or in several consecutives steps as the reactive load increases and, thus, need to be switched off during light load conditions to prevent overvoltage conditions and avoid power loss due to excessive reactive power compensation. Figure 2-18 demonstrates the daily operations of fixed and switched CAPs. As shown in the figure, fixed capacitors are only sized to meet the minimum amount of reactive power needed, and switched CAPs can be switched in gradually as the load increases and switched off as the load decreases.

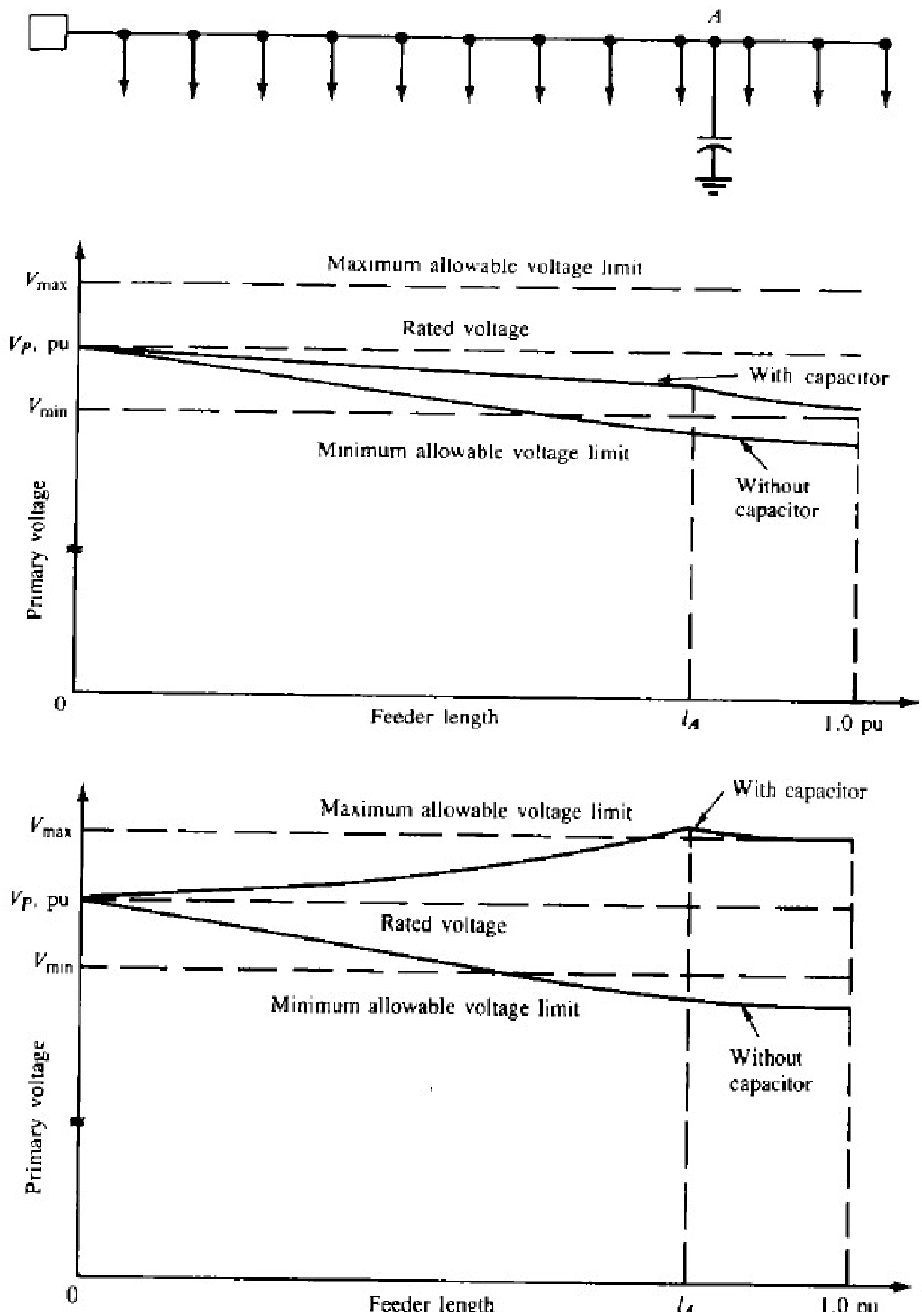

Figure 2-17 The effects of a fixed capacitor on the voltage profile of: (a) a feeder with a uniformly distributed load, (b) at heavy load, and (c) at light load [14]

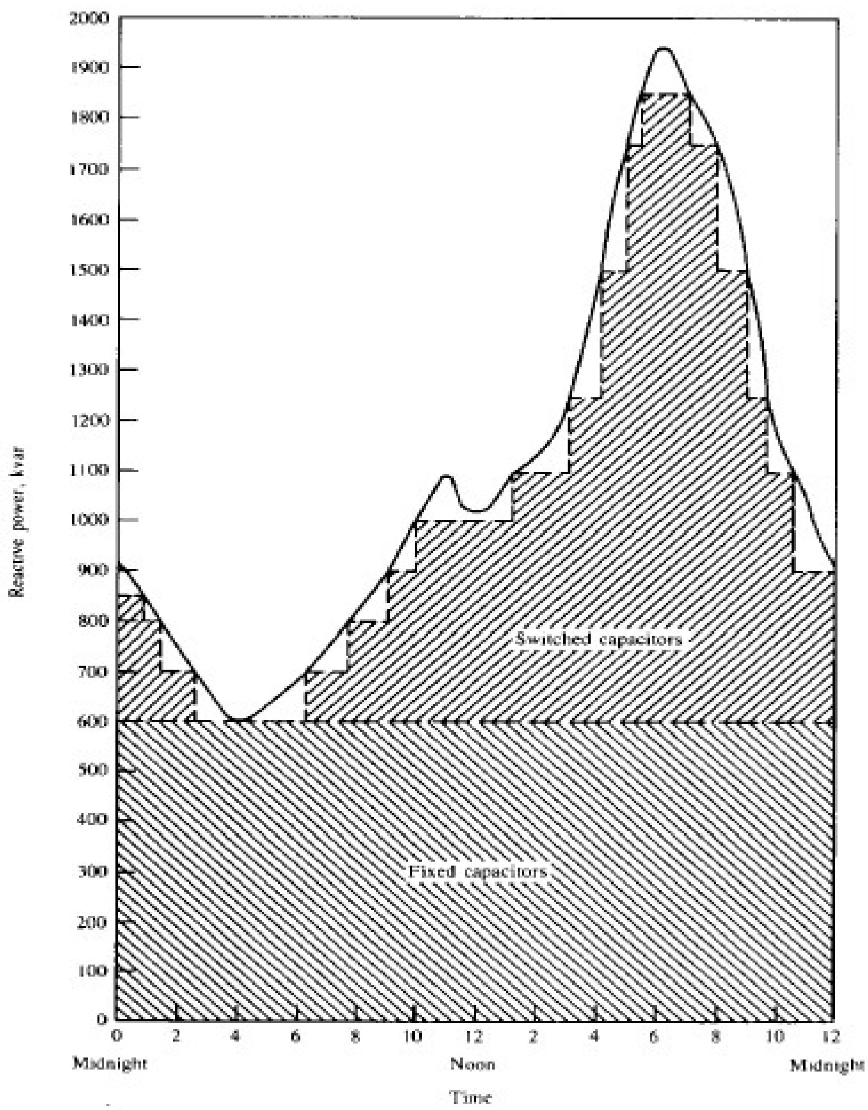

Figure 2-18 Operations of the fixed and switched capacitors to meet the daily reactive power demands [14]

There are two types of control for switched shunt capacitors. One is manual control, which can be employed at distribution substations. The other one is simple rule-based control schemes, which include time-switched, voltage-controlled, current-controlled, voltage-time combined controlled, voltage-current combined controlled, and temperature-controlled CAPs

[14]. The time-switch control is the least expensive one. Figure 2-19 illustrates two of the most commonly used capacitor control types in different areas.

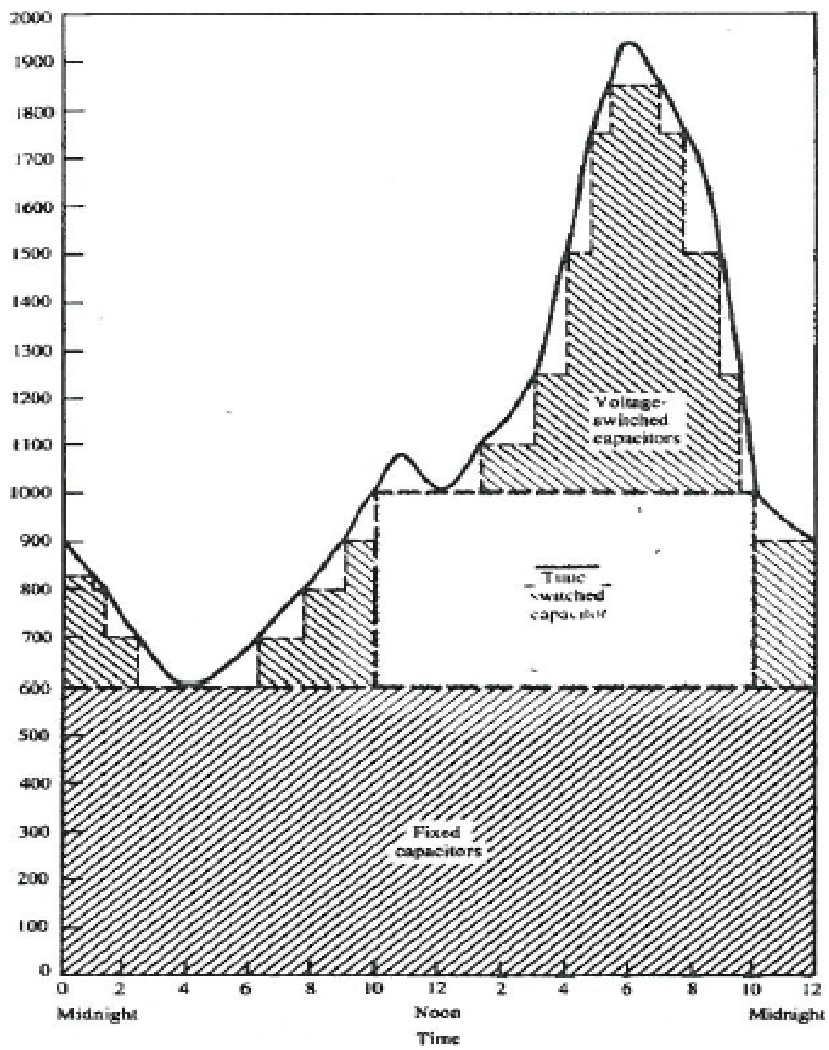

Figure 2-19 Control schemes for switched capacitor banks [14]

In the two testbeds introduced above, there are two fixed CAPs in the IEEE 34 node system and four fixed CAPs in the Residential Notional System.

2.3 Impact Study of High-Penetration PV on the Distribution System

Electric-power distribution systems have traditionally been designed assuming that the primary substation is the sole source of power. With the merging and application of DRER to distribution systems, the power source is introduced into the distribution system causing unexpected operating conditions. As one of the fastest developing renewable energy sources, PV technology is widely adopted at both the residential and commercial levels. However, PV output varies throughout the day and may be intermittent depending on the environment—solar radiation at the location where the PV is installed. From a control point of view, PV can have a significant impact on system voltages, power quality, operations of control devices, and power losses [17]. In addition, these effects vary with the size and location of PV generation, the method of voltage regulation and control, and the inherent characteristics of the distribution networks. Therefore, it is necessary to address the impact of PV on the system before it can be applied to the system.

2.3.1 Potential Steady State Impact of Renewables and Literature-Proposed Investigation Approach

The PV integrated in the FREEDM system is residential-scale, is installed on the customer's roof, and is connected to the secondary side of the distribution transformer. Dr. Katiraei's recent paper looked into both the steady state and the dynamic impact of utilityscale PV generators on distribution systems [18]. As Dr. Katiraei addressed in the paper, residential-scale PV requires a system-wide impact study, which may not be feasible from an economic standpoint. Therefore, very few papers have an in-depth discussion of a real situation that may occur in a distribution system with high residential PV penetration. In Dr. Liu's work [19], the impact of high-penetration PV on distribution system voltage performance is presented, giving an investigative approach. In her paper, PV itself can work under different control conditions, such as providing only reactive power, controlling voltages, or controlling the total service power factor. Therefore, different PV operating modes, together with different penetration levels and conventional system voltage regulating status will result in a different voltage profile in the test system. However, IEEE P1547.7 does not recommend allowing the DRERs to actively regulate the utility voltage [20]. The research objective of the FREEDM System Center is to create a "smart" distribution system that utilizes SSTs instead of conventional control devices, such as VRs or CAPs.

The IEEE P1547.7 gives a general outline of the potential impact that DRER, not limited to PV, may have on the system's steady-state performance. However, the limitation of the guide is that it only applies to DRER technologies of aggregate capacity of 10MVA or less that are interconnected with an area External Power Supply (EPS) at a typical primary or secondary distribution voltage.

The understanding of the steady-state performance of the area EPS is essential to ensure that the proposed DRER is applied appropriately while taking into account existing DRERs. When considering the effect the addition of DRER has on the steady-state performance of the area EPS, the steady-state performance of the DRER and the connected loads must also be considered. Modeling and simulation software are most often used to conduct system impact studies. In our case, PSCAD/ EMTDC is chosen to be the platform of modeling and simulation, and the structure of each electronic device was introduced in the previous chapter.

The steady impact study for distribution studies is typically done by addressing power flow, and potential steady-state impacts that need to be investigated include the following categories:

1) Reverse power flow under high penetration scenarios.
2) Changes in feeder voltage, including voltage rise and unbalance.
3) Interaction with CAPs, LTC transformers, and VRs.
4) Reactive-power flow fluctuations due to operation of switched CAPs.
5) Change in power losses, where a relatively large reverse power flow may increase losses.

To be specific, a result of the load-flow study is the data required to perform a more detailed voltage analysis, including the analysis of voltage drop, voltage unbalance, and voltage sags or swells. The ANSI C84.1 [21] standard defines the recommended service and utilization voltage limits for 120V level, which is accepted by most utilities.

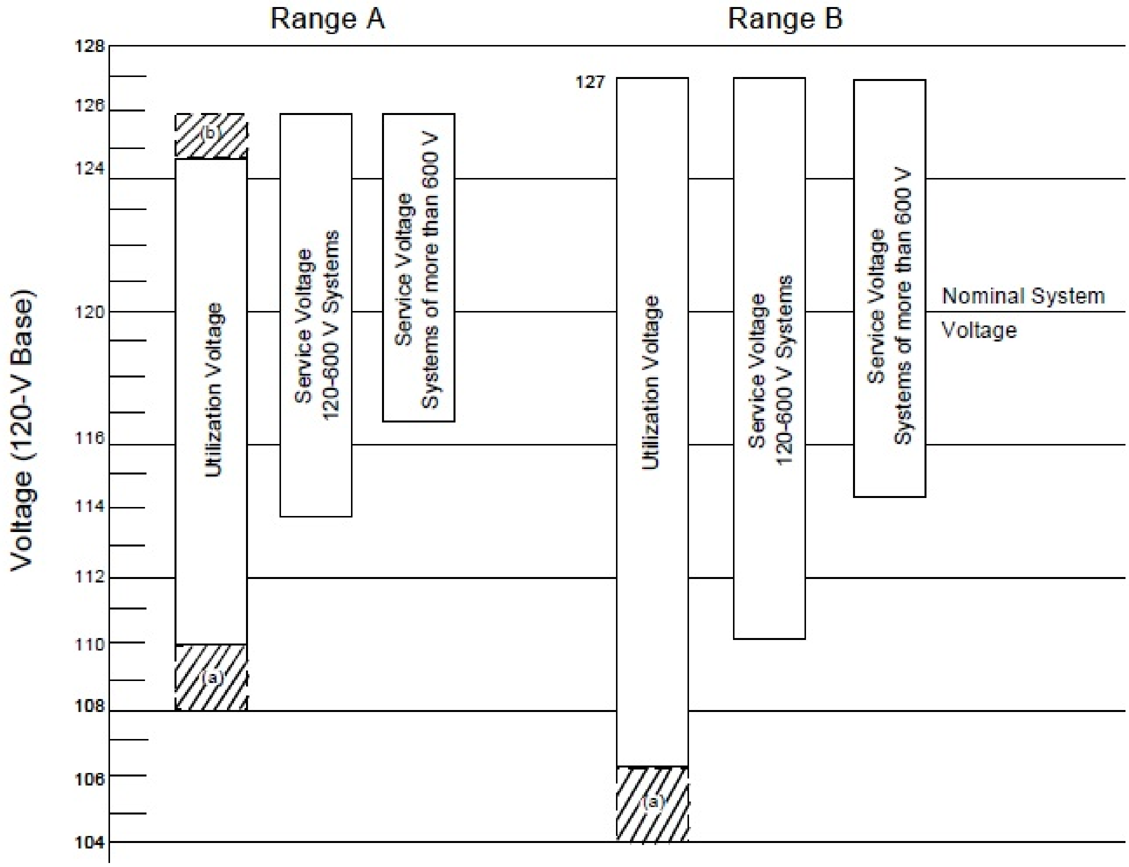

Figure 2-20 ANSI C84.1 voltage range for 120V level [21]

As indicated in Figure 2-20, the Range A service voltage range is the primary feeder voltage that needs to be well regulated under normal operating conditions. The voltage range of each category is shown in Table 2-3, where +/-5% is followed in this work.

Table 2-3 Voltage range for 120V level

	Service		Utilization	
	Min	Max	Min	Max
Range A (Normal)	-5%	+5%	-8.3%	+4.2%
Range B (Emergency)	-8.3%	+5.8%	-11.7%	+5.8%

Besides maintaining the required voltage level, voltage unbalance, sags, and swells are all important aspects of voltage study. One of the features of a distribution system is unbalanced loading. With a single-phase DRER applied to the distribution system, voltage unbalance studies are needed to determine the level of unbalance between phases. The installation of a single-phase DER or a three-phase DER on unbalanced circuits should be modeled using a three-phase power flow analysis tool to identify any complications that might arise on the circuit.

A voltage sag and swell study looks at the potential for DRER to produce or affect temporary voltage excursions. Voltage rise and variation may also occur because of PV output intermittency. The study should consider the Area EPS configuration, DRER interconnection configuration and equipment, and DRER characteristics. The study should also reflect the impact of DRER under varying expected topologies and loading conditions. Voltage issues often occur because of the addition of DRER on the electrical distribution system.

Reverse power flow happens when PV generation offsets the feeder load, which is very likely during sunny noon time in a high-penetration case. Care must be taken to examine relaying and metering to ensure that any possible reverse power flow will not trip the feeder or provide erroneous load readings to the system operators. This condition could be caused by installing a number of smaller units rather than a single large unit [21]. In addition to substation equipment, feeder equipment such as automatic circuit reclosers and VRs must also be evaluated to ensure the maintenance of proper service to the customers on the circuit. Note that uni-directional VRs will mis-operate when the generation exceeds the load beyond the

VRs. These units should be replaced with bi-directional VRs when the generation may exceed the load at any time during the year.

Voltage variation has a direct impact on the operation of voltage-controlled devices, such as VR, LTC, and voltage-controlled CAPs. Usually, there are limited operation times set for these devices within a certain time period. Frequent operations will shorten the expected life cycle and increase maintenance requirements for these devices. When the VR is uni-directional and reverse power flow happens, a more serious voltage rise may be caused by the unintentional operation. Consequentially, due to the frequent operation of CAPs, reactive power flow fluctuates, which may even affect the power flow of the sub-transmission and transmission systems.

Additional power injection provided by distributed PV will also change the line losses. For low-to-moderate penetration levels, line losses tend to decrease until they reach a minimum. However, high penetration may cause line losses to increase [18].

In this chapter, the steady-state impact study of high-penetration residential PV on a smart distribution system will be investigated following the guidelines provided in IEEE 1547.7. The study involved simulating varying operating conditions of the feeder and determining how the voltages vary under these different conditions. Based on the study's results, the necessity of the VVC strategy development is justified.

2.3.2 Impact Study of High-Penetration PV on Green Hub-Type and FREEDM-Type Residential Notional Systems

In order to decide the normal operation conditions that may take place, the actual load and the PV daily profile are obtained. The average residential load data of November 1999 is provided by Progress Energy, and the real-power output of the rooftop PVs in the FREEDM System Center on a typical sunny day in November 2010 is also recorded. The resolution of the load profile is 30 minutes, and the resolution of the PV profile is 5 minutes. The raw data is analyzed and represented in per-unit (p.u.) form. As shown in Figure 2-21, the residential load usually has two peaks: one is in the morning but the heaviest load happens after work. The energy requirement pattern mainly depends on customer characteristics. PV starts to produce real power from 7:45 a.m. until 6:15 p.m. During noon time when customer needs are quite flat and the sun's radiation is sufficient, PV real power generation exceeds the load consumption from 11:00 a.m. to 4:00 p.m., which results in a reverse power flow and potentially high voltage.

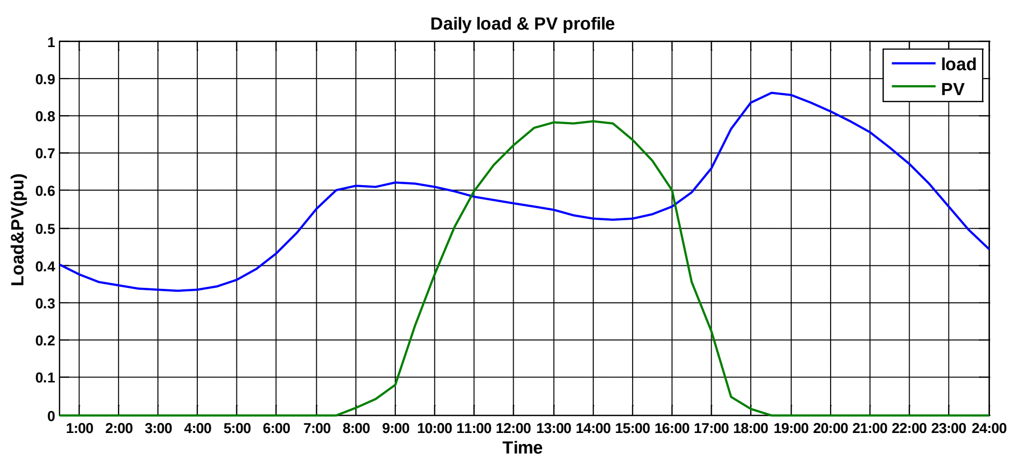

Figure 2-21 Daily load and PV profile

Based on the observation, the following possible system operating conditions are simulated by scaling the PV and loads.

C1) High load, no PV (kld=1, kpv=0)

C2) High load, medium PV (kld=1, kpv=0.5)

C3) Medium load, medium PV (kld=0.5, kpv=0.5)

C4) Medium load, high PV (kld=0.5, kpv=1)

C5) Medium load, no PV (kld=0.5, kpv=0)

Actual loads and PV output are expressed as a percentage of the peak load or its installation capacity. The ratio of kld=1 and kpv=1 means that the loads are the heaviest and the PVs are giving out their maximum real power. A ratio of kld=0.5 and kpv=0.5 means that loads and PVs equal 50% of their peak load or installation capacity. And a ratio of kpv=1 means that the PVs are not generating any real power.

Case 1 represents the peak load condition without any PV generation around 7:00 p.m. Case 2 represents a heavy-load condition with certain PV real power output, like at 5:30 p.m. Case 3 is the crossing point when the customer’s needs equal the PV generation, such as at 11:00 a.m. and 4:00 p.m. Case 4 is the most severe situation that can happen in a conventional distribution feeder when the difference between PV generation and load consumption is at its maximum, such as at 2:00 p.m. Case 5 represents most of the day when the load is moderate and there is no PV generation, from 12:00 a.m. to 6:00 a.m. Out of these five cases, case 1 and case 4 are the two extreme operating conditions during normal operations. Case 1 may result in a severe voltage drop and a low-voltage profile at the end of the feeder, while case 4 may cause high voltage.

In the following study, several assumptions have been made:

1) The substation transformer has no voltage regulation capability, and the source voltage is set to be 1.0 p.u. in all cases.
2) VRs and CAPs are kept in the Green Hub-type distribution system. All conventional control devices are removed from the FREEDM-type distribution system.
3) Each load bus has solar PV connected to it with the installation capability the same as the peak real power of its corresponding load.
4) Since the fixed-load model in PSCAD has certain dynamic behaviors, all the loads are represented using resistance and inductance instead of using a fixed load. The loads are distributed evenly on the secondary side of the distribution transformer.

Figure 2-22 shows the load connection in the Green Hub-type system and the FREEDM-type system in the PSCAD simulation platform. As indicated in the figure, all the loads, no matter whether they were delta- or Y-connected originally, are modeled per phase and distributed evenly on the two windings of the secondary side of the distribution transformer. PV with the same size as the corresponding load is connected at the secondary side of the distribution transformer, too. The difference between the Green Hub-type system and the FREEDM-type system is that the Green Hub-type distribution system utilizes magnetic transformers as a distribution transformer and conventional control devices to regulate voltages. The distribution transformers in the FREEDM-type distribution system are SSTs. As an intelligent power electronics device, the SST also plays the role of voltage regulation and Var compensation so there is no need of conventional control devices in the FREEDM-type distribution system. The application of SST makes the distribution system be a FREEDM-type smart distribution system.

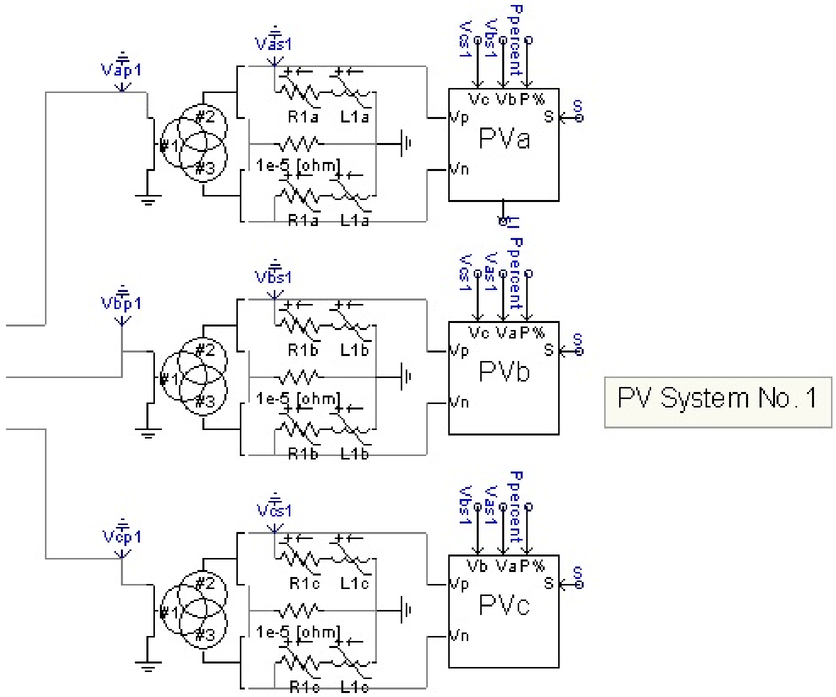

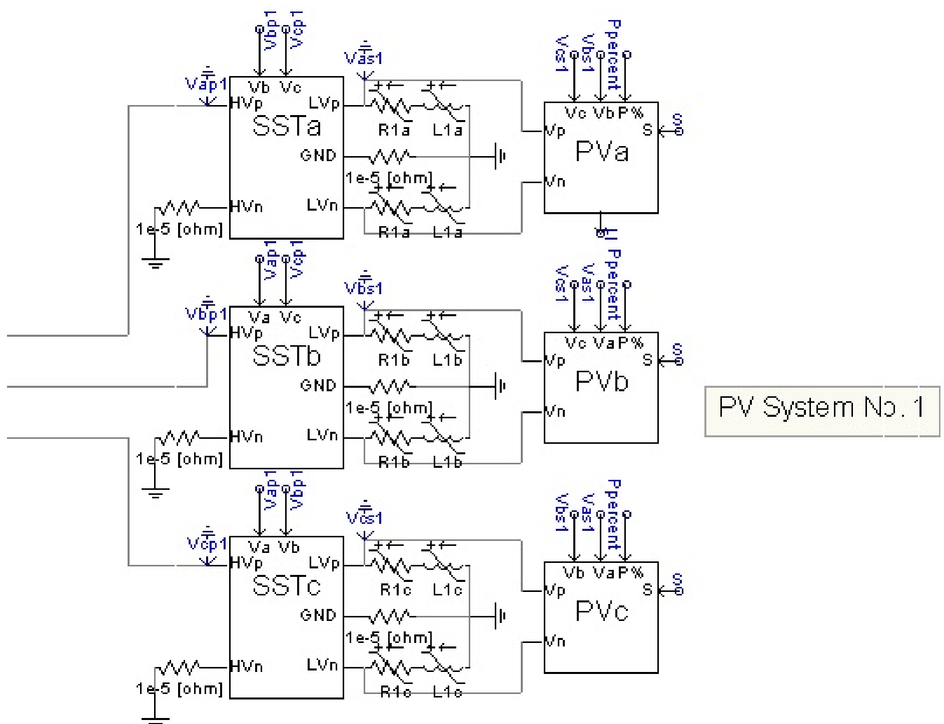

Figure 2-22 Load connection in PSCAD (1) Green Hub-type system, and (2) FREEDM-type system

As described above, the difference between Residential Notional System I (a Green Hub-type distribution system) and Residential Notional System II (a FREEDM-type distribution system) lies in the distribution transformers that connect the loads and the primary feeder. In Residential Notional System I magnetic transformers are used, while in Residential Notional System II SSTs are applied. Besides, conventional voltage-control devices are kept in Residential Notional System I, while they are removed from Residential Notional System II.

2.3.2.1 Impact Study of Residential Notional System I

According to the detailed data given in previous sections, Residential Notional System I is modeled in PSCAD and the implemented simulation model is shown in Figure 2-23.

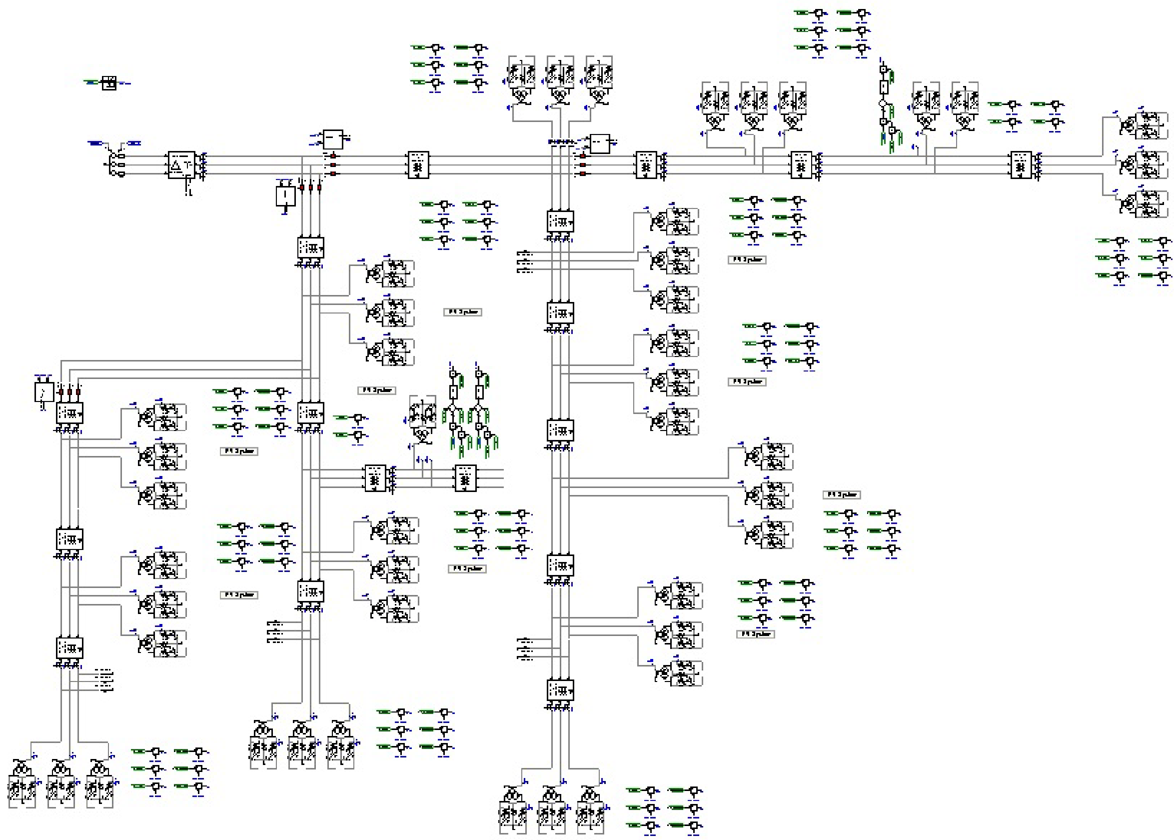

Figure 2-23 PSCAD implementation of Residential Notional System I

Figure 2-24 shows the voltage profiles of the two feeders on a phase basis based on the PSCAD-based simulations. Note that the first nine nodes in the figure (on the *x*-axis) correspond to the first feeder, and nodes 10-16 correspond to the second feeder.

As expected, under heavy load conditions with no PV (case 1), the load profile is lowest and the profile improves with even modest PV compensation (case 2). With full PV compensation under a normal load (case 3), the voltage profile is even higher and is quite flat (a low voltage drop on the feeder). When the PV generation exceeds the load under normal conditions (case 4), it pushes the voltages even higher; the voltage profile is flat, and some parts turn slightly upward, rather than downward. Clearly, the voltage issue in C1 is the most severe since many nodes in each phase are lower than 0.95 p.u. Note also that the voltage rise resulting from high PV generation in C5 is not severe and does not cause any voltage violations in Residential Notional System I.

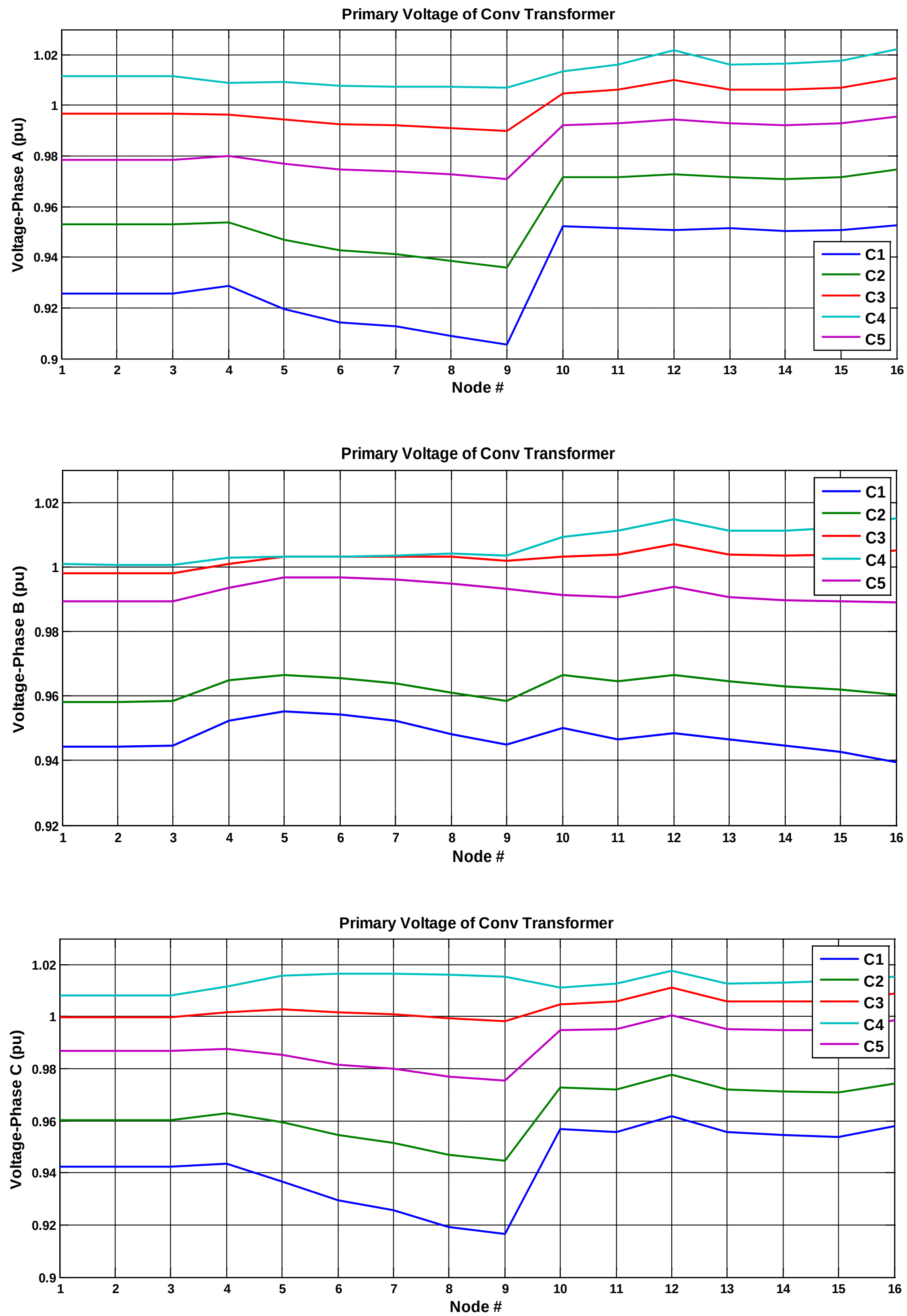

Figure 2-24 Comparison of phase voltages (p.u.) under different system operating conditions

To better assess the voltage variation (VV) at each node during these operating conditions, Figure 2-24 shows the VV under the different operation conditions considered. The VV for each node is calculated using the following equation:

$$VV_i = Max(V_{ix}) - Min(V_{ix}) \tag{2.1}$$

where i is the node number, and V_{ix} is the node voltage under operation condition x. As Figure 2-25 illustrates that VV on the first feeder is especially high and about 10% toward the end nodes of the first feeder. Given that PV output is quite intermittent and can change quickly (e.g., cloud conditions), this much VV may not be acceptable (e.g., flicker concerns).

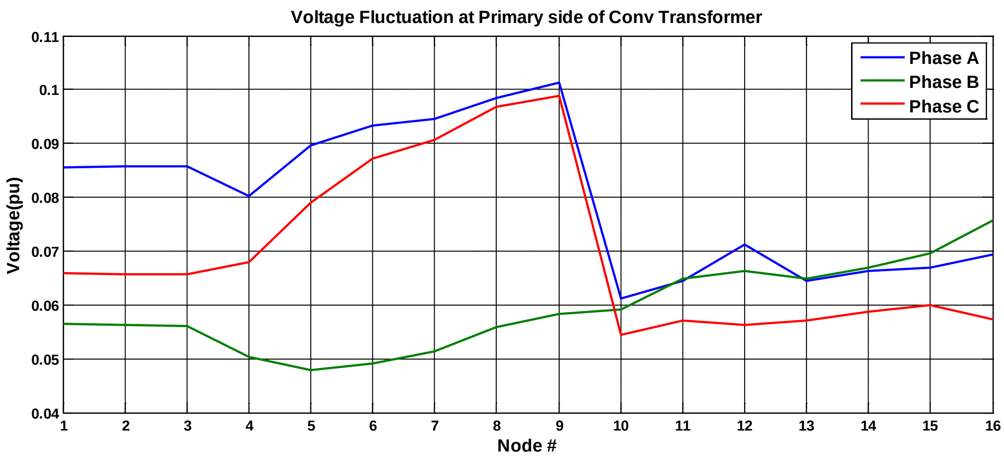

Figure 2-25 Voltage variation (in p.u.) along feeder for all three phases

The results in Figure 2-25 also indicate that there is considerable voltage unbalance between phases. To assess the voltage unbalance on this system, the voltage unbalance (VU) of a certain node i between phases is calculated using:

$$VU_i = Max(V_{iy}) - Min(V_{iy}) \tag{2.2}$$

where i is the node number and y represents phases A, B, and C. Figure 2-26 shows the VU profile for the test system. As the figure illustrates, the VU increases with loading and is highest during heavy loading (condition C1), about 0.04 p.u. Hence, power injection from PVs tends to decrease the VU. For example, having some PV during heavy loading (case C2) helps improve the VU considerably, as comparing the profiles of C1 and C2 indicates. Unfortunately, the intermittent nature of PV can makes the VU vary considerably during heavy loading conditions. In order to investigate the effect of PV intermittency on the feeder voltage, the cloud-passage effect on PV output and the system voltage profile is investigated.

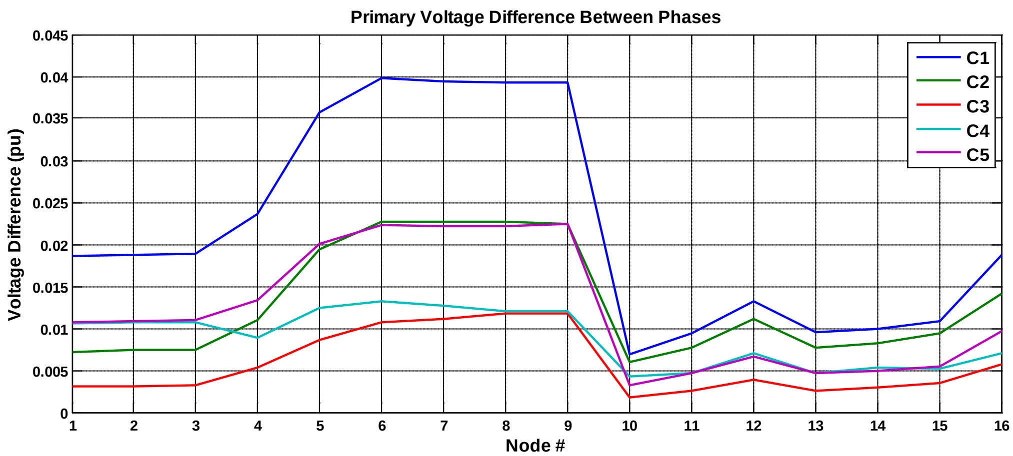

Figure 2-26 Voltage unbalance along feeder under different system operating conditions

Solar radiation can change very quickly. In the previously studies [16], [22], and [23], it is recorded that a cloud can travel as fast as about 43 feet per second, which results in the quickest ramp rate of 705 watts per square meter (W/m^2). Therefore, it takes only a few seconds for a clear sky to change to heavy cloud cover. Then, a cloud-passage scenario is created to test the system response in the following. The cloud transient is simulated by a decrease in solar irradiation from 1000W/m^2 to 300W/m^2 over a 7-second period of time. Then, after 1 second, the cloud is assumed to pass by with an increasing rate of 350W/m^2/sec.. The solar radiation profile used is shown in Figure 2-27.

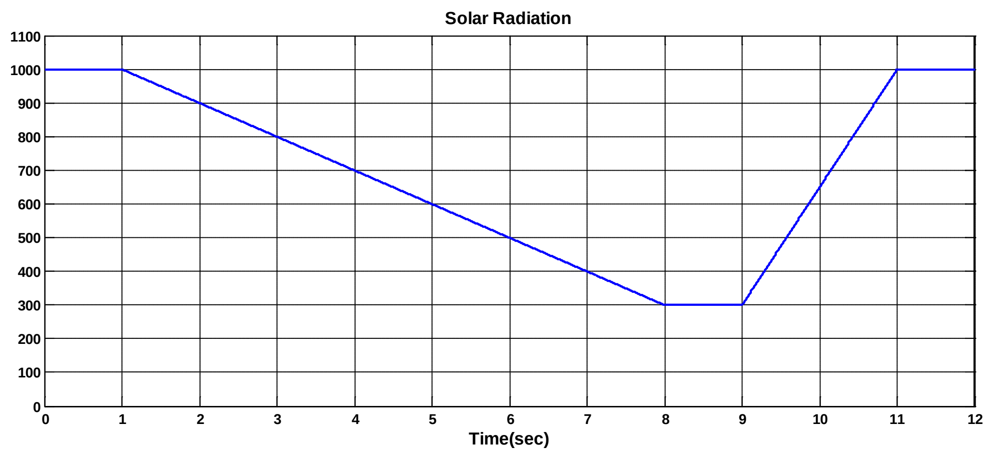

Figure 2-27 Solar radiation profile due to the passage of clouds

Since the PV output in case 4 is the largest during the day, the effect of cloud passage will be most severe under this condition. Choose case 4 to demonstrate the PV output and system VV during a cloud-passage event, and the result is shown in Figure 2-28. Due to solar radiation variation, the real power generated by PV changes will affect the voltage at the corresponding node to which the PVs are connected. Taking the PV connected to node 4 (the furthest node on feeder 1) and the voltage at the primary side of the corresponding distribution transformer as an example, the effect of PV intermittency at each phase is given in

Figure 2-28. Note that the installation capacity of the PVs at node 4 is 20.02kW for phase A, 10.01kW for phase B, and 85.47kW for phase C, respectively.

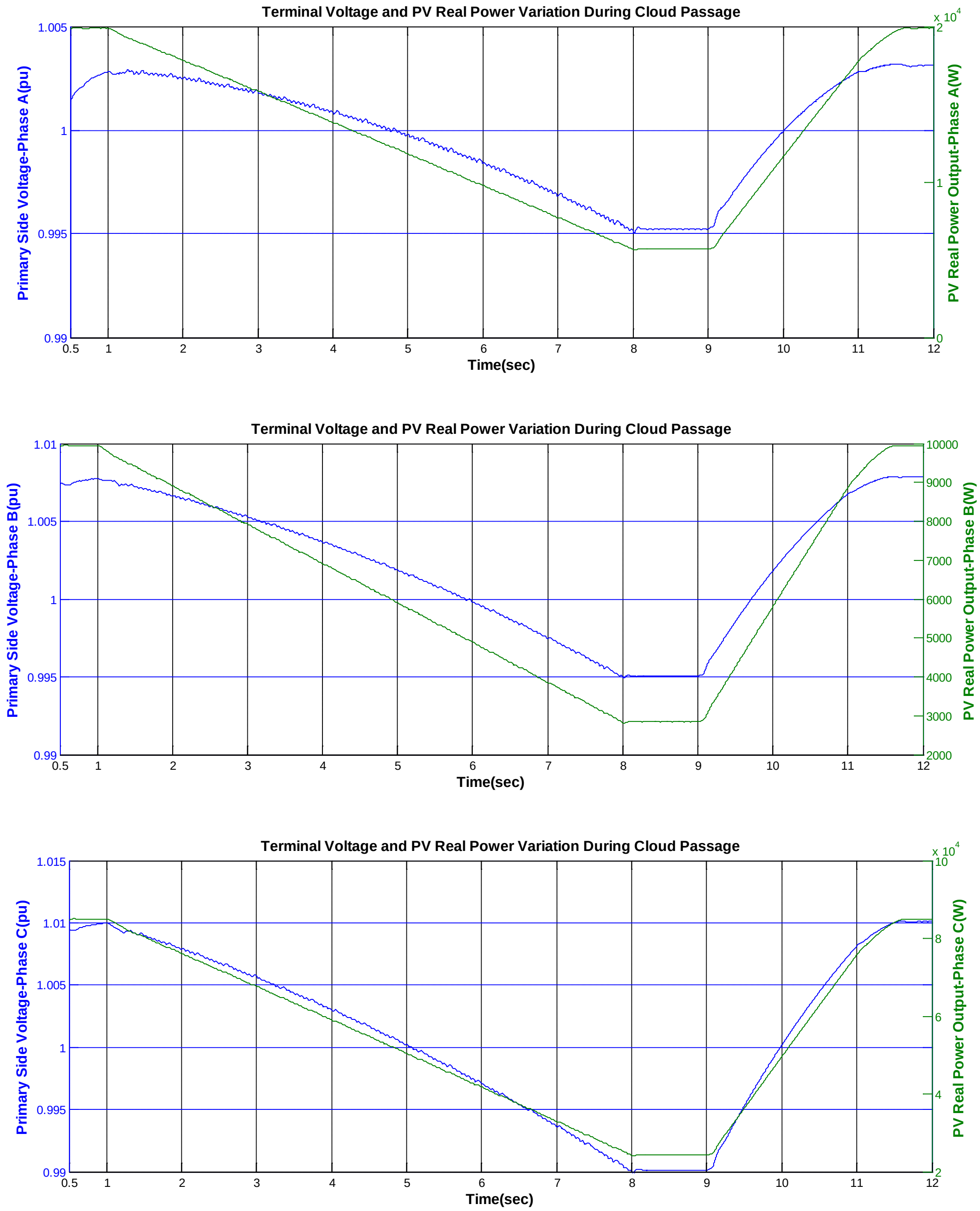

Figure 2-28 Terminal voltage and PV real-power variation during cloud passage at node 4

Note that the PV real-power output change follows the change in solar radiation and the VV follows the PV real-power output change. Due to the intermittency, the most severe voltage drop is about 0.03 p.u. in phase C. The effect is considerably higher and may even effect the control decision, which will be discussed in detail in later chapters.

The results show that high-penetration PV on a feeder will affect the VV on a feeder. PV will, in general, improve the voltage profile and reduce both voltage drop and the VU. However, due to the PV's sensitivity to cloud cover, the VV can be excessive.

2.3.2.2 Impact Study of Residential Notional System II

By replacing the conventional magnetic-distribution transformers with SSTs, Residential Notional System I turns into Residential Notional System II. The PSCAD implementation of Residential Notional System II is shown in Figure 2-29.

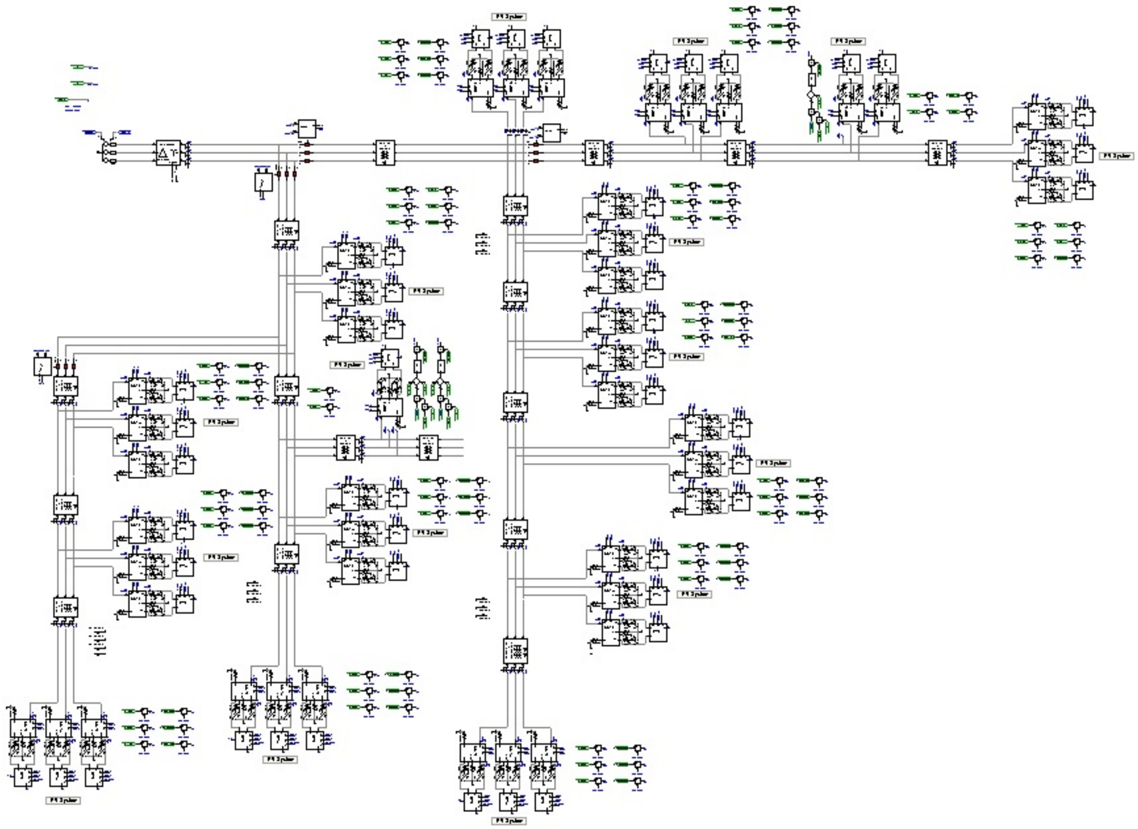

Figure 2-29 PSCAD implementation of Residential Notional System II

As introduced earlier, one of the main features of SST is that it can automatically work under a per-unit power factor without receiving any control commands. Therefore, all the reactive load inquiries on the secondary side will be provided by their corresponding SSTs. Based on the PSCAD simulations, Figure 2-30 shows the voltage profiles of the two feeders on a phase basis. Note again that the first nine nodes of the figure (on the *x*-axis) correspond to the first feeder and nodes 10-16 correspond to the other feeder.

As expected, reducing the apparent load will result in a better voltage profile than will Residential Notional System I under the same system operating conditions. Besides, the impact of PV real-power output to the system voltage profile is of the same trend as in Residential Notional System I. The voltage profile is the lowest under heavy-load conditions with no PV (case 1) and improves with even modest PV compensation (case 2). With full PV compensation under a normal load (case 3), the voltage profile is even higher and quite flat with a very low voltage drop on the feeder). When the PV generation exceeds the load under normal conditions and reverse power flow occurs (case 4), it pushes the voltages even higher. Then, the voltage profile is flat and some parts turn slightly upward, rather than downward. Note also that the voltage rise in this case is not severe and does not cause any voltage violation.

Compare the same operating conditions between Residential Notional System I and Residential Notional System II. The voltage profile in the conventional system under heavy loading condition (case 1) is far lower than the lower voltage limits. The lowest voltage in Residential Notional System I is only about 0.91 p.u. in phase A. While in Residential Notional System II, the lowest voltage is 0.94 p.u. in phase C, and the voltage in phases A and B are all within range A. In another extreme case, the reverse power-flow case 4, the voltage profile is quite flat in both Residential Notional System I and Residential Notional System II. Fortunately, high voltage over the upper limits doesn’t happen with this system structure, but attention still needs to be paid since the reverse power flow is not a usual case in the distribution system.

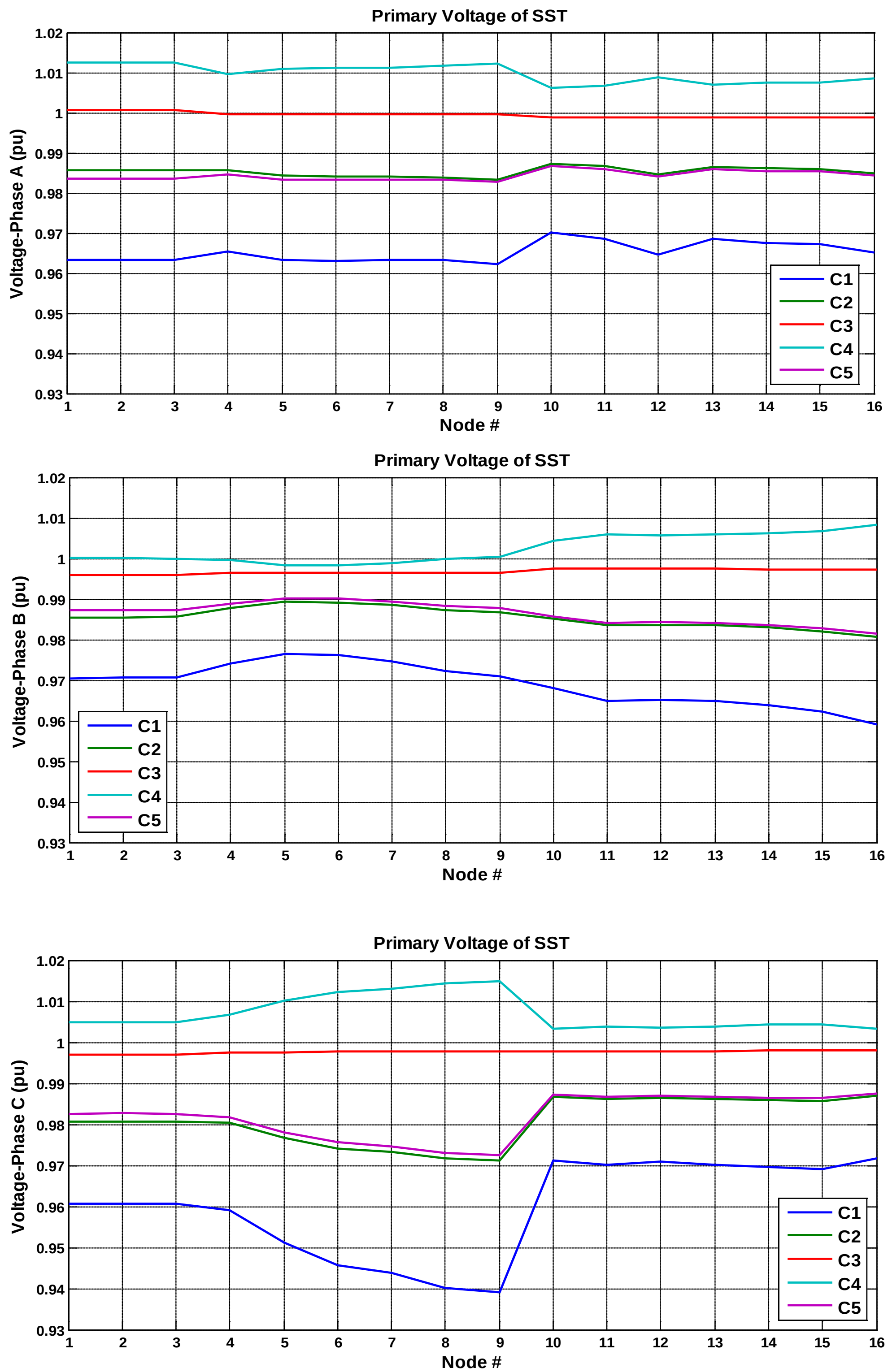

Figure 2-30 Comparison of phase voltages (p.u.) under different system operating conditions

Equation (2.1) is used, then, to assess the VV at each node during these operating conditions. Figure 2-31 shows the VV under the different operation conditions considered. As illustrated, the VV on the first feeder is still high, about 8% on phase C toward the end nodes of the first feeder. The fluctuation is improved compared with 10% on phase C in Residential Notional System I. Phase A is quite flat around 4% to 5% in Residential Notional System II, while phase A is almost the same pattern as phase C in Residential Notional System I. The fluctuation in phase B also decreases here.

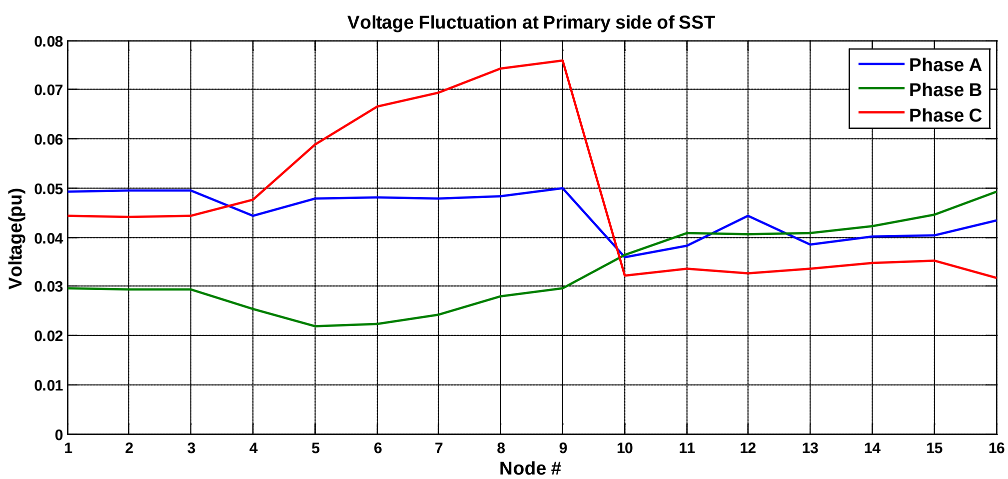

Figure 2-31 Voltage variation (in p.u.) along the feeder

Then, equation (2.2) is adopted to investigate the VU issue in Residential Notional System II, which is shown in Figure 2-32. Similarly, as in Residential Notional System I, VU increases with loading and is highest during heavy loading (condition C1). Hence, power injection from PVs tends to decrease VU. Case 3 shows a considerable difference here when PV output just offsets the loading. The voltage difference here is almost negligible and quite flat along the feeder. However, although the voltage difference in case 3 is the smallest, it still has the same trend as the other cases in Residential Notional System I. The main reason is that not only is the real power needed equal to the PV output, but also the reactive power is provided by SST directly.

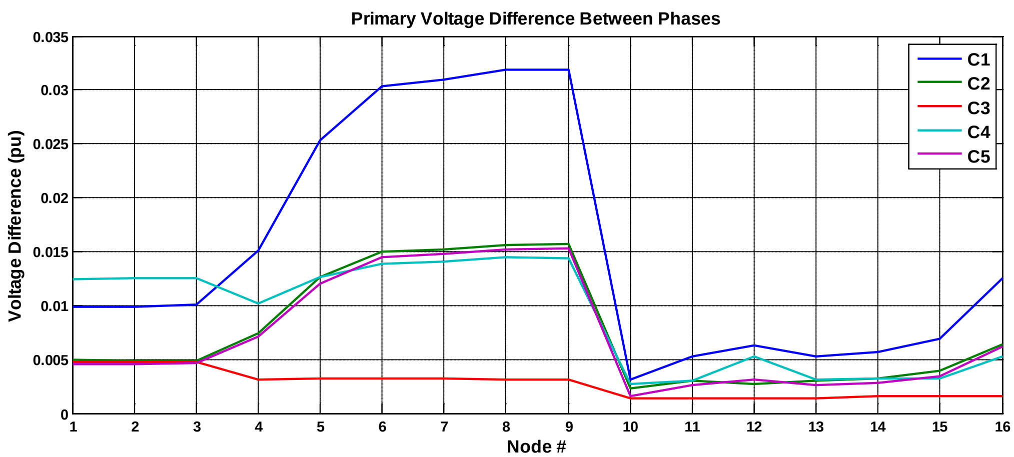

Figure 2-32 Voltage unbalance along the feeder under different system operating conditions

In the following, the same cloud-passage scenario is investigated, and the voltage and PV output profiles during the cloud passage at node 4 are demonstrated in Figure 2-33. Note that the installation capacity of the PVs at node 4 is 20.02kW for phase A, 10.01kW for phase B, and 85.47kW for phase C, respectively. Due to solar-radiation variation, the real power generated by PVs changes accordingly and, thus, will affect the voltage at the node to which the PVs are connected.

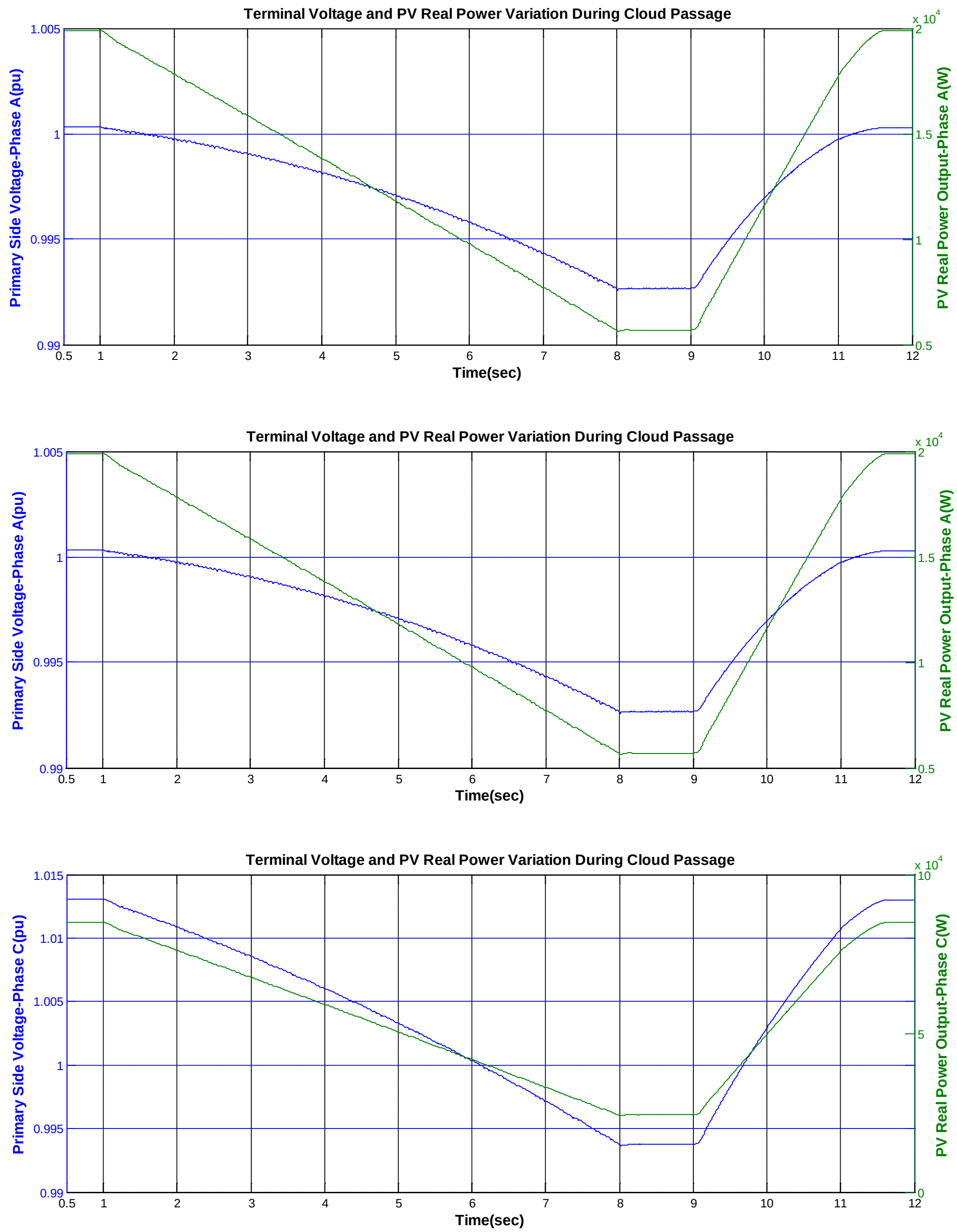

Figure 2-33 Terminal voltage and PV real-power variation during cloud passage at node 4

Note that the PV real-power output change follows the change in solar radiation, and the VV follows the PV real-power output change. Due to the intermittency, the most severe voltage drop is about 0.03 p.u. in phase C, the same VV as in Residential Notional System I. This demonstrates that the intermittency of PV generation is kind of a critical issue in both the Green Hub-type system and the FREEDM-type system.

Overall, the results show that high-penetration PV on a feeder will affect the VV on a feeder. Together with new enabling technology, such as SSTs, the system voltage profile will be greatly improved when residential high-penetration PV is presented. Voltage drop and the VU issue will be relieved, too. However, high voltage during reverse power flow and the VV during cloud passage are issues to which attention needs to be paid.

2.4 Conclusion

In this chapter, the key features of the smart distribution system, the concept of Green Hub and FREEDM systems are introduced. Then, the new enabling technologies that make the distribution system "smart" are presented. Two testbed systems, modeled from realistic existing feeders with detailed data, are discussed and modified to be Green Hub-type and FREEDM-type distribution systems, respectively. The main difference between the two distribution systems is that the Green Hub-type system uses magnetic transformers as distribution transformers and conventional control devices to regulate voltages; the distribution transformers in the FREEDM-type distribution system, on the other hand, are SSTs. As an intelligent power-electronics device, the SST also plays the role of VR and Var compensation so conventional control devices are not needed in the FREEDM-type distribution system.

A literature survey has been conducted on the topic of the impact of renewables on distribution systems. Potential steady-state impacts are mentioned, and standard investigation approaches are followed. Then, the steady-state impact of high penetration of residential PV on the Green Hub-type and the FREEDM-type of both testbeds is demonstrated in the second part of this chapter. The results show that when high-penetration PV appears in the distribution system, conventional voltage regulation devices cannot respond quickly enough. Also, the voltage profile along the distribution feeder needs to be regulated within acceptable limits. In order to deal with the new distribution system structure and new voltage regulation devices, Volt/Var control strategy needs to be developed for the FREEDM-type distribution system.

CHAPTER 3. A Centralized Volt/Var Control Scheme for the FREEDM System

3.1 Introduction

This section describes the motivation for a VVC; commonly used VR and Var compensation devices are also listed here. Different from conventional distribution systems, the concept of the FREEDM system, a smart distribution system that accommodates DRER and SST, is presented. Instead of conventional VVC devices, SSTs are going to provide the Var injections requested by VVC applications. In order to justify the necessity of developing VVC for FREEDM systems, a comprehensive impact study of high-penetration PV is conducted followed by the IEEE standard.

3.1.1 Overview of Volt/Var Control

Power distribution systems may experience both over-voltage and under-voltage violations during daily operations [14]. In a conventional distribution system, the substation is usually viewed as the sole source for the whole system. Therefore, current flows through the transformer and line impedance causes voltage drops, which reduce the voltage magnitude from a maximum value nearest to the substation to a minimum value at the farthest end of the circuit, as shown in Figure 3-1. As loading conditions change, the voltage profile along the feeder also changes accordingly. Without VVC, over-voltage can be experienced under a light load condition, and under-voltage can happen during a heavy load.

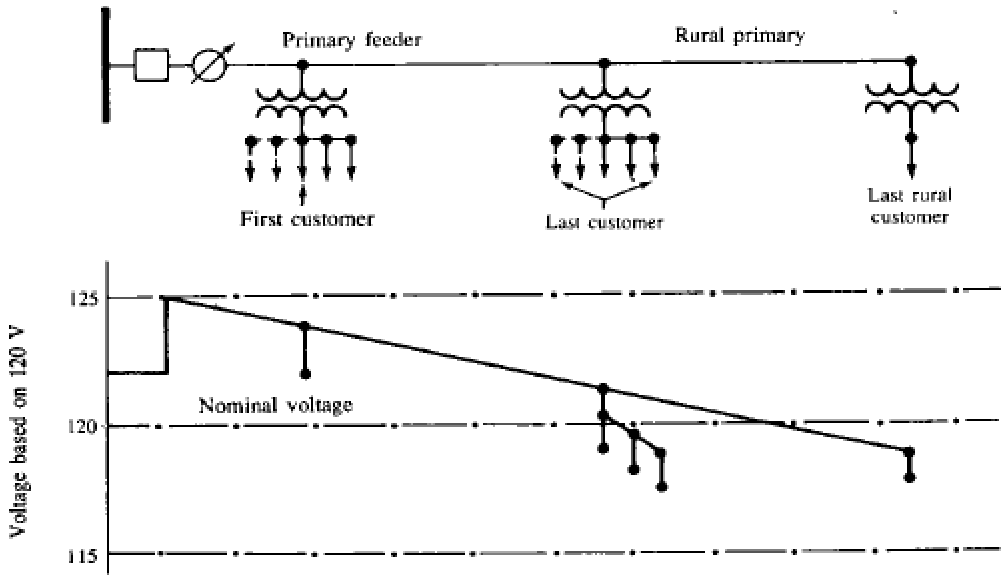

Figure 3-1 Voltage profile of a radial system (a) one-line diagram of the feeder, and (b) voltage profile

As one of the main criteria to justify system performance, voltages at the customer terminals in the system have to be within acceptable limits. As illustrated in Figure 2-20 and Table 2-3, the recommended service voltage range A by ANSI C84.1 [21] standard is +/-5% of the nominal value. Therefore, VVC will work on regulating system voltage within acceptable limits in normal daily operations. VVC is achieved by supplying or absorbing reactive power to keep voltage within normal range under different system operation conditions. The complete list of the means required to do voltage regulation is found in [14], [15]:

1) Use of generator VRs
2) Application of voltage-regulating equipment in the distribution substations
3) Application of capacitors in the distribution substation
4) Balancing the loads on the primary feeders

5) Increase of the feeder conductor size

6) Changing the feeder sections from single-phase to multiphase

7) Transferring loads to new feeders

8) Installing new substations and primary feeders

9) Increasing the primary voltage level

10) Application of VRs on the primary feeders

11) Application of shunt capacitors on the primary feeders

12) Application of series capacitors on the primary feeders

In short, the ways to regulate voltage can be classified in three categories:

1) Var compensation, such as reactive generators or shunt capacitors

2) Direct voltage regulation, such as VRs or LTCs

3) Modifying the feeder characteristics, such as series capacitors

In past decades, comprehensive investigations have been performed on the VVC topic, and a lot of conventional control methods have been proposed [24]-[29]. Typically, VVC is performed in an integrated manner in both flattening the voltage profile over the feeder and achieving system-wide optimization goals, such as minimizing the power loss/electrical demand/energy consumption of the system.

Nowadays, many power venders, such as COOPER and ABB [30], [31], provide conventional centralized VVC applications. Taking the COOPER Volt/Var management system as an example, the VVC application monitors real-time voltages, watts, and Vars from LTCs, regulators, capacitors, medium-voltage sensors, and additional monitoring points, such as customer meters, as shown in Figure 3-2. Using this real-time set of analog measurements, the VVC application, which sits at the control station, will trigger a control period during which the VR devices are assigned an operational cost.

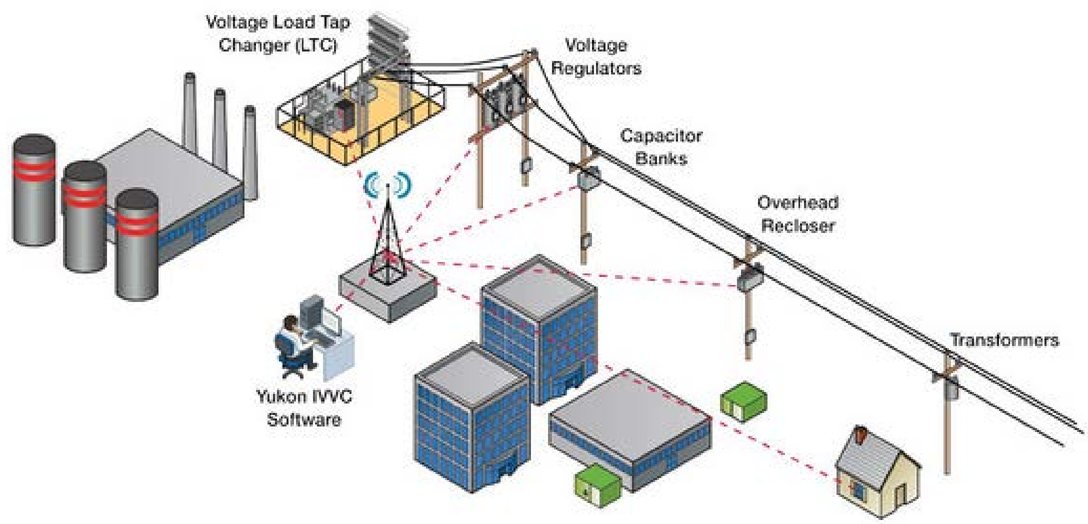

Figure 3-2 COOPER VVC application illustration [30]

It is mentioned in many articles that a VR periodically (every 15 min.) receives the state of the power system [29]. According to an ABB report [31], the operating frequency can be adjusted based on customer needs, and the VVC also retains 15-minute circuit-load history for all circuits and all switching activity. Loss-performance reporting analyzes circuit loss performance over extended periods of time (month, quarter, year), thus promoting effective tuning for optimum efficiency. The user-friendly interface and a sizable keypad enables easy operation at any time of day.

3.1.2 Volt/Var Control in the FREEDM System

With the integration of high-penetration DRERs and SSTs in the FREEDM system, the system's performance and voltage profile will differ from conventional distribution systems. In order to investigate the needs for doing VVC in the FREEDM system, an impact study of high-penetration residential PV on a smart distribution system was investigated in the previous chapter following the guidelines provided in IEEE 1547.7.

The test system that is going to be used in this centralized VVC proposal is the IEEE 34 node test feeder, which is characterized by its long line length and heavy peak load, as introduced in Chapter 2. The one-line diagram of the IEEE 34 system is shown in Figure 3-3. In order to convert the conventional IEEE 34 system into a FREEDM system, several changes have been made:

1) Instead of connecting directly to a primary feeder, all the loads are now connected via SSTs.
2) PVs with the same installation capacity as local peak loads are connected at the secondary side of the distribution transformer.
3) Conventional control devices (VRs and CAPs) are removed.

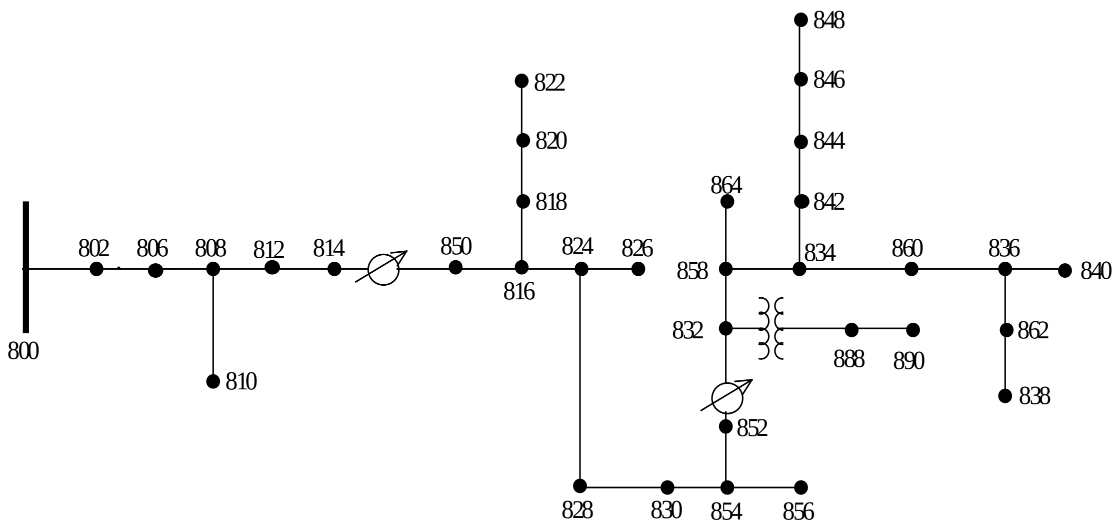

Figure 3-3 IEEE 34 node test feeder

In the study, various load and PV profiles are adopted in order to show the challenge in regulating voltages in a normal power system's daily operations. With the presence of over-voltage and under-voltage, VVC is necessary to keep the distribution feeder's voltage within acceptable limits and, at the same time, achieve some system-wide optimization goal.

3.2 A Centralized Volt/Var Control Scheme

In this section, the VVC problem will be formulated, and potential solution approaches will be presented. A two-phase centralized VVC based on gradient and linear programming methods is proposed. Then, the VVC application is tested using the FREEDM IEEE 34 system, and the control effect is analyzed based on the simulation result.

3.2.1 Volt/Var Control Problem

As the investigation above on the impact study of high-penetration PV on the smart distribution systems indicate, a VVC is necessary in order to adjust the system voltage profile, regardless of the conditions under which the system is operating, while at the same time achieving a system-wide optimization goal. In the following discussion, the objective of the VVC is selected as minimizing system-power loss while keeping the voltages within limits. In a smart distribution system, no conventional VR or Var compensation devices are involved; only SSTs are used as control devices. The VVC problem itself is basically an optimal power flow (OPF) problem in the following form:

$$minP_{loss} = \sum G_{ij} \left[V_i^2 + V_j^2 - 2V_i V_j \cos(\delta_i - \delta_j)\right] \quad (3.1)$$

subject to:

$$g(x,u) = 0 \quad (3.2)$$

$$V^{min} \leq V \leq V^{max} \quad (3.3)$$

$$Q_{SST}^{min} \leq Q_{SST} \leq Q_{SST}^{max} \quad (3.4)$$

The objective function (3.1) is the summation of the line loss of each line section in the system, where G_{ij} is the conductance of the line between bus i and bus j.

The equality constraint (3.2) is the power mismatch equation:

$$\begin{cases} \Delta P_i = P_i^{sp} - P_i(x) = 0 \\ \Delta Q_i = Q_i^{sp} - Q_i(x) = 0 \end{cases} \quad (3.5)$$

where x is the state variable and u is the control variable.

$$\begin{cases} P_i^{sp} = P_{gi} - P_{li} \\ Q_i^{sp} = Q_{gi} - Q_{li} \end{cases} \tag{3.6}$$

and

$$\begin{cases} P_i(x) = V_i \sum V_j (G_{ij} cos\theta_{ij} + B_{ij} sin\theta_{ij}) \\ Q_i(x) = V_i \sum V_j (G_{ij} sin\theta_{ij} - B_{ij} cos\theta_{ij}) \end{cases} \tag{3.7}$$

where P_{gi} and P_{li} are the real power generation and real load, respectively, at bus i, Q_{gi} and Q_{li} are the real power generation and real load, respectively, at bus i.

The inequality constraint (3.3) on the state variable enforces the system voltage limitations on all nodes throughout the system. The inequality constraint on the control variable indicates that the actual reactive power injection by each SST should be within its capacity limitation.

In the FREEDM system, SSTs are connected with every load and are capable of regulating the secondary side voltage. Therefore, the voltage doesn't need to be as tight as indicated in [21] on the primary side of the SST. The VVC problem formulation in this work not only aims to regulate the voltage, but also to minimize the system power loss.

In addition, with the presence of a great number of unbalanced loads in the distribution feeders, load balance becomes important for reducing power loss and mitigating power flow overloading. Therefore, in the future, phase balancing also needs to be considered as a factor in reducing the distribution system's power loss. In one of the early works, Dr. Baran proposed a network reconfiguration scheme to keep the phase balanced [32]. The problem is formulated in the form of a minimal spanning tree. Both of the objectives, loss reduction and load balancing, will be satisfied by changing the status of the sectionalizing switches. Following a similar problem formulation, Dr. Nicolae introduced a neural network in conjunction with a heuristic method, which enables different reconfiguration switches to be turned on or off and connected consumers to be switched between phases to keep the phases balanced for the combined problem [33]. As more renewable resources are integrated into the distribution network, it becomes very difficult to achieve load-balancing with conventional network reconfiguration methods by changing the status of line switches, because of the intermittency of renewables. In order to resolve the problem, Dr. Lin proposed a loop power controller to be applied, instead of the open-tie switch, for the control of real power and reactive power flows by adjusting the voltage ratio and phase-shift, according to branch impedance and load imbalance so that the load balance of the distribution feeders could be obtained [34]. It claims that the distribution feeder pair with LPC can improve controllability and operational flexibility of the distribution system, mitigate voltage fluctuation with fast reactive power compensation, control the real and reactive power flow, reduce power system loss with improved load-balancing of the distribution system, and enhance system robustness for integration with more renewable energy.

Nowadays, the problem of phase-unbalancing is solved using two methods: the reconfiguration method and the rephasing strategy. In the reconfiguration technique, the unbalancing problem can be solved by the switches present in the network. To improve the efficiency of the network in the rephrasing technique, the loads of all three phases of the network should be appropriately distributed among the phases. Methods of creating a balance in the phases of the distribution feeders are resolved using the trial-and-error method, the mixed integer programming technique, and intelligent methods. Recently, Dr. Hooshmand proposed a new method based on bacterial-foraging oriented by the particle swarm optimization algorithm (BF-PSO) [35]. The objective function includes the neutral voltage of the sup-supporting feeder, the rephasing cost, the voltage drop, and the line losses. The four objectives are made fuzzy and then integrated as the fuzzy multi-objective function. The effectiveness of BF-PSO in finding the optimal rephasing strategy in the radial and meshed networks is demonstrated by comparing the control results with other intelligent methods.

3.2.2 A New Two-Stage Centralized Volt/Var Control Scheme

3.2.2.1 Candidate Approaches

In order to solve the VVC problem, intensive literature research has been done. The VVC problem is a type of OPF problem, which has a long history of development. The goal of OPF is usually to find the optimal settings for a given power system such that a certain objective function can be achieved while system limitations are satisfied. Many articles and textbooks have an in-depth discussion of the OPF problem [36]-[40]. The formation of OPF is usually:

$$\min_{x \in R^n} f(x) \tag{3.8}$$

subject to:

$$g(x) = 0 \tag{3.9}$$

$$\underline{x} \leq x \leq \overline{x} \tag{3.10}$$

$$\underline{h} \leq h(x) \leq \overline{h} \tag{3.11}$$

The objective function of OPF would be:

1) Minimize generation cost
2) Minimize total power generation
3) Minimize electrical losses
4) Minimize shift of generation
5) Minimize bus voltage derivation
6) Minimize generation emission
7) Minimize number of control actions

The non-linear equality constraint of OPF is usually a power-balance function:

$$\begin{cases} v_i \sum v_j \, [G_{ij} \cos(\theta_i - \theta_j) + B_{ij} \sin(\theta_i - \theta_j) - P_i = 0 \\ v_i \sum v_j \, [G_{ij} \sin(\theta_i - \theta_j) + B_{ij} \cos(\theta_i - \theta_j) - Q_i = 0 \end{cases} \tag{3.12}$$

The inequality constraints of OPF would be:

1) Generation limits: $\underline{P} \leq P \leq \overline{P}$, $\underline{Q} \leq Q \leq \overline{Q}$
2) Voltage limits: $\underline{V} \leq V \leq \overline{V}$
3) Angle difference constraint: $-\frac{\pi}{4} \leq \theta_{ij} \leq \frac{\pi}{4}$, θ_{ij} is the angle difference between bus *i* and bus *j*
4) Transmission line limits: $\underline{S_{ij}} \leq S_{ij} \leq \overline{S_{ij}}$ from bus *i* to bus *j*
5) Security constraints: such as $\underline{V_k} \leq V_k$ (with line nm out) $\leq \overline{V_k}$, $\underline{S_{ij}} \leq S_{ij}$ (with line nm out) $\leq \overline{S_{ij}}$, which means OPF would prevent the post-contingency voltage on bus *k* or the post-contingency flow on line *ij* from exceeding

their limits for an outage of line *nm*. A system that is operated so that it can withstand any single failure is called secure, and the additional constraints to ensure that any single failure does not result in overloads are called security constraints [36].

The control variables of OPF would be:

1) Real/ reactive power generation
2) Generator voltage
3) LTC transformer tap position
4) Phase shifter
5) Switchable capacitors and reactors
6) Reactive power injection for a static Var compensator

According to different selected objective functions and constraints, the optimization problem can be classified generally into the following categories [37]:

1) A linear problem where both objectives and constraints are in linear form with continuous control variables
2) A non-linear problem where either objectives or constraints or both are non-linear with continuous control variables
3) A mixed-integer linear problem where control variables are both discrete and continuous

Due to the complexity of the OPF problem, various solution approaches have been proposed to solve the problem more reliably. Dr. Allen Wood [40] indicates that almost every mathematical programming method can be applied to this problem. It takes researcher and developer decades to test and justify each solution approach. The most promising schemes are:

1) Gradient method
2) Newton method
3) Linear programming method
4) Quadratic programming method
5) Interior point method
6) Intelligent methods, such as genetic algorithms and particle swarm optimization

The gradient method will find the direction of maximum increase in the objective function, and the negative of the gradient will serve as the update direction while additional step-size search steps are also necessary to determine the best update length. However, the functional inequality constraints, such as the bus voltage on the PQ bus (i.e., load bus), are difficult to handle; the method can become very time-consuming or practically impossible at some point [37], [38], and [40]. Although a penalty method can be used to consider the inequality constraints in the objective function, it has very little effect on the algorithm [39].

Since the Newton method has the second derivative information built into it, it does not have difficulty converging and can handle the inequality constraints, as well. The difficulty with the Newton method arises because near the limit the penalty is small. So the optimal solution tends to allow the variable to float over its limit. Besides, handling inequality constraints is very difficult in either the gradient or Newton approach [38].

The LP method is one of the fully developed methods now in common use. It can easily handle inequality constraints as long as the problem to be solved can be made linear without suffering a loss of accuracy. Non-linear objective functions and constraints can also be handled in a linearized fashion. The main advantages of a linear programming optimal power flow (LPOPF) solution are the reliability of the optimization, the ability to quickly recognize problem infeasibility, the capability to easily accommodate operating limits, and the tendency to converge rapidly. However, the number of segments resulting from LP affects the solution's speed and precision. If the segment sizes are large, some issues may arise [36] and [37].

Quadratic programming can also be applied to solve the OPF problem with proper improvements. Because of the non-convexity of the OPF problem, Dr. Lavaei proposed a convex relation for the classical OPF problem and pointed out that under a sufficient condition, the OPF problem is equivalent to a convex problem. The dual of OPF is a semi-definite program, and a sufficient condition guarantees that the duality gap is zero. A globally optimal solution of the OPF problem is recoverable from a dual optimal solution [41] and [42].

The interior-point method is essentially an LP method. Compared to other well-known LP methods, the interior-point method maintains their accuracy while converging more quickly. However, the interior point method in general suffers from poor initial, termination, and optimality criteria and, in most case, is unable to solve nonlinear and quadratic objective functions [37].

Obviously, in the VVC problem formulation, both the objective function and the equality constraints are non-linear. In the following, a two-phase optimization scheme is proposed using both the gradient method and the LP method to better achieve the goal. As presented previously, the gradient method has difficulty in handling inequality constraints, and there is a good chance that the LPOPF cannot return feasible solutions if the starting point is out of the feasible region. Therefore, the gradient method is used to find the feasible operating point before minimizing the power loss. After the feasibility search, an LP-based OPF is applied to minimize the power loss within the feasible region.

3.2.2.2 Proposed Scheme

With all the potential mathematical approaches introduced earlier, Dr. Potkonjak proposed an algorithm-selection method in [43]. The VVC problem can then be classified in two parts: the first is to regulate the voltage within acceptable limitation, and the second is to find the minimum power loss within the feasible region. As discussed above, the gradient method performs well when dealing with non-linear optimization with only equality constraints. It can be utilized to force the voltage back into the feasible region when the initial system's operating condition is not feasible. After the feasibility search, the original VVC problem can be linearized into the standard formation of LP. Thus, both equality and inequality constraints can be handled. Therefore, in the following two-phase problem, a centralized VVC scheme will be proposed:

1) Phase I: Gradient-based feasibility search
2) Phase II: LP-based power-loss minimization

3.2.2.2.1 Phase I: Gradient-based feasibility search

In the smart distribution system, the only control variable is reactive power injection at each node to which SSTs are connected. Therefore, if the original system's operating condition is not within the feasible region, typically voltage violation, the reactive power injection should be adjusted so that voltages can be forced back into the required operating range. Then, the objective of the feasibility search is:

$$\min f(x) = \sum w_i (V_i - V_{lb})^2 \tag{3.13}$$

subject to:

$$g(x) = 0 \tag{3.14}$$

where w_i is the weight factor. When a voltage violation happens at node i, $w_i = 1$. Otherwise, set $w_i = 0$.

Now, apply the Lagrangian function and the gradient method. Then, the minimum of the Lagrangian function

$$\mathcal{L} = f + \lambda g \tag{3.15}$$

can be found when the following criteria set is satisfied:

$$\left[\frac{\partial \mathcal{L}}{\partial x}\right] = \left[\frac{\partial f}{\partial x}\right] + [\frac{\partial g}{\partial x}]^T \lambda = 0 \tag{3.16}$$

$$\left[\frac{\partial \mathcal{L}}{\partial u}\right] = \left[\frac{\partial f}{\partial u}\right] + [\frac{\partial g}{\partial u}]^T \lambda = 0 \tag{3.17}$$

$$[\frac{\partial \mathcal{L}}{\partial \lambda}] = g = 0 \tag{3.18}$$

where x is the vector of the state variables and u is the vector of the control variables.

Then, from the first equation of a necessary condition (3.16), we can find λ

$$\lambda = -([\frac{\partial g}{\partial x}]^T)^{-1} \frac{\partial f}{\partial x} \tag{3.19}$$

By substituting λ back into the second necessary condition (3.17), the gradient can be obtained:

$$\nabla f = \frac{\partial f}{\partial u} = -[\frac{\partial g}{\partial u}]^T \lambda \tag{3.20}$$

Since reactive power change is more sensitive to voltage change than to angle, the coupling can be neglected. Therefore, the equality constraint only considers the reactive power mismatch:

$$g(x) = Q_i^{sp} - Q_i(x) = 0 \tag{3.21}$$

And the state variables consist of only voltages $x = [V]$.

Then,

$$\frac{\partial f}{\partial x} = [\frac{\partial f}{\partial V}] = \begin{bmatrix} 2w_2(V_2 - V_{lb}) \\ \vdots \\ 2w_n(V_n - V_{lb}) \end{bmatrix} \tag{3.22}$$

where

$$w_i = \begin{cases} 0, \text{if no voltage violation exists at node } i \\ 1, \text{if the voltage is out of limits} \end{cases}$$

And $\frac{\partial g}{\partial x}$ considers only the right lower part of a full Jacobian matrix, which is the sensitivity of voltage with respect to reactive power variations:

$$\frac{\partial g}{\partial x} = [\frac{\partial \Delta Q}{\partial V}] \tag{3.23}$$

and

$$\frac{\partial g}{\partial u} = [\frac{\partial \Delta Q}{\partial Q_{SST}}] \tag{3.24}$$

where $\frac{\partial Q}{\partial Q_{SST}}$ is an identity matrix.

Then after we obtain the gradient, Q_{new}^{sp} can be updated using

$$Q_{new}^{sp} = Q_{old}^{sp} - \gamma \nabla f \tag{3.25}$$

where γ is the update step size of the steepest gradient.

Then, the feasible operating-point search step is as follows:

1) Run the distribution power flow (DPF) to get the initial system operating condition.
2) Check convergences to see if all voltages are within the limitations. If yes, there is no need to do a feasible operating-point search; just exit the loop. Otherwise, process the next step.
3) Solve for the gradient $\frac{\partial g}{\partial u}$ using the method proposed.
4) Update the control variables.
5) Go back to step 2 to update the state variable by the rerun DPF.

Then, the flowchart of the feasibility search iteration is:

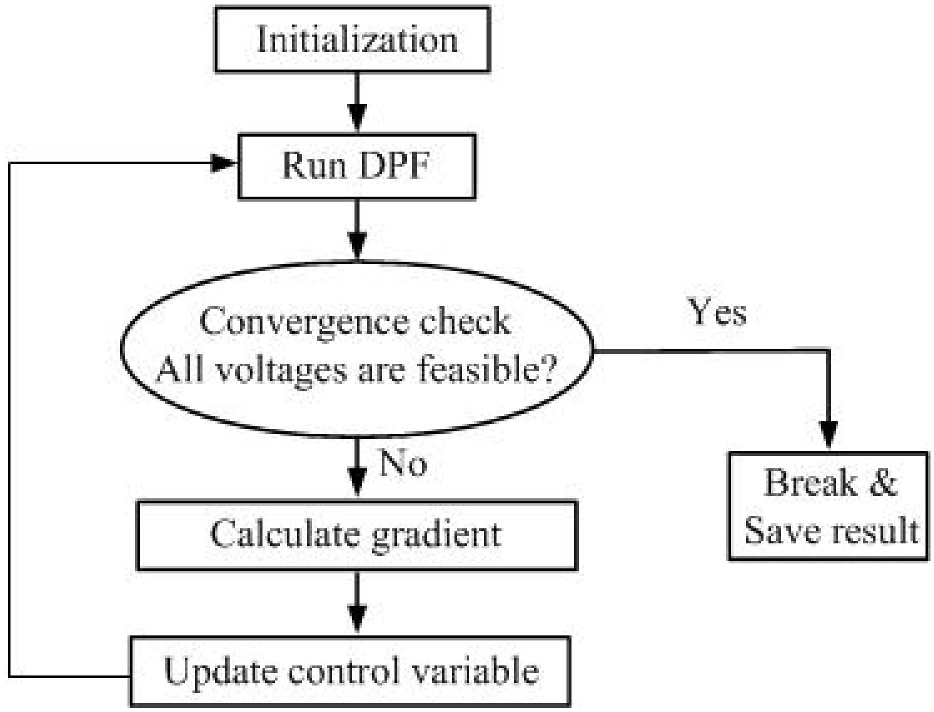

Figure 3-4 Flowchart of feasibility search

Since the feasibility search will end when the voltages are feasible, the final operating condition might be very close to the boundary of the feasible region. Therefore, in order to check for optimality, we can increase the reactive power injection of each SST by a ratio, say 25% more of the result recommended by the feasibility search. If the initial start point of the power-loss minimization is more inside the feasible region, there is a chance that the optimal point may end up better.

3.2.2.2.2 Phase II: LP-based power-loss minimization

After the feasibility search, an LP-based OPF is used to minimize system power loss within the feasible region.

$$\min P_{loss} = \sum G_{ij}\left[V_i^2 + V_j^2 - 2V_iV_j\cos(\delta_i - \delta_j)\right] \tag{3.26}$$

subject to:

$$g(x,u) = 0 \tag{3.27}$$

$$V^{min} \leq V \leq V^{max} \tag{3.28}$$

$$Q_{SST}^{min} \leq Q_{SST} \leq Q_{SST}^{max} \tag{3.29}$$

where $x = \begin{bmatrix}\theta \\ V\end{bmatrix}$ are the state variables of the system, and $u = [Q_{SST}]$ are the control variables. The equality constraint is a power mismatch equation (3.5). Obviously, both the objective function and the equality constraints are non-linear. In order to use LP to solve the problem, first we need to make the problem formulation linear with respect to both the state and control variables.

The linearized objective function is shown as follows:

$$\Delta P_{loss} = \begin{bmatrix}\frac{\partial P_{loss}}{\partial \theta} & \frac{\partial P_{loss}}{\partial V} & \frac{\partial P_{loss}}{\partial Q_{SST}}\end{bmatrix}\begin{bmatrix}\Delta\theta \\ \Delta V \\ \Delta Q_{SST}\end{bmatrix} = c\begin{bmatrix}\Delta x \\ \Delta u\end{bmatrix} \tag{3.30}$$

where $\frac{\partial P_{loss}}{\partial Q_{SST}}$ is a zero vector. The elements in the linearized vector can be calculated using power-flow equations.

The linearized equality constraint is shown as follows:

$$\Delta g = \begin{bmatrix}\frac{\partial \Delta P_i}{\partial \theta} & \frac{\partial \Delta P_i}{\partial V} & \frac{\partial \Delta P_i}{\partial Q_{SST}} \\ \frac{\partial \Delta Q_i}{\partial \theta} & \frac{\partial \Delta Q_i}{\partial V} & \frac{\partial \Delta Q_i}{\partial Q_{SST}}\end{bmatrix}\begin{bmatrix}\Delta\theta \\ \Delta V \\ \Delta Q_{SST}\end{bmatrix} = [J|H]\begin{bmatrix}\Delta x \\ \Delta u\end{bmatrix} \tag{3.31}$$

where $\begin{bmatrix} \frac{\partial P_i}{\partial \theta} & \frac{\partial P_i}{\partial V} \\ \frac{\partial Q_i}{\partial \theta} & \frac{\partial Q_i}{\partial V} \end{bmatrix}$ is the Jacobian matrix that can be calculated directly by taking partial derivatives.

After linearization, the original VVC problem is now in the following form:

$$\min \Delta P_{loss} = c \begin{bmatrix} \Delta x \\ \Delta u \end{bmatrix} \tag{3.32}$$

subject to:

$$[J|H] \begin{bmatrix} \Delta x \\ \Delta u \end{bmatrix} = 0 \tag{3.33}$$

$$V^{min} \leq V \leq V^{max} \tag{3.34}$$

$$Q_{SST}^{min} \leq Q_{SST} \leq Q_{SST}^{max} \tag{3.35}$$

where $c = [\frac{\partial P_{loss}}{\partial \theta} \quad \frac{\partial P_{loss}}{\partial V} \quad \frac{\partial P_{loss}}{\partial Q_{SST}}]$, J is the Jacobian matrix, and $H = \begin{bmatrix} \frac{\partial \Delta P_i}{\partial Q_{SST}} \\ \frac{\partial \Delta Q_i}{\partial Q_{SST}} \end{bmatrix}$.

Clearly, the new problem formulation is an LP problem, which can be solved using an LP solver. By substituting the linearize problem into an LP solver, an update of control variables ΔQ_{SST} will be obtained to lower the power losses. The new control variables Q_{SST}^{new} can be updated using:

$$Q_{SST}^{new} = Q_{SST}^{old} + \Delta Q_{SST} \tag{3.36}$$

Then, update the state variable by rerunning DPF, and try to determine whether the following criteria are satisfied:

$$\Delta Q_{SST} < \varepsilon \tag{3.37}$$

or

$$V \leq V^{min} \text{ or } V^{max} \leq V \tag{3.38}$$

or

$$\Delta P_{loss} > 0 \tag{3.39}$$

The first criterion indicates that the iteration can be terminated when the update of the control variable is small enough. The second criterion enforces the voltage limitation. The third criterion means that when the change of power loss is positive, the objective starts to increase and the iteration should be ended. No matter which one is satisfied first, the optimal point is said to be achieved. Otherwise, continue to update the control variables and form LP using the new state variables.

However, as indicated above, the LP method can only be used when the original problem to be solved can be linearized without a loss of accuracy. Since the problem is highly non-linear, the linearization may lose accuracy and drift away from the actual DPF result when the update of the control variable is too large for each step. In order to deal with different system topologies and various operating conditions, improvements of the LPOPF are required.

Applying LP to a non-linear problem is an approximate approach, and there is a mismatch between the actual DPF result and the LP-approximated result. As shown in Figure 3-5, with a certain update of the control variables, the LP solver will return an approximate solution y_{app}. On the other hand, after updating the reactive power information at each node and running DPF, we can get an exact solution y^*. It is clear that, if the update of control variables is too large, the linearization may lose accuracy and drift away from the actual DPF result. In addition, if the current operating point is close to the limitation boundary, there is a good chance that y_{app} will go out of the boundary when the update step is too large.

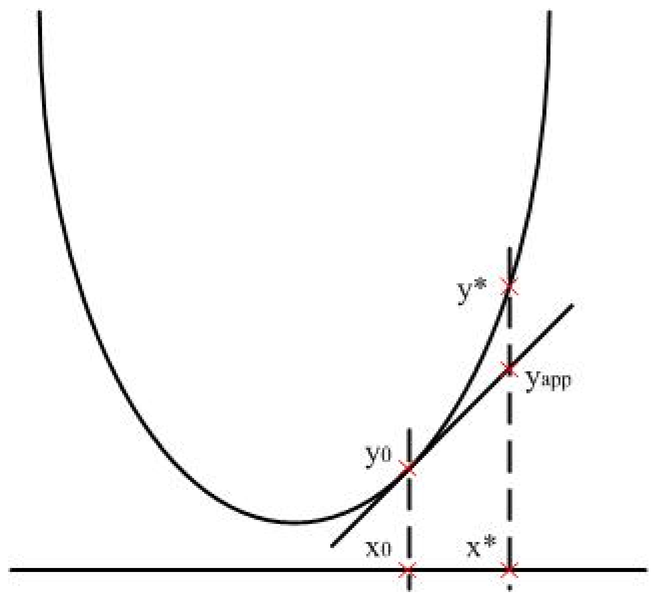

Figure 3-5 Demonstration of the difference between the actual problem and a linearized approximate problem

Thus, it is necessary to determine the proper maximum update of control variables for each step, so that the LP returned result is reliable and trustworthy and still feasible. Therefore, the criteria used here to determine whether the LP solution is good enough are:

$$\% \frac{P_{mis}}{\Delta P_{loss}} = \frac{|\Delta P_{loss} - fval|}{\Delta P_{loss}} < \varepsilon\% \quad (3.40)$$

and

$$V^{min} \leq V \leq V^{max} \quad (3.41)$$

where ΔP_{loss} is the actual power-loss reduction that resulted from DPF, and $fval$ is the LP-returned power-loss reduction.

If the criteria is not satisfied, then update the ΔQ_{limit} for each iteration using

$$\Delta Q_{limit} = \Delta Q_{limit} * Q_{ratio} \tag{3.42}$$

where Q_{ratio} is the decrease ratio and satisfies $0 < Q_{ratio} < 1$.

Until both criteria are satisfied, the ΔQ_{limit} can be used as a limitation for the maximum update step for each LP iteration.

There are two approaches that involve a ΔQ_{limit} search in the LPOPF: One is to determine the ΔQ_{limit} first before performing the power-loss minimization; the other is to include ΔQ_{limit} in the inner loop of the LPOPF.

Then, the approach of LPOPF with ΔQ_{limit} determined first is:

1) Start with an initial feasible point y^o given by the gradient base feasibility search and an initial ΔQ_{limit} .
2) Run the DPF to get the state variables.
3) Form the linearized objective function by calculating the c matrix.
4) Form the linearized equality constraint by calculating $[J|H]$.
5) Set up the inequality constraints.
6) Solve the LP problem using the MATLAB solver "linprog."
7) Perform the convergence check for the ΔQ_{limit} search. If the criteria are satisfied, process the next step. Otherwise, update the ΔQ_{limit} settings and reset all. Go back to the same initial feasibility point in step 1 again.
8) Run the DPF to get the state variables.

9) Form the linearized objective function by calculating the c matrix.

10) Form the linearized equality constraint by calculating $[J|H]$.

11) Set up the inequality constraints with the ΔQ_{limit} that guarantees the accuracy of a linear approximation.

12) Solve the LP problem using the MATLAB solver "linprog."

13) Perform a convergence check for power-loss minimization. If the criteria are satisfied, save the current settings as the optimal point. Otherwise, update the control variables and rerun DPF in step 8 until the criteria are satisfied.

Then, the flowchart of LPOPF with the ΔQ_{limit} search is:

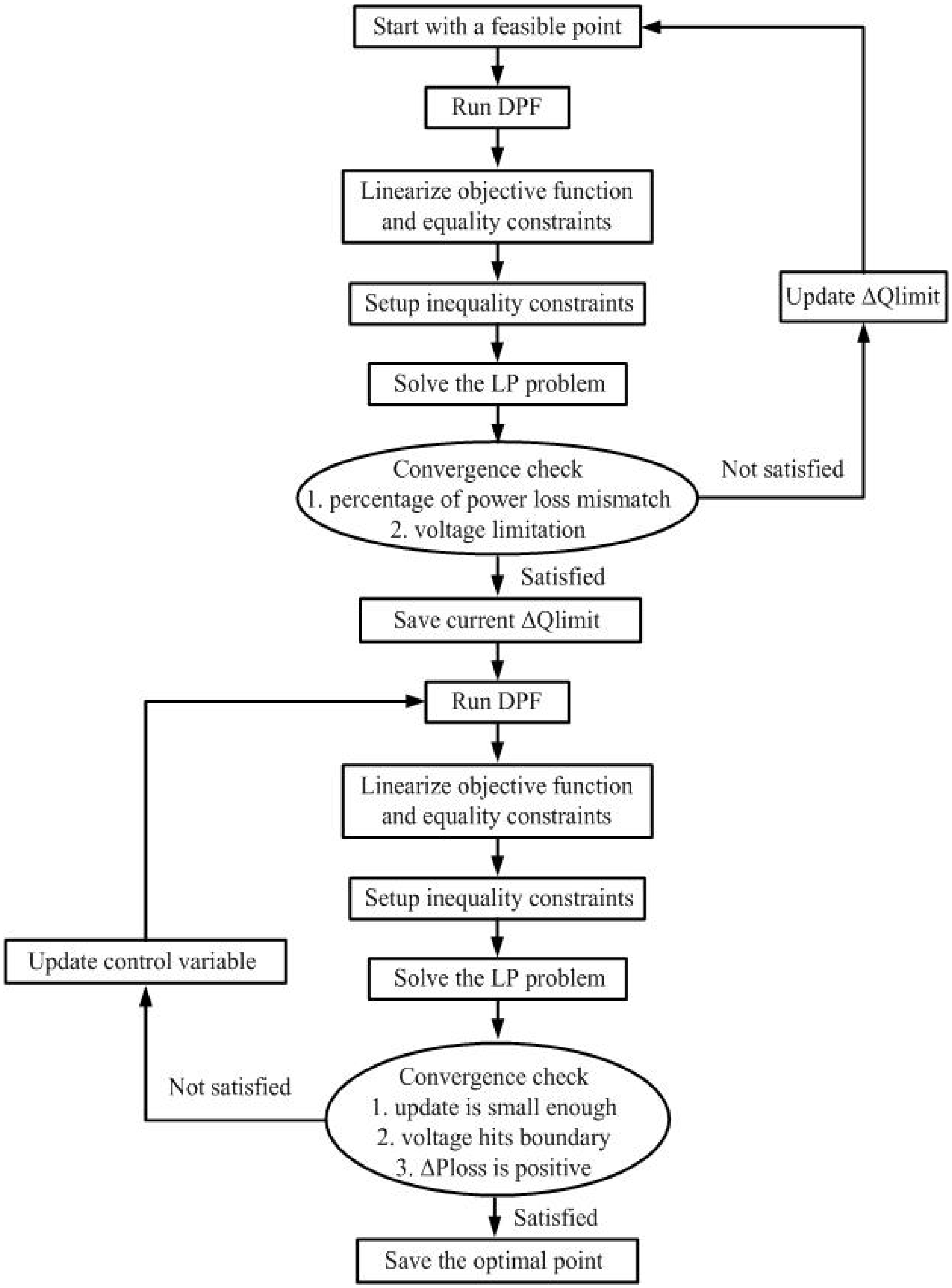

Figure 3-6 Flowchart of LPOPF

The full version of the gradient and the LP-based VVC is demonstrated in Figure 3-7.

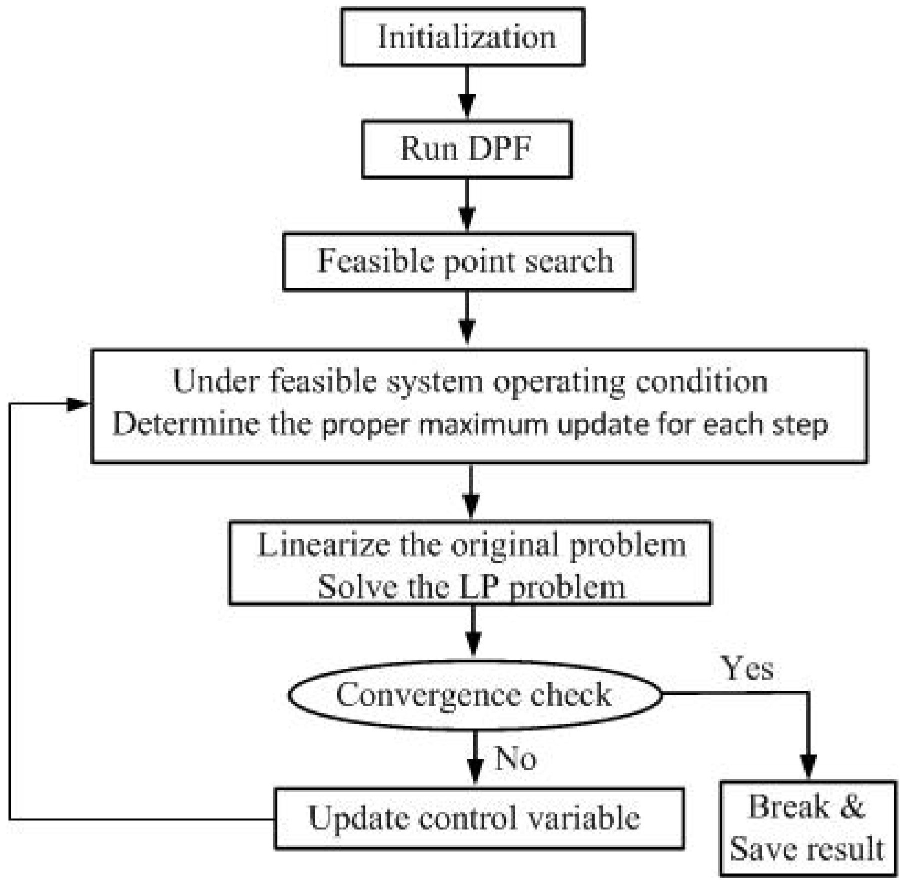

Figure 3-7 Flowchart of the two-phase VVC

The second optimization approach that combines the ΔQ_{limit} search and power-loss minimization is also proposed here; it is going to be called back and forth LPOPF (BF LPOPF).

The basic idea of BF LPOPF is:

1) Start with an initial feasible point y^o, given by the gradient-based feasibility search, and an initial ΔQ^0_{limit}.

2) Run the DPF to get the state variables.

3) Form the linearized objective function by calculating the *c* matrix.

4) Form the linearized equality constraint by calculating $[J|H]$.

5) Set up the inequality constraints.

6) Solve the LP problem using the MATLAB solver “linprog.”

7) Update the control variables. Run the DPF to get the new state variables y^i.

8) Check to see whether y^i is feasible or not. If yes, check to see if current ΔQ_{limit} is small enough. The optimal is said to be achieved if ΔQ_{limit} is small enough. Otherwise, save y^i as the new initial feasible point y^o_{new} , save ΔQ^i_{limit} and the new Q limitation, $\Delta Q^0_{limit\_new}$, then go back to step 2. If the optimal is not reached, update ΔQ^i_{limit} , and go back to step 1.

The process can be illustrated better by Figure 3-8.

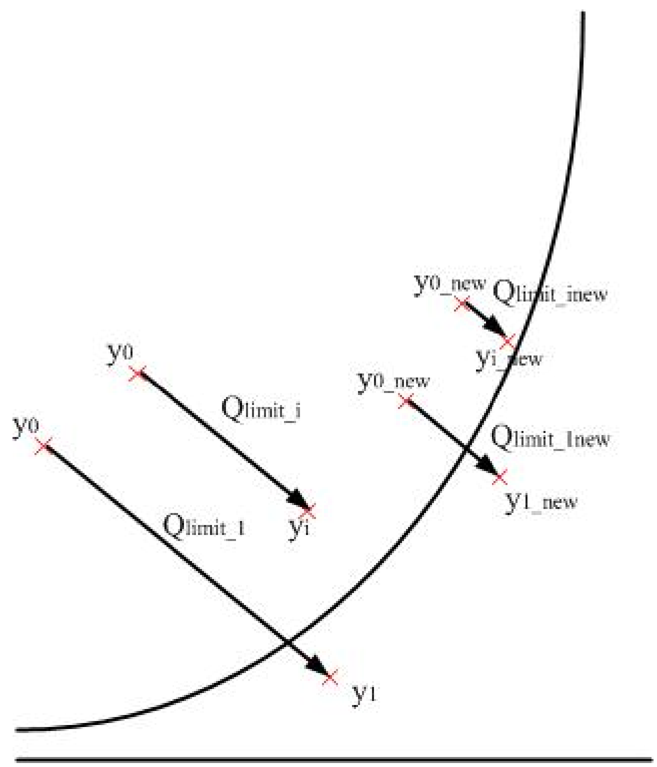

Figure 3-8 Procedure demonstration of BF LPOPF

Then the flowchart of BF LPOPF is:

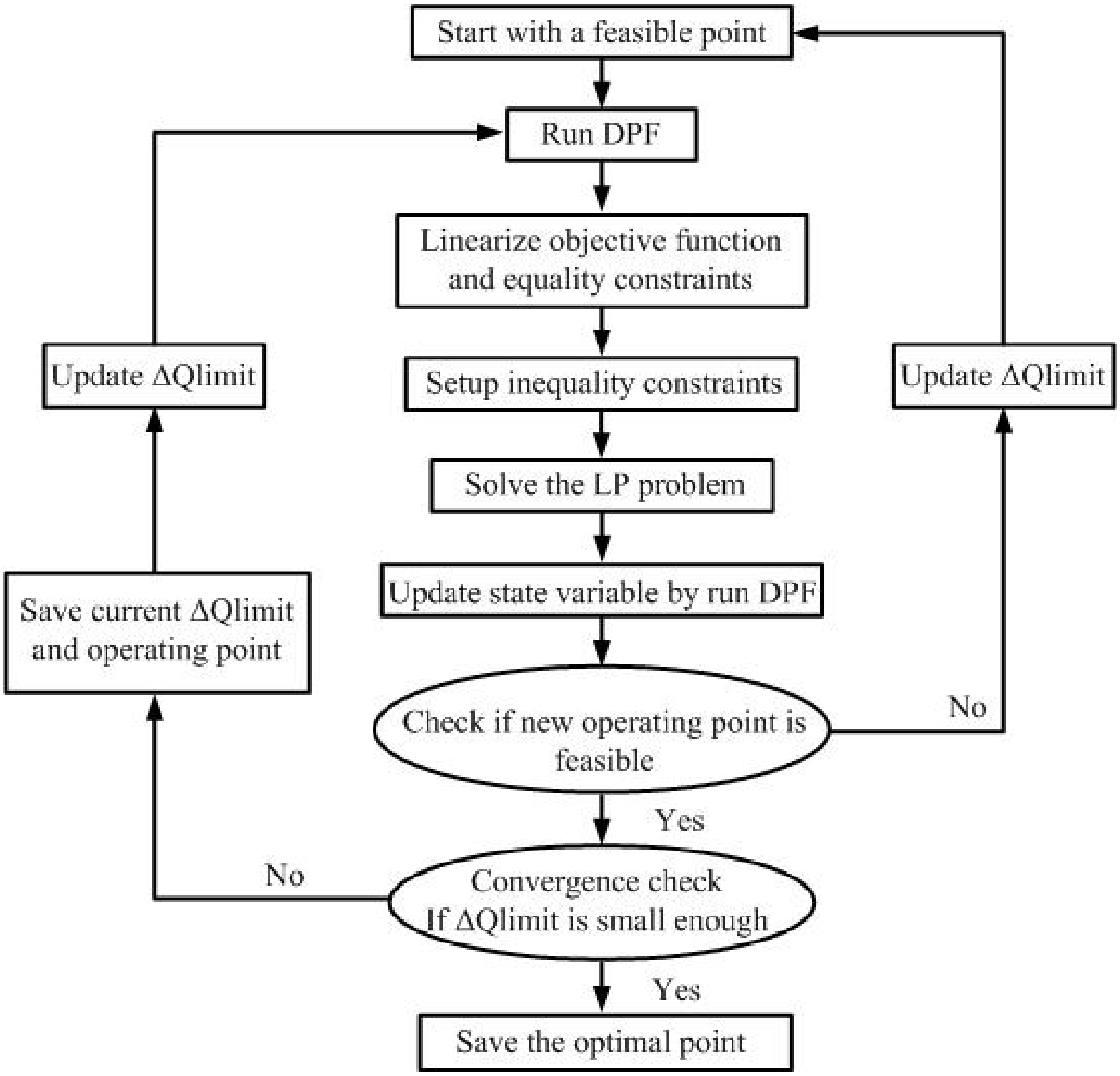

Figure 3-9 Flowchart of BF LPOPF

According to Dr. Stott [44], since power-loss minimization is strongly non-separable, it is quite unlikely that those mathematical approaches proposed above will have good convergence to accurate minimum-loss solutions. Therefore, although the method proposed in this article aims at minimizing power loss, there is no guarantee that the optimal point found is the global minimum.

3.3 The FREEDM IEEE 34 Test System and Result Analysis

As introduced above, several changes have been made in the IEEE 34 system to make it a FREEDM system that accommodates DRERs and SSTs. One of the main features of an SST is that it can automatically work under a per-unit power factor without receiving any control commands. Therefore, all the reactive load inquiries on the secondary side will be provided by the corresponding SSTs. When the VVC application starts to minimize power loss and maintain voltages within limitations, the SSTs are going to receive the command to inject reactive power into the system or draw reactive power from the system. Under different system operating conditions, the VVC will return different reactive power commands.

3.3.1 System Operating Conditions Without VVC

For the FREEDM IEEE 34 system without a VVC, an SST provides the reactive power demanded by the loads; therefore, the initial system condition is with a real load only. Use phase A as an example to show the voltage profile at the original system operating condition. Note that although the IEEE 34 system has 34 nodes, some of the feeders are only single-phase; therefore, the total number of nodes for phase A is only 30.

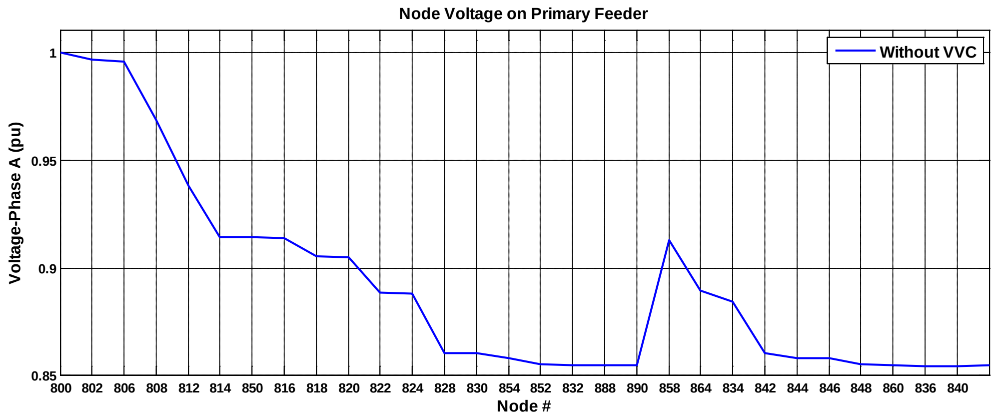

Figure 3-10 The voltage profile of phase A without VVC

Clearly, the lowest voltage in the system is only 0.8518 p.u., which is far below the lower voltage limitation. Also, the real power flowing through the substation is also measured, and the power loss for each phase can be calculated using the following equation:

$$P_{loss} = P_{sub} - \sum P_{load} \tag{3.43}$$

Then, the power loss in the system without VVC is documented in Table 3-1.

Table 3-1 Power loss without VVC

	Pa(kW)	*Pb*(kW)	*Pc*(kW)
Power flow through the substation	698.0123	658.2004	669.2435
Total load	606.0002	584.0000	578.9995
Original power loss	92.0122	74.2004	90.2440

3.3.2 The Simulation Results of a Feasibility Search

Since the voltages are not feasible, the gradient-based feasibility search starts take action. The goal of the feasibility search is to force the voltage back into its limitations. Therefore, the minimum voltage along the feeder is the main concern. In Figure 3-11, the iteration time with its corresponding minimum voltage is documented to show the performance of the feasibility search.

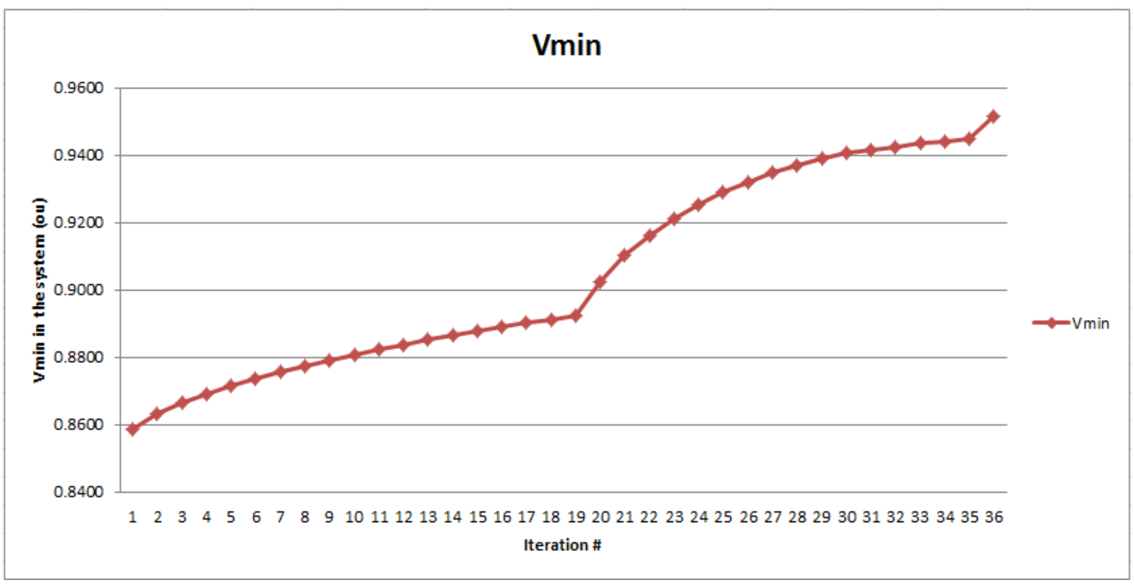

Figure 3-11 The iteration of the feasibility search

Clearly shown in Figure 3-11, V_{min} increases as the iteration proceeds and finally reaches the acceptable value after 36 iterations. The new power-flow information measured at the primary side of each SST with a feasible operating condition is shown in the following table. As shown in Figure 3-12, the SSTs are required to provide a huge amount of reactive power to boost the voltage. Note that there are only 12 loads connected to phase A, which means that there are only 12 SSTs. That is why only 12 injections are required.

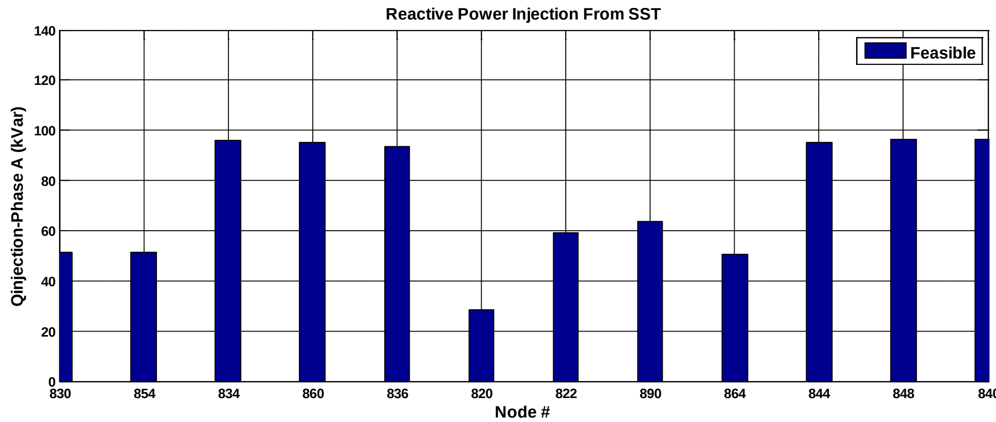

Figure 3-12 The reactive power injection after the feasibility search

The new voltage profile of phase A in p.u. along the feeders after the feasibility search is shown in Figure 3-13.

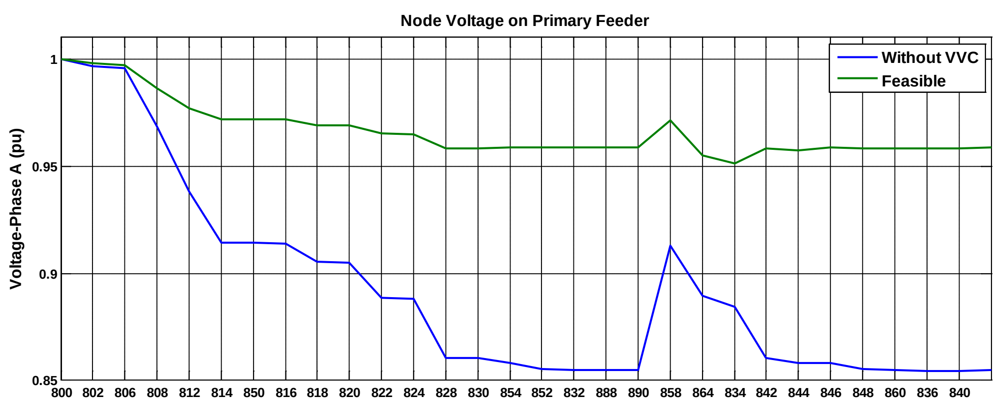

Figure 3-13 The voltage profile of phase A after the feasibility search

Now, the minimum voltage in the system is 0.9514 p.u. All of the voltages are within the feasible region, which demonstrates that the gradient-based feasibility search works properly.

Similar to the original operating condition, the power flowing through the substation is documented to calculate the power loss in Table 3-3. As expected, the power loss is much higher than the original case because of the huge reactive injection from the SSTs to boost the voltage. The total amount of required reactive power from the SSTs is also documented.

Table 3-2 Power loss after feasibility search

	Pa(kW)	*Pb*(kW)	*Pc*(kW)
Power flow through the substation	855.3208	775.8523	815.8465
Total load	606.0012	584.0033	578.9917
Power loss	249.3196	191.8490	236.8548
	Qa(kVar)	*Qb*(kVar)	*Qc*(kVar)
Total reactive power injection	877.4249	787.4649	847.439

3.3.3 The Simulation Result of Power-Loss Minimization

There are two approaches to involve the ΔQ_{limit} search in the LPOPF. One is to determine the ΔQ_{limit} first before processing the power-loss minimization. The other is to include the ΔQ_{limit} in the inner loop of LPOPF.

3.3.3.1 LPOPF Simulation Result

After the feasible operating point is determined, it's time to run the LP-based OPF to minimize the power loss within the feasible region. The first step is to determine the ΔQ_{limit} so that the new update operating points resulting from LP and DPF will be close enough and the voltage violation is avoided.

With an initial $\Delta Q_{limit} = 5$kVar, and an update ratio of $Q_{ratio} = 0.6$, the percentage of power-loss mismatch is calculated using:

$$\% \frac{P_{mis}}{\Delta P_{loss}} = \frac{|\Delta P_{loss} - fval|}{\Delta P_{loss}} < \varepsilon\% \tag{3.44}$$

Another main criterion of the ΔQ_{limit} search iteration is to guarantee that with a certain update of the reactive power injection, the voltage is still feasible.

The ΔQ_{limit} search iteration result is documented in Figure 3-14. The left-hand axis shows V_{min} in the system, and the right-hand axis is the value of $\frac{P_{mis}}{\Delta P_{loss}}$. As expected, a larger ΔQ_{limit} has a better chance of resulting in a voltage violation. As ΔQ_{limit} decreases from the initial setting of 5kVar in the first iteration to 1.08kVar in the 4th iteration, the V_{min} resulting from the iteration is increasing. The $\% \frac{P_{mis}}{\Delta P_{loss}}$ grows from 28.26% to 30.17%, which is not too large a difference. As long as the LP returned power-loss reduction and the DPF-given results are in the same direction and the orders of magnitude are the same, the LP approximation is said to be accurate enough to solve the original nonlinear optimization problem.

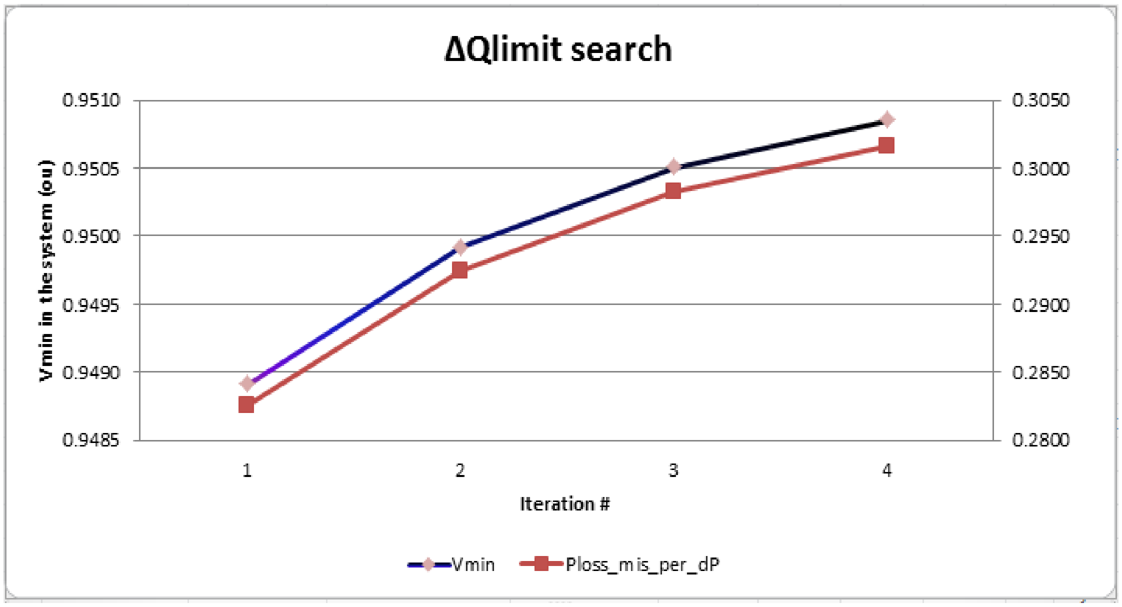

Figure 3-14 Iteration of the limitation search

Therefore, from the ΔQ_{limit} search result, $\Delta Q_{limit} = 1.8$kVar is the largest ΔQ_{limit} that can be accepted. However, if ΔQ_{limit} is set to be 1.8kVar, only one update can maintain the voltage within the feasible region. So, in the following LPOPF, the conservative approach, setting ΔQ_{limit} to a small enough value, is used to make sure we can achieve the best system operating conditions not only when the power loss is minimized, but also when the voltages are still feasible. If ΔQ_{limit} is small, it will require more iterations to get to the optimal operating point, but the results will be more accurate.

In the following, $\Delta Q_{limit} = 0.2$kVar is used as the maximum update of control variables per iteration. Then, the LPOPF gives the optimization result as shown in Figure 3-15. The left-hand axis shows the total system power loss, and the right-hand axis is the minimum voltage in the system. As Figure 3-15 shows, the system power loss lessens in the optimization iteration process, and, at the same time, the minimum voltage also decreases.

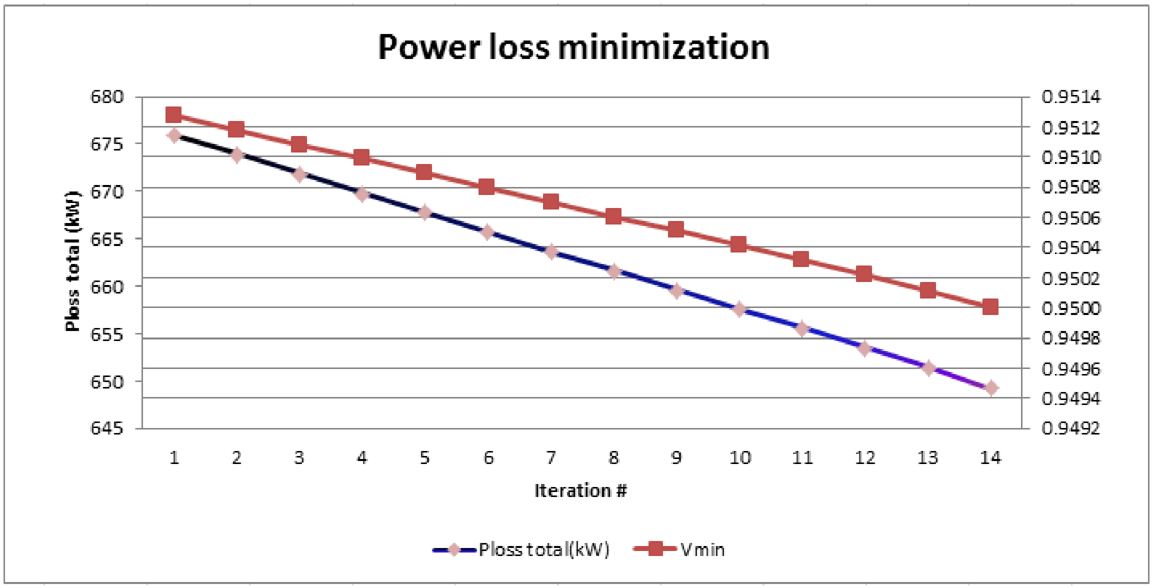

Figure 3-15 The iteration of the power-loss minimization

The optimal operating point that is returned by the LPOPF is documented. Figure 3-16 shows the reactive power needed from the SSTs in phase A to achieve the optimal point.

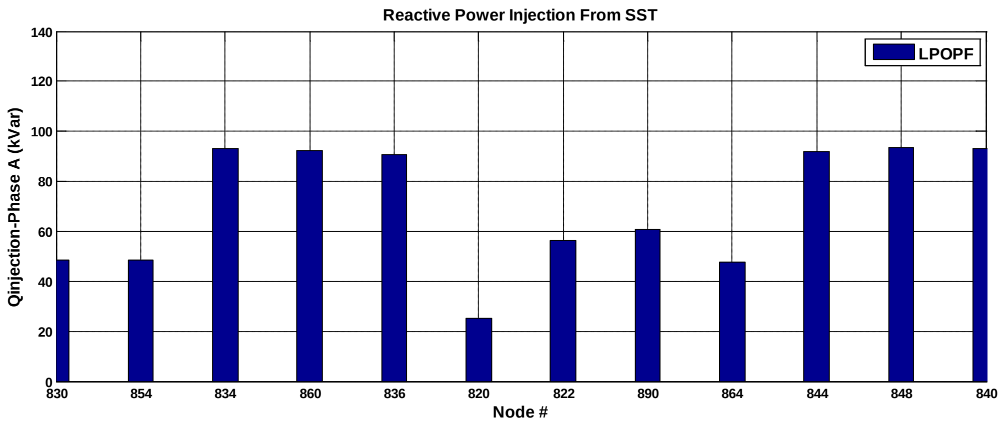

Figure 3-16 Reactive power injection after the LPOPF

The voltage profile of phase A in p.u. along the feeders of the optimal point is shown in Figure 3-17.

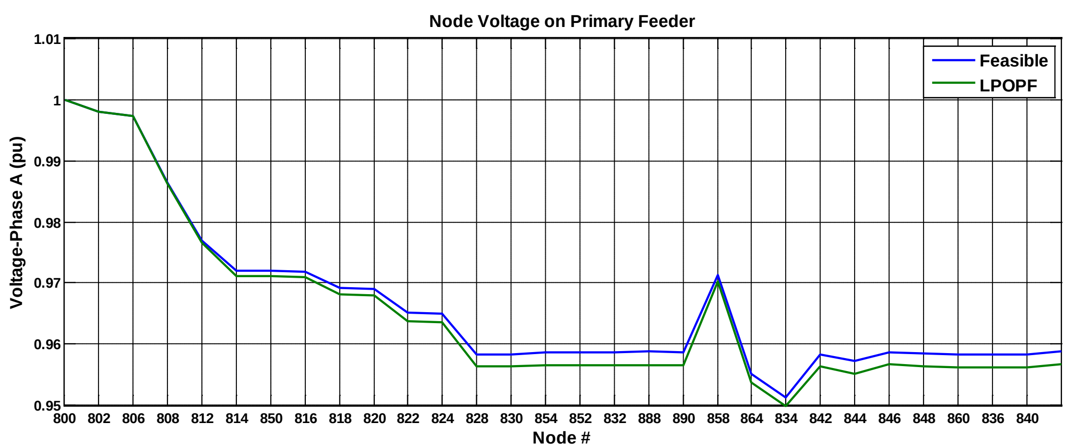

Figure 3-17 The voltage profile of phase A after the LPOPF

Then, the use of the power flow through the substation and the total load to calculate the power loss, are documented in Table 3-3. The total required reactive power from the SSTs is also documented.

Table 3-3 Power loss after LPOPF

	Pa(kW)	*Pb*(kW)	*Pc*(kW)
Power flow through the substation	841.4338	766.4906	808.1505
Total load	606.0013	584.0024	578.9930
Power loss	235.4325	182.4882	229.1575
	Qa(kVar)	*Qb*(kVar)	*Qc*(kVar)
Total reactive power injection	841.4245	739.4645	822.2356

The power-loss reduction for each phase is then calculated using the difference between the power loss of the initial feasible point and the final optimal point.

$$P_{loss\_red} = P_{loss\_feasible} - P_{loss\_final} \tag{3.45}$$

Then, we calculate the percentage of power-loss reduction using the following equation:

$$\%P_{loss\_red} = \frac{P_{loss\_feasible} - P_{loss\_final}}{P_{loss\_feasible}} \tag{3.46}$$

The comparison of all power losses during the optimization is documented in Table 3-4.

Table 3-4 Power loss comparison

Power loss (kW)	*Pa*(kW)	*Pb*(kW)	*Pc*(kW)
Original	92.0122	74.2004	90.244
After feasibility search	249.3196	191.849	236.8548
After LPOPF	235.4325	182.4882	229.1575

Table 3-4 Continued

Reduction	13.8871	9.3608	7.6973
Percentage of reduction	0.0557	0.0487925	0.032498

Similarly, as we calculated the power-loss reduction, we can also calculate the reduction of reactive power provided by the SSTs:

$$Q_{inj\_red} = Q_{inj\_feasible} - Q_{inj\_final} \tag{3.47}$$

Then, the percentage of power-loss reduction can be calculated using the following equation:

$$\%Q_{inj\_red} = \frac{Q_{inj\_feasible} - Q_{inj\_final}}{Q_{inj\_feasible}} \tag{3.48}$$

The comparison of the total reactive power injection from the SSTs during the optimization is documented in Table 3-5.

Table 3-5 Reactive injection comparison

Total reactive power injection	Qa(kVar)	Qb(kVar)	Qc(kVar)
After feasibility search	877.4249	787.4649	847.439
After LPOPF	841.4245	739.4645	822.2356
Reduction	36.0004	48.0004	25.2034
Percentage of reduction	0.0410	0.0609	0.0297

The result indicates that the proposed centralized VVC scheme can successfully control the voltages and minimize the power loss to a practical level. Table 3-4 and Table 3-5 show the reactive power needed to boost the voltage to a feasible point and the reactive power needed at the optimal point. As indicated, the power loss is reduced by about 10%, on average, from Phase I to Phase II, which is a considerable reduction in reality.

3.3.3.2 The BF LPOPF Simulation Result

In order to justify the optimization result, apply BF LPOPF to the feasible system operating condition we got from Phase I. The optimal operating point that is returned by the BF LPOPF is shown in Figure 3-18, where the reactive power needed by the SSTs is indicated.

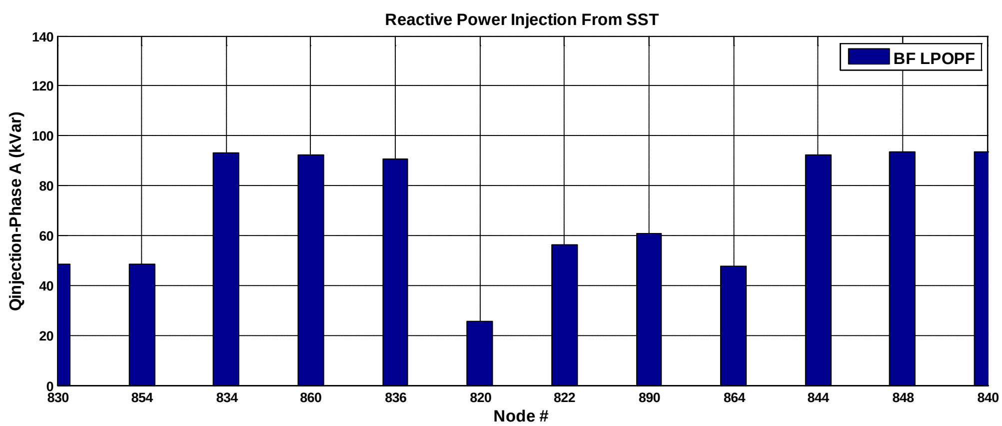

Figure 3-18 The reactive power injection after the BF LPOPF

The voltage profile of phase A in p.u. along the feeders after the BF LPOPF is shown in Figure 3-19.

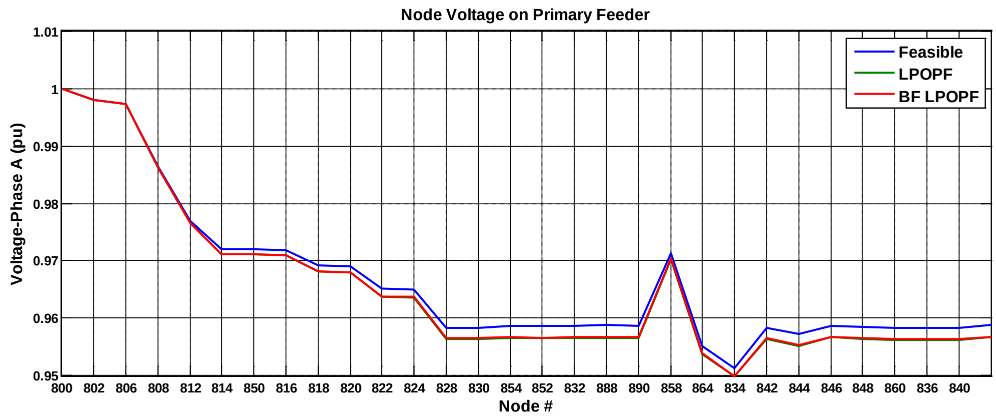

Figure 3-19 The voltage profile of phase A after the BF LPOPF

Then, the use of the power flow through the substation and the total load to calculate the power loss are documented in Table 3-6. The total required reactive power from the SSTs is also documented.

Table 3-6 Power loss after BF LPOPF

	Pa(kW)	*Pb*(kW)	*Pc*(kW)
Power flow through substation	842.2164	767.0796	808.7269
Total load	606.0014	584.0025	578.9929
Power loss	236.2150	183.0771	229.7340
	Qa(kVar)	*Qb*(kVar)	*Qc*(kVar)
Total reactive power injection	843.5695	742.3245	824.1241

Use the same real-power reduction calculation equations presented previously to get the result for the BF LPOPF in Table 3-7.

Table 3-7 Power loss reduction and comparison

Power loss (kW)	*Pa*	*Pb*	*Pc*
Original	92.0122	74.2004	90.2440
After feasibility search	249.3196	191.8490	236.8548
After BF LPOPF	236.2150	183.0771	229.7340
Reduction	13.1046	8.7719	7.1208
Percentage of reduction	0.0526	0.0457	0.0301

The comparison of the total reactive power injection from the SSTs during the optimization is documented in Table 3-8.

Table 3-8 Reactive injection reduction and comparison

Total reactive power injection	*Qa*(kVar)	*Qb*(kVar)	*Qc*(kVar)
After feasibility search	877.4249	787.4649	847.4390
After BF LPOPF	843.5695	742.3245	824.1241
Reduction	33.8554	45.1404	23.3149
Percentage of reduction	0.0386	0.0573	0.0275

Similarly, as in the previous approach, the BF LPOPF can successfully maintain the voltages within acceptable limits and minimize power loss to a practical level. Table 3-8 and Table 3-9 show the reactive power needed to boost the voltage to a feasible point, and the reactive power needed at the optimal point. As indicated, the power loss reduces by about 10%, on average, from Phase I to Phase II, which is a considerable reduction in reality.

3.3.3.3 Check for Optimality Using the LPOPF

It is probable that the optimal point found is not the global minimum point. Especially in our case, the initial point of power-loss minimization is the result of the feasibility search, which is usually close to the boundary of the feasible region. We may want to start with an initial point that is further inside the feasible region. For example, in the following test we magnify the suggested reactive power injection returned by the feasibility search by 25% more. Then, the new initial point of Phase II will be as shown in Figure 3-20.

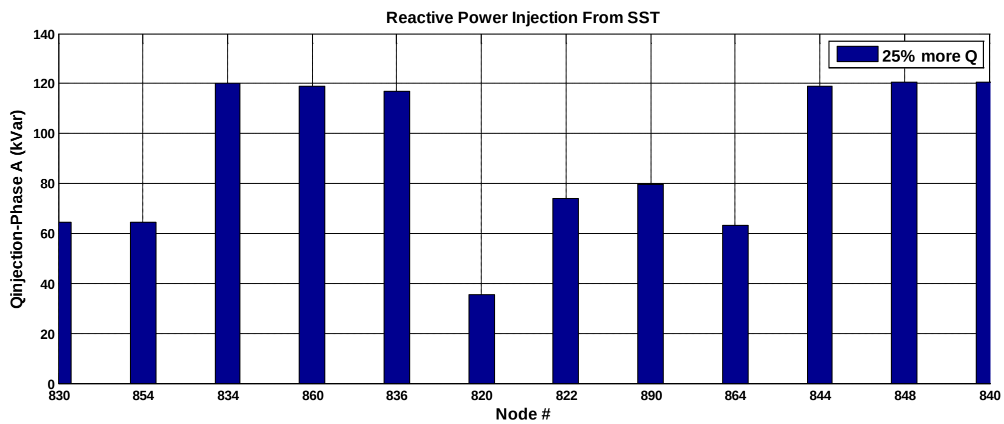

Figure 3-20 25% more reactive power injection after the feasibility search

The voltage profile of phase A in p.u. along the feeders after injecting 25% more reactive power is shown in Figure 3-21. From the comparison with the original feasibility search result, it is clear that with more reactive power injected, the operating condition is farther from the boundary of the feasible region.

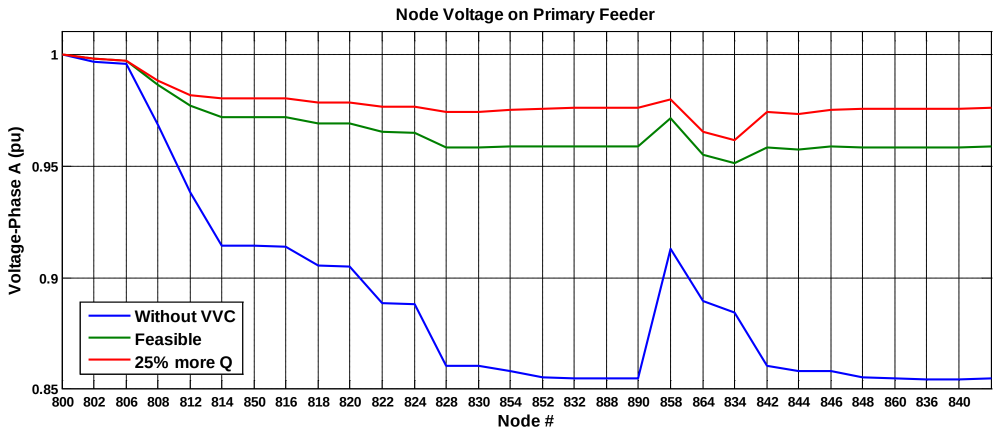

Figure 3-21 The voltage profile of phase A after injecting 25% more reactive power

Then, the use of the power flow though the substation and the total load to calculate power loss is documented in Table 3-9. The total required reactive power from the SSTs is also documented.

Table 3-9 Power loss for 25% more reactive power injection

	Pa(kW)	*Pb*(kW)	*Pc*(kW)
Power flow through the substation	943.0851	839.1845	897.4367
Total load	606.0012	584.0033	578.9917
Power loss	337.0839	255.1812	318.4450
	Qa(kVar)	*Qb*(kVar)	*Qc*(kVar)
Total reactive power injection	1096.796	984.333	1059.2657

Then, the power-loss minimization iteration by the LPOPF is shown in Figure 3-22. The left-hand axis shows the total system power loss, and the right-hand axis is the minimum voltage in the system. As the iteration progresses, the power-loss decreases from 896.9040kW to 711.6275kW, while the minimum voltage decreases from 0.9613 p.u. to 0.9503 p.u.

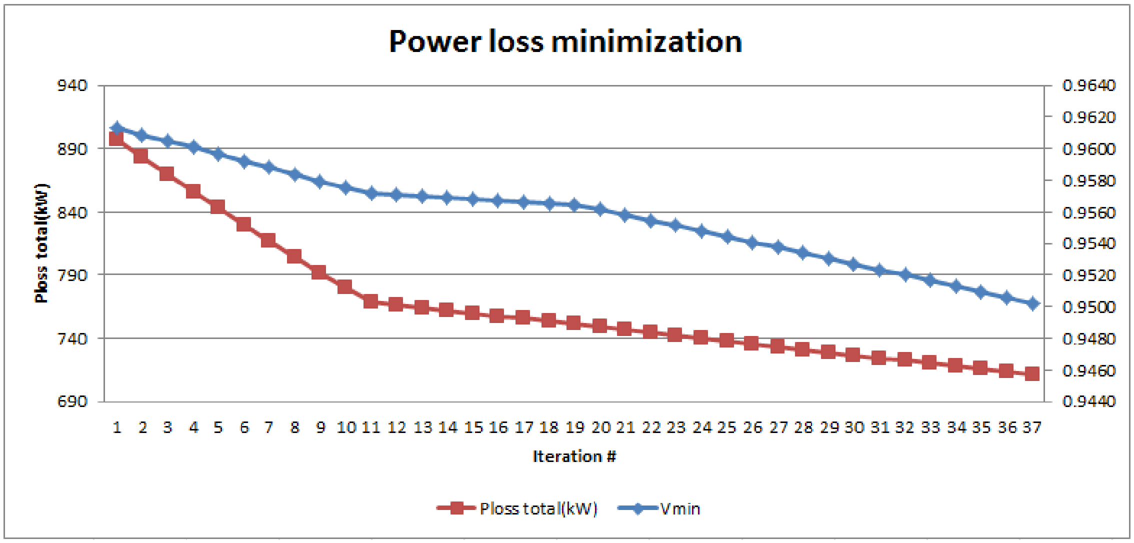

Figure 3-22 The power-loss minimization iteration

The new optimal point with minimum power loss given by the LPOPF is documented, and the reactive power-injection requirement is shown in Figure 3-23.

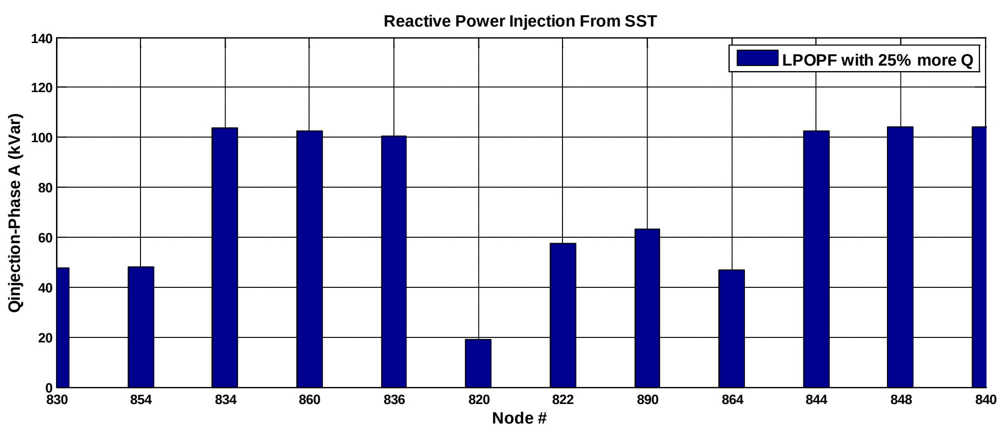

Figure 3-23 The reactive power injection after the LPOPF

The voltage profile of phase A in p.u. along the feeders after the LPOPF is shown in Figure 3-24.

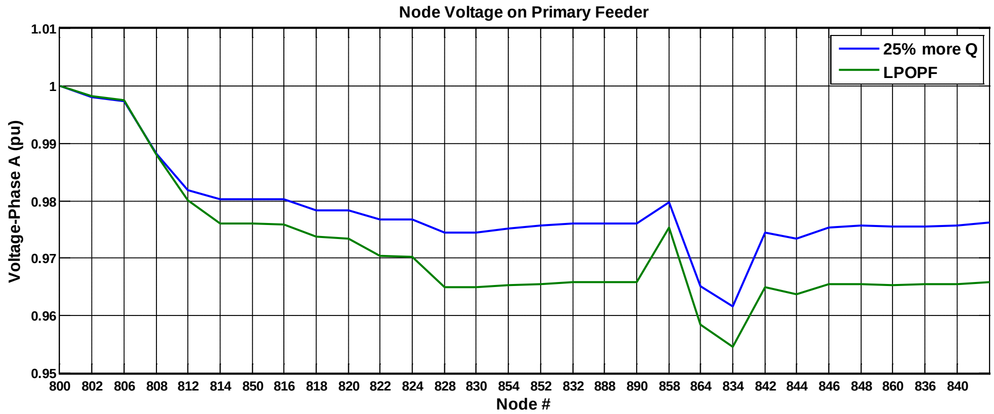

Figure 3-24 The voltage profile of phase A after the LPOPF

The use of the power flow through the substation and the total load to calculate the power loss is documented in Table 3-10. The total required reactive power from the SSTs is also documented.

Table 3-10 Power loss after LPOPF

	Pa(kW)	*Pb*(kW)	*Pc*(kW)
Power flow through the substation	858.3426	778.7734	841.3613
Total load	606.0031	584.0037	578.9876
Power loss	252.3395	194.7698	262.3737
	Qa(kVar)	*Qb*(kVar)	*Qc*(kVar)
Total reactive power injection	899.9852	721.9287	894.0945

Using the same real-power reduction calculation equations presented previously to get the results for the LPOPF of the optimality check, the results are documented in Table 3-11.

Table 3-11 Power loss reduction and comparison

Power loss (kW)	*Pa*	*Pb*	*Pc*
After feasibility search	337.0839	255.1812	318.4450
After LPOPF	252.3395	194.7698	262.3737
Reduction	84.7444	60.4114	56.0713
Percentage of reduction	0.2514	0.2367	0.1761

The comparison of the total reactive power injection from the SSTs during the optimization is documented in Table 3-12.

Table 3-12 Reactive injection reduction and comparison

Total reactive power injection	*Qa*(kVar)	*Qb*(kVar)	*Qc*(kVar)
After feasibility search	1096.7960	984.3330	1059.2657
After LPOPF	899.9852	721.9287	894.0945
Reduction	196.8108	262.4043	165.1712
Percentage of reduction	0.1794	0.2666	0.1559

As shown in Table 3-11 and Table 3-12, the LPOPF, under the condition of injecting 25% more reactive power required by the feasibility search, can also successfully maintain the voltages within acceptable limits and minimize the power loss to a practical level. With 25% more reactive power injection compared to the feasibility search result, the power loss reduction is larger because the starting point is further inside the feasible region. As indicated in Table 3-11, there is about a 22%, on average, power-loss reduction from Phase I to Phase II.

3.3.3.4 Check for Optimality Using the BF LPOPF

Start with the new feasibility point, which is with 25% more reactive power injection indicated by the feasibility search, and apply the BF LPOPF to see how it works. Then, the BF LPOPF iteration is shown as in Figure 3-25. As the iteration progresses, the power loss decreases from 843.0211kW to 710.7568kW while the minimum voltage also decreases from 0.9597 p.u. to 0.9500 p.u.

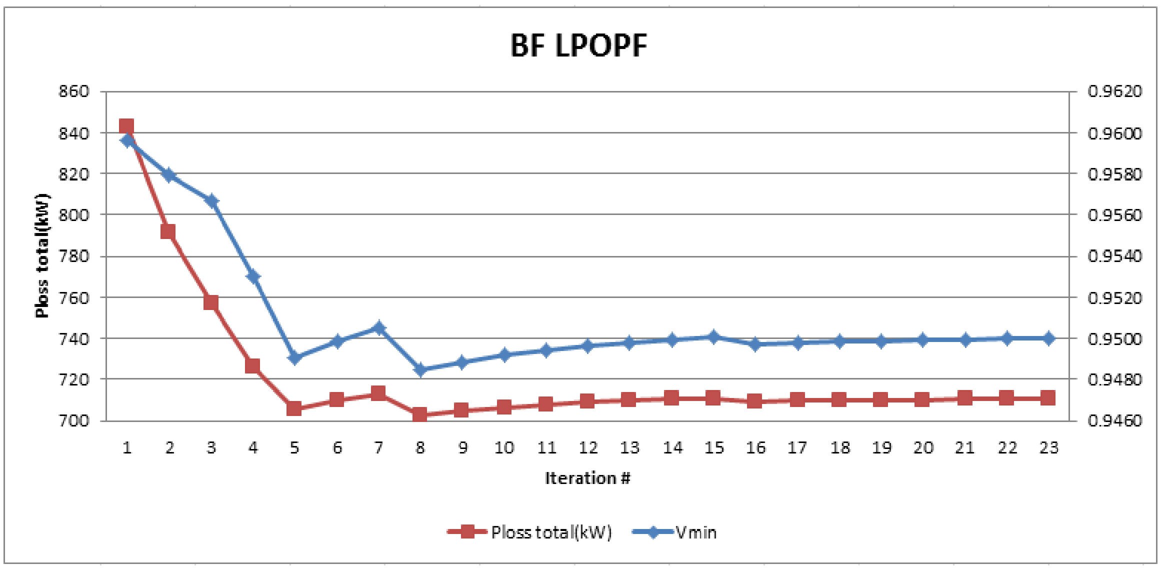

Figure 3-25 The power-loss minimization iteration

Then, the new optimal point with minimum power loss given by the BF LPOPF is documented. The reactive power injection requirement is shown in Figure 3-26.

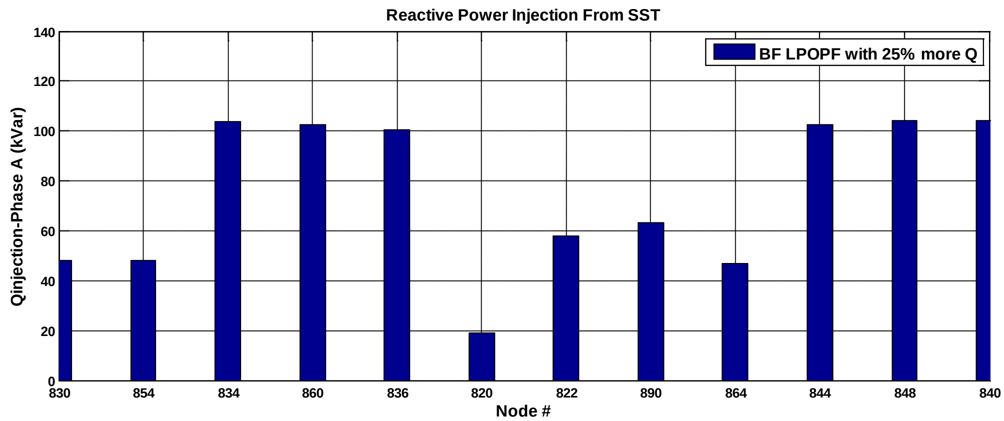

Figure 3-26 The reactive power injection after the BF LPOPF

The voltage profile of phase A in p.u. along the feeders after the BF LPOPF is shown in Figure 3-27.

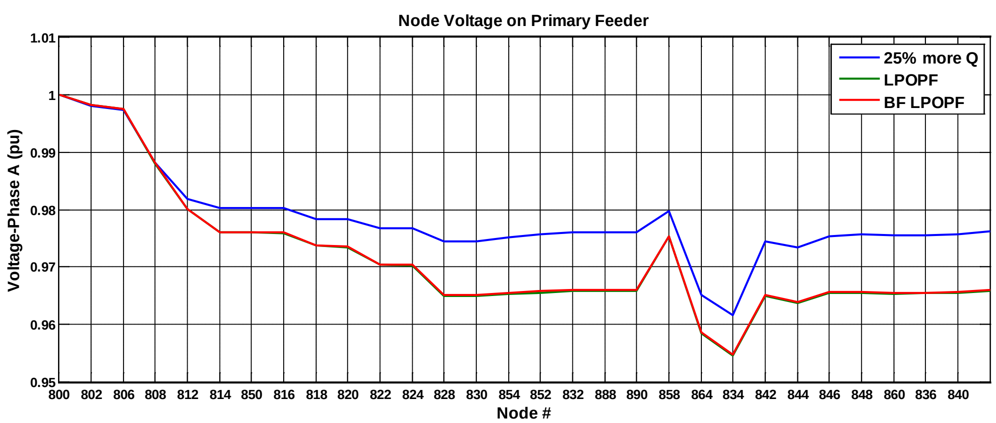

Figure 3-27 The voltage profile of phase A after the BF LPOPF

Then, using the power flow through the substation and the total load to calculate power loss is documented in the following table. The total required reactive power from the SSTs is also documented.

Table 3-13 Power loss after BF LPOPF

	Pa(kW)	*Pb*(kW)	*Pc*(kW)
Power flow through the substation	858.5770	779.0001	842.1739
Total load	606.0033	584.0036	578.9872
Power loss	252.5737	194.9965	263.1867
	Qa(kVar)	*Qb*(kVar)	*Qc*(kVar)
Total reactive power injection	900.8553	723.0883	891.969

Using the same real-power reduction equations presented previously to get the result for the LPOPF of the optimality check, the results are documented in Table 3-14.

Table 3-14 Power loss reduction and comparison

Power loss (kW)	*Pa*	*Pb*	*Pc*
After feasibility search	337.0839	255.1812	318.4450
After BF LPOPF	236.2150	183.0771	229.7340
Reduction	100.8689	72.1041	88.711
Percentage of reduction	0.2992	0.2826	0.2786

The comparison of the total reactive power injection from the SSTs during the optimization is documented in Table 3-15.

Table 3-15 Reactive injection reduction and comparison

Total reactive power injection	Qa(kVar)	Qb(kVar)	Qc(kVar)
After feasibility search	1096.7960	984.3330	1059.2657
After BF LPOPF	900.8553	723.0883	891.969
Reduction	195.9407	261.2447	167.2967
Percentage of reduction	0.1786	0.2654	0.1579

As shown in Table 3-14 and Table 3-15, the BF LPOPF, under the condition of injecting 25% more reactive power required by the feasibility search, can also successfully maintain the voltages within acceptable limits and minimize the power loss to a practical level. With 25% more reactive power injection compared to the feasibility search result, the power-loss reduction is larger because the starting point is further inside the feasible region. As indicated in Table 3-15, the average power-loss reduction from Phase I to Phase II is about 28%.

3.3.3.5 Results Comparison and Analysis

In order to compare the power-loss minimization results given previously, Table 3-16, which includes the power loss per phase, the reactive power injection per phase, and the minimum voltage information, is given.

Table 3-16 Optimal point power loss comparison for all the test cases

	Original $Qinj$		25% more $Qinj$	
	LPOPF	BF LPOPF	LPOPF	BF LPOPF
P_{la}(kW)	235.4325	236.215	252.3395	252.5737
P_{lb}(kW)	182.4882	183.0771	194.7698	194.9965
P_{lc}(kW)	229.1575	229.734	262.3737	263.1867
Q_{inja}(kVar)	841.4245	843.5695	899.9852	900.8553
Q_{injb}(kVar)	739.4645	742.3245	721.9287	723.0883

Table 3-16 Continued

Q_{injc}(kVar)	822.2356	824.1241	894.0945	891.969
V_{min}	0.95	0.95	0.9503	0.95

Then the total system power loss and reactive power injection are calculated as the summation of three phase values. As shown in Table 3-17, the minimum power loss achieved by applying the LPOPF with the original feasibility search result as the initial point provides the best solution, which is with a total system power loss of 647.0782kW and a total reactive power injection of 2403.1246kVar.

Table 3-17 Total power loss comparison

		P_{l_total}(kW)	Q_{inj_total}(kVar)
Original Q_{inj}	LPOPF	647.0782	2403.1246
	BF LPOPF	649.0261	2410.0181
25% more Q_{inj}	LPOPF	709.483	2516.0084
	BF LPOPF	710.7569	2515.9126

From the results comparison in Table 3-16 and Table 3-17, starting with the same feasible point, LPOPF and BF LPOPF returned optimal points that are quite close to one another, and there is no significant difference. However, when starting with different feasible points, the optimal points may differ, which means that there is no guarantee that the returned optimal point is the global optimal. From the scenario that has been completed, directly utilizing the feasibility search result as the initial feasible starting point for power-loss minimization will give us a better optimal point.

3.4 Conclusion

In this chapter, the potential centralized control strategies for power distribution systems are investigated and the applications are presented. Based on the new feature of the FREEDM-type smart distribution grid, a new two-phase centralized VVC scheme is proposed. The objective of the VVC is formulated as minimizing system power loss while regulating the voltage profile within acceptable limits. Phase I control is then targeted at regulating voltages when a voltage violation exists. The feasibility search is based on the gradient method to find the steepest decent update direction. Then, based on a feasible operating condition, the Phase II optimization is aiming at minimizing the power loss within the feasible region. Since the adopted optimization scheme is LP-based, it is necessary to make sure the linearization doesn't lose accuracy. Therefore, the limitation of the reactive power change step size is added as an improvement, so that the VVC-returned update system status will not drift away from the actual system response. Another improvement made here is the BF LPOPF, where the back and forth method is adopted to find the optimal operating point.

The proposed centralized VVC scheme is then tested on the FREEDM IEEE 34 node test feeder. In order to check the optimality with different initial feasible conditions, an additional test is made with 25% more reactive power injections. The result shows that LPOPF has a better performance than BF LPOPF. The optimization result with a starting point at the original feasible point is better than that with 25% more reactive power injections. Based on the simulation result, it is clear that the proposed scheme can achieve the optimization goal of minimizing power loss while maintaining voltages within the feasible region.

CHAPTER 4. A Decentralized Volt/Var Control Scheme for the FREEDM System

4.1 Introduction

A radial feeder is the most common topology for a low-voltage distribution network. A radial network leaves the substation and passes electricity through long distribution lines and cables to the terminal customer. Given the inherent nature of the distributed power grid, field devices and remote terminal units (RTU) usually make operation and control decisions based on local measurements. However, when dealing with system-wide optimization problems, such as a VVC, a central operator is necessary to collect any excessive information from RTUs and coordinate their operations. The existing Distribution Management System (DMS) is based on this centralized control architecture: data acquisition through the Supervisory Control and Data Acquisition (SCADA) system, centralized decision-making, and the transmission of control decisions to the field equipment [45]. As indicated in Figure 3-2, the DMS system in centralized control fashion usually sits at the substation, communicates with all the field devices, and makes decisions based on system-wide information. The legacy SCADA system is typically built using a star topology in which data is exchanged directly between the control center and remote field devices. The vertical control approach usually is composed of a control master and multiple slave RTUs. Meter slave RTUs are programmed to report their measurements periodically and act as a database. Control and operational decisions will be made accordingly at the central controller and sent to control or protection devices, such as CAPs, LTC transformers, relays, and circuit breakers. The information exchange of centralized hierarchical control is demonstrated in Figure 4-1.

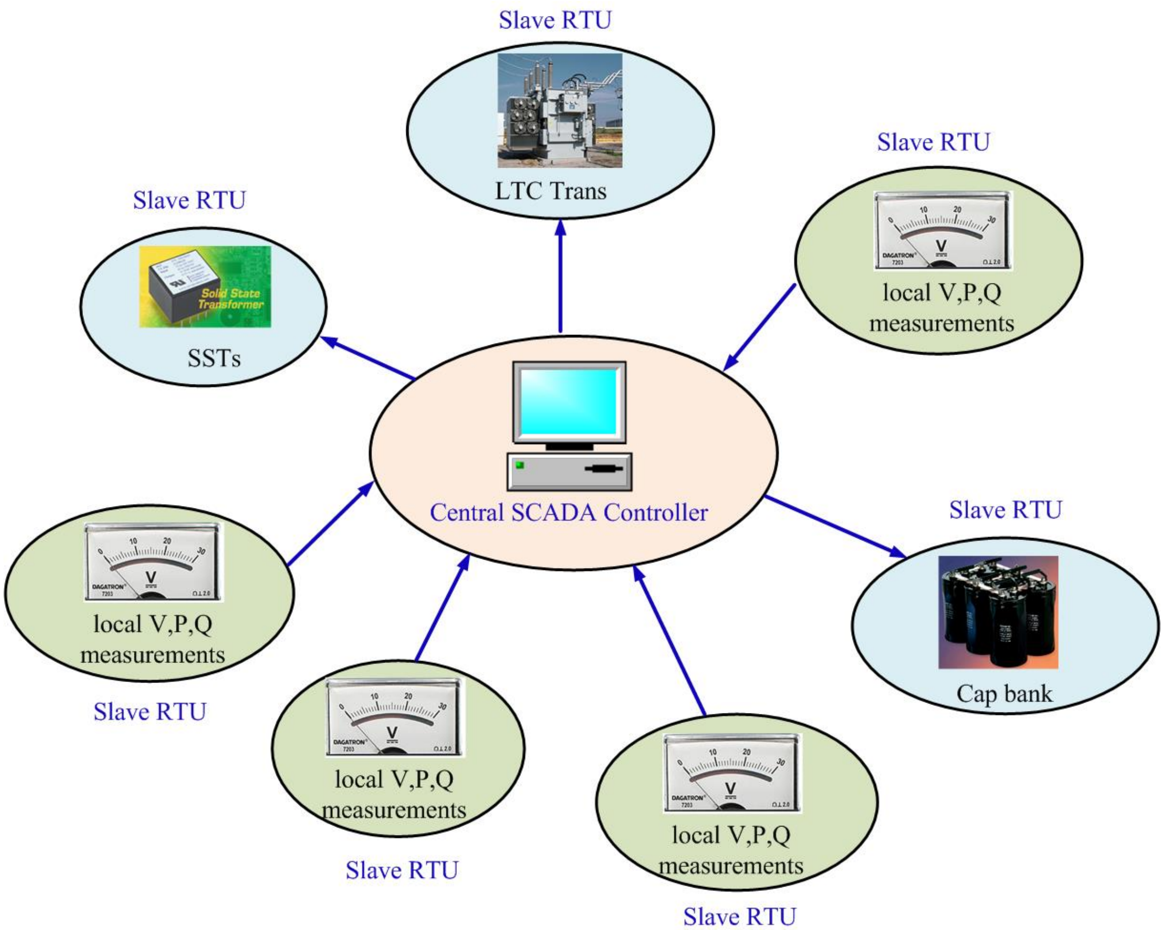

Figure 4-1 Illustration of centralized control

The development and implementation of new power electronics devices and advances in communications and computer technologies raise opportunities to control DRERs in power distribution systems. At the same time, the needs for decentralized control are becoming critical as the power system and prevailing constraints increase in size. With the appearance of smart processors, virtual sub-areas can be established by grouping several RTUs together. You can follow a different direction in forming those virtual clusters, such as electric distance or similar characters. Once the sub-areas are formed, instead of communicating with all of the RTUs, the central SCADA now only needs to exchange information with the slave processors, which work on achieving the optimization goal within their own areas. A central master is needed to eliminate any boundary mismatches between sub-areas. The topology of decentralized control is demonstrated in Figure 4-2.

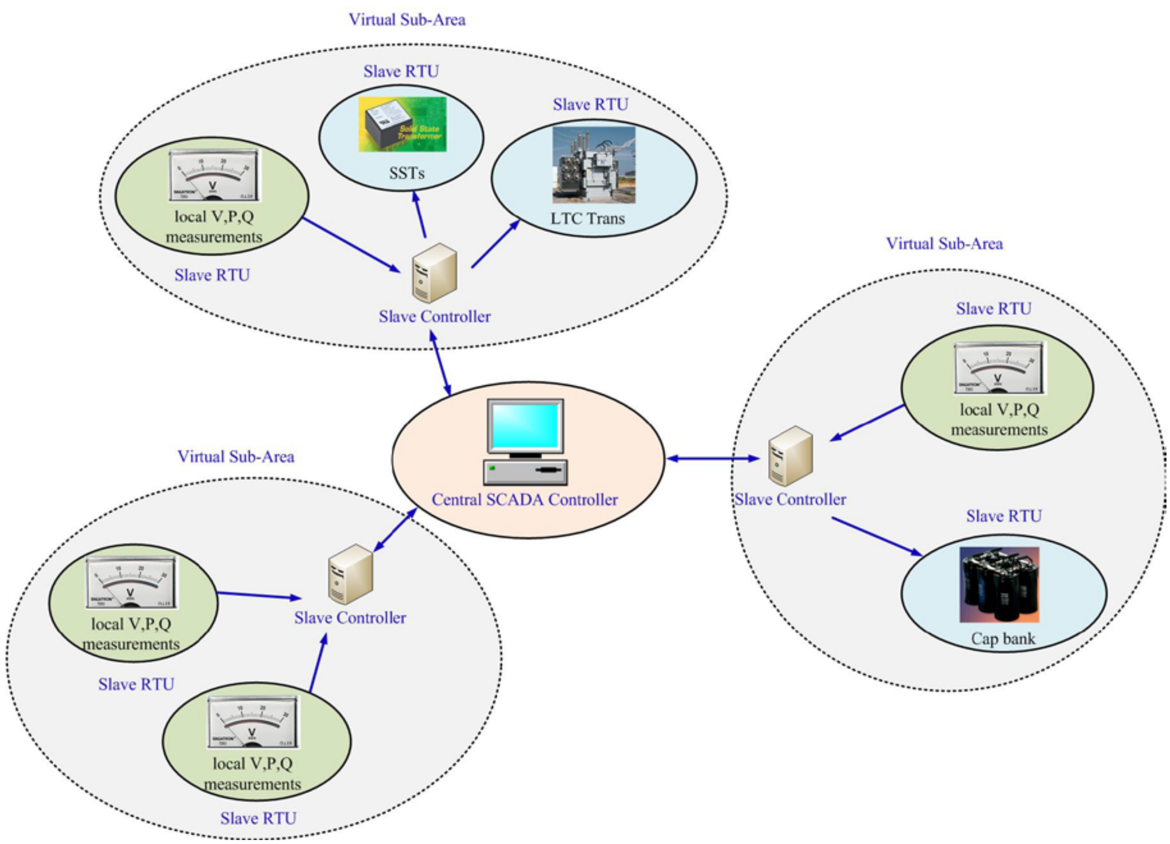

Figure 4-2 Illustration of decentralized control

Distinctions among centralized, decentralized, and distributed types of control strategy are obvious. In order to find the optimal operating point by utilizing centralized control, the central controller needs system-wide information, and the optimization problem is large-scale and time-consuming. Decentralized control is indeed a master-slave control where the original problem is partitioned into smaller subproblems. Each subproblem is processed by slave controller in its own area. The master controller is working on eliminating the mismatches among the sub-areas and coordinating them to achieve the system-wide optimization goal. In distributed control, there is no master controller to coordinate the performance of the sub-areas. Each local agent aims at the optimal in its own area and exchanges information with its neighbors. Generally speaking, distributed control is designed to be able to operate properly in the presence of limited, sometimes unreliable, communications links, and often in the absence of a central control mechanism [46].

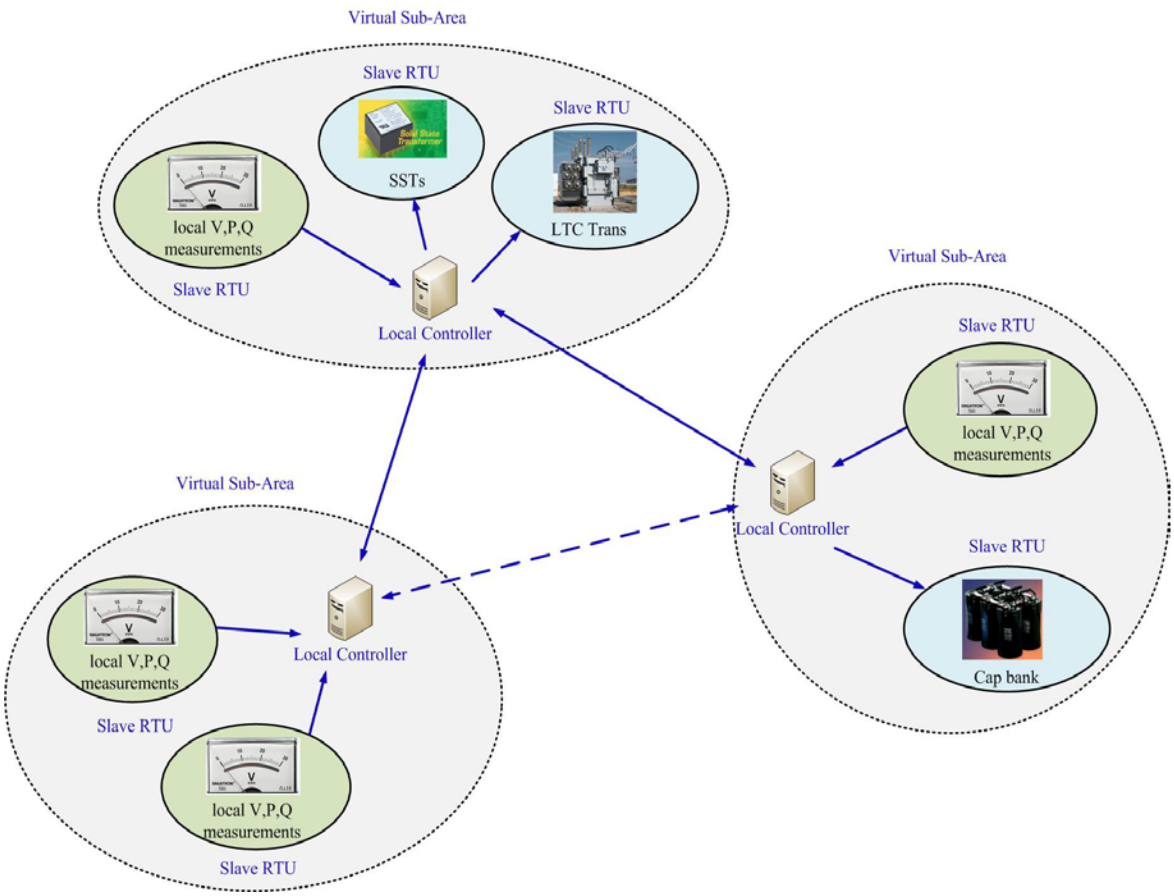

Figure 4-3 Illustration of distributed control

4.1.1 Pros and Cons of Centralized and Decentralized Control

Traditional approaches to the centralized monitoring and control of the power system would not only need high-performance computers to meet rigid time requirements but would also need to build up expensive and complicated communications networks to transmit local measured data to the central control center [46]. Any failure occurring in the system would result in insufficient information being received by the VVC central controller and would, thus, inhibit the making of proper control decisions accordingly. Besides, due to the dependency of centralized VVC on the communications infrastructure, power system control and management is more vulnerable to potential security attacks. Therefore, the drawback of centralized control is apparent in accommodating renewable energy in a distribution network. Centralized control is insufficient to deal with the increasing uncertainty and complexity in future power-system applications as more DRER units appear [47].

Decentralized control usually is made up of a number of processors that are closely coupled within a small physical space. Compared with centralized control, communications links in decentralized control are relatively short, and the dependence of control on the communications infrastructure is also less. Since the originally large-scale problem is decomposed into multiple smaller subproblems, the computation time needed is greatly reduced as a result. However, since the sub-areas also aim to achieve the same system-wide optimization goal as centralized control, the master controller needs information from each slave controller. Given the possibility that the sizes of subproblems may be different and processing time is unpredictable, the master problem may need to wait a little to receive the sub-area data.

In comparison, the reliability of the communications network is not as crucial in distributed control. When communication delays are hard to predict and unreliable, distributed control can be used instead of centralized or decentralized control. Distributed control can not only save a large amount of capital investment in communications networks, but it also limits the effect of local operations within the related local area. In distributed control, each agent can communicate with its neighbors and make decisions autonomously, which reduces the complexity in each distributed controller. However, since each sub-area agent is working only on its own objective and there is no master coordinator present, it is not possible for all of the sub-areas to solve a common problem.

In the FREEDM-type distribution system where every load is connected via an SST, instead of utilizing conventional VVC devices, such as LTC, VR, and CAPs, the SSTs are used as Var resources to regulate system voltages while achieving system-wide optimization goals. With high PV penetration, SSTs are used at each load node to accommodate PVs into the primary distribution feeder. Since the load condition of a distributed system is usually unbalanced, the SSTs are installed per phase so they can be dispatched separately to meet different needs in each phase. Therefore, control variables and operation limits are much more important than in a conventional distributed system since each load node is now capable of providing and absorbing reactive power. Thus, the complexity and uncertainty of a centralized VVC optimization problem in the FREEDM system is much more challenging. In addition to the heavy computational burden, the accuracy and response time of a centralized VVC is highly dependent on the communications infrastructure since the central controller will need to make decisions by utilizing all of the system information. Fortunately, with the appearance of smart meters and microprocessors embedded in the SSTs as RTUs in the FREEDM system, residential-level devices can be used to correct any voltage violation in their local area.

4.1.2 Literature Review on Potential Decentralized Control Approaches and Applications

Typically, all the mathematical methods mentioned in the previous chapter can be used to solve the subproblems after the problem is partitioned into a cluster of subproblems [48]. The potential approaches for decentralized VVC can be classified into two categories:

1) Traditional mathematical methods, such as the gradient-projection algorithm, quadratic programming, augmented Lagrange method [48], [49], and Dantzig Wolfe.
2) Evolutionary algorithms, such as a genetic algorithm (GA), particle swarm optimization (PSO), and graph theory [50]-[52].

A recent application of decentralized algorithms is on economic dispatch. By applying a consensus algorithm, Dr. Chow proposed a distributed decision-making procedure where the local controller constantly reports its information state to the consensus manager, and the consensus manager negotiates with the neighboring agents on the communications network [47]. After the negotiation iterative process, the state parameters of all local controllers will reach the same value. A multi-agent-based distributed control approach is proposed in Dr. Baran's paper [53], which considers the sensitivity of voltage with respect to the reactive power injection. The optimization problem is solved in a distributed manner by decomposing the original problem into smaller subproblems, each assigned to a particular agent. The supervisory subproblem is needed to ensure that the distributed solution will converge to the optimal point. Similar to Dr. Baran's problem formulation, the impact of control actions of different kinds of control devices is studied first in Dr. El-Saadany's recent work [54]. After the impact study, a two-way communications-based distributed control is proposed for all agents to achieve a common objective. Each control agent has its own objective and constraints regarding the preferences and capabilities of the device. The local controller is then grouped with its neighbors in Dr. Klump's paper to form reactive support groups [55]. In this case, rather than considering all devices as potential destinations for reactive control messages, each node is associated with a reactive support group. A voltage-coupling index algorithm is adopted to achieve the control goal where the voltages within the same group are highly coupled with each other.

Evolutionary algorithms also demonstrate their strengths in solving a large-scale nonlinear optimization problem. Dr. Michalewicz's paper provides an overview of these algorithms and a set of numerical optimization test cases [52]. As one of the more promising solution approaches, PSO has drawn a lot attention. The state-of-the-art and mathematical techniques of PSO are described in detail in [50], [51]. As a highly non-separable problem, there is no guarantee that a global optimum can be found for VVC by any conventional method. PSO, on the other hand, has shown particular promise for the problems for which there is no specialized method available or all specialized methods give unsatisfactory results. Very limited PSO applications on power system operations and control are available. In [56], Dr. Yoshida gives an insight discussion on applying PSO for VVC when considering a voltage-security assessment, and indicates the possible use of PSO to solve mixed-integer nonlinear optimization problems. In Dr. Sharma's [57] recent research, PSO is utilized to solve a reactive power optimization problem to minimize power losses in a transmission network. The proposed method is successfully applied on the IEEE 6 bus system. In another recent work [58], Dr. Swarnkar applies improved PSO to a distributed system for the solution of combined economic emissions dispatch problem. The proposed scheme is tested on the IEEE 30 system and compared with other evolutionary computation techniques to demonstrate its advantage in handling the optimal power-flow problem.

Discussions are still ongoing on the distributed VVC schemes. The main challenge to applying the distributed algorithm is to partition the original large-size optimization problems into subproblems while identifying the coupling between subproblems and feed this information back to a coordinate master station.

In the previous chapter, the centralized VVC problem is formulated and made linear with respect to both state and control variables, which results in a large-scale LP problem. In Dr. Kleinberg's recent paper, the portions of the network served by the same source or sources of reactive power flow are grouped into common areas once positive power-flow directions are established. Then, the distributed power flow and distributed state estimation techniques are investigated for distribution system analysis [59]. Following a similar problem-solving procedure, the DW decomposition method draws the author's attention. Since the DW concept was proposed by Dr. George B. Dantzig and Dr. Philip Wolfe in the 1960s, the DW decomposition method, which can reduce the dimension of the problem in a very effective way by separating it into several subproblems coordinated by a master problem, has been used to solve large-scale LP problems [60], [61]. The DW concept has already been applied to the economic dispatch and unit commitment problems [62]-[66].

4.2 Proposed DW-based Decentralized Control Scheme

Previously, centralized VVC was solved in a two-phase fashion, where a gradient-based feasibility search will first force all the voltage within the acceptable limit and the LP algorithm will try to minimize the system power loss within the feasible region. In the same way as the previous problem formulation (3.1), the objective of Volt/Var optimization is to minimize the real power loss while keeping voltages within acceptable limits.

$$minP_{loss} = \sum G_{ij} \left[V_i^2 + V_j^2 - 2V_i V_j \cos(\delta_i - \delta_j)\right]$$

subject to:

$$g(x,u) = 0$$

$$V^{min} \leq V \leq V^{max}$$

$$Q_{SST}^{min} \leq Q_{SST} \leq Q_{SST}^{max}$$

In this chapter, the DW decomposition method will be applied to the second phase of the VVC to bring down the already made linear VVC optimization problem into subproblems. After decomposition of the original LP problem, parallel processing of the subproblems becomes possible, which will greatly reduce the computational burden and the dependence of the control application on the communications infrastructure. In the following, a decentralized control scheme based on DW decomposition will be proposed and explained in detail. Simulation test results will be presented for the FREEDM IEEE 34 system and the FREEDM Residential Notional System.

4.2.1 The DW Decomposition Scheme

Large-scale LP problems usually have some special structural form that can be exploited to develop efficient computational procedures. One common structure is where there are a number of separate activity areas that are linked through common resource constraints. Consider an LP problem of the form:

$$min M_1 \mathrm{x}_1 + M_2 \mathrm{x}_2 + \cdots + M_n x_n \tag{4.1}$$

subject to:

$$L_1 x_1 + L_2 x_2 + \cdots + L_n x_n \leq b_0 \tag{4.2}$$

$$\begin{cases} A_1 x_1 \leq b_1 \\ A_2 x_2 \leq b_2 \\ \quad \dots \\ A_n x_n \leq b_n \end{cases} \tag{4.3}$$

$$x_1, x_2 \dots x_n \geq 0 \tag{4.4}$$

where $x_1, x_2 \dots x_n$ are vectors of the dimensions $n_1, n_2 \dots n_n$, respectively, and $b_1, b_2 \dots b_n$ are vectors of the dimensions $m_1, m_2 \dots m_n$, separatelyrespectively. If the LP problem is put into standard form:

$$min c^T x \tag{4.5}$$

subject to:

$$Ax \leq b \tag{4.6}$$

$$x \geq 0 \tag{4.7}$$

where $x = [x_1, x_2 \dots x_n]$, $c = [M_1, M_2 \dots M_n]$, $b = [b_1; b_2; \dots; b_n]$, and the matrix A are in a special “block angular” structure [67]:

$$A = \begin{bmatrix} L_1 & L_2 & \dots & L_n \\ A_1 & & & \\ & A_2 & & \\ & & \dots & \\ & & & A_n \end{bmatrix} \tag{4.8}$$

The block angular structure can be clearly illustrated in Figure 4-4.

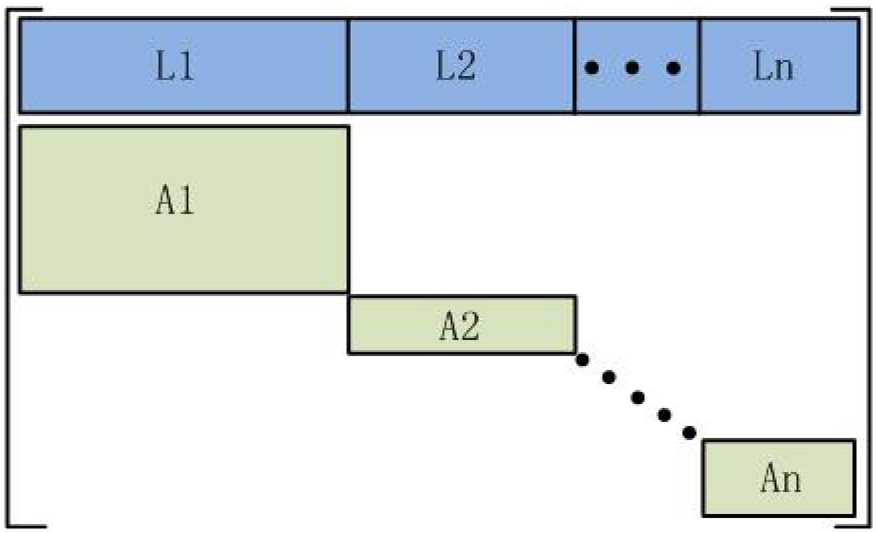

Figure 4-4 Block angular structure

A problem in this form can be solved by the DW decomposition method, which solves subproblems separately in each iteration. The subproblems are LP problems within their own area. The objectives of the subproblems vary from iteration to iteration and are determined by the master coordinator based on the results from previous iterations. The master problem eliminates mismatched information between subproblems so that the overall optimization problem will be solved ultimately. The equations above can be rewritten in a more general form:

$$min \sum_{i}^{n} M_i x_i \tag{4.9}$$

subject to:

$$\sum_{i}^{n} L_i x_i \leq b_0 \tag{4.10}$$

$$A_i x_i \leq b_i \tag{4.11}$$

$$x_1, x_2 \dots x_n \geq 0 \tag{4.12}$$

This may be viewed as a problem of minimizing the objective of n different linear programs that are independent except for the first set of constraints. This way a large linear optimization problem can be converted into n smaller ones of the following type:

$$min (M_i - \omega_i L_i) x_i \tag{4.13}$$

subject to:

$$A_i x_i \leq b_i \tag{4.14}$$

$$x_i \geq 0 \tag{4.15}$$

These subproblems are coordinated by a master problem, which provides them with a simplex multiplier ω_i from the dual solution. At each iteration, the structure of the subproblems is invariant, changing only the multiplier. The subproblems are optimized at the end of each iteration, and their answers are sent to the master problem. The answer consists of reactive power exchanges at each stage in all border buses with tie lines. Since the subproblems are decoupled, the individual reactive power flows may differ in any border bus at any stage.

The master problem, which includes the overall objective function and all linking constraints, must eliminate those infeasibilities.

If at the i^{th} iteration, the current optimal solution for a subproblem n is x_n^i, then the full control variable vector is:

$$x^i = [x_1^i, x_2^i \dots x_n^i] \tag{4.16}$$

while the master problem will have a weighted factor λ_i corresponding to that returned control variable vector.

Using the accumulated answers of the previous solution of subproblems, the i^{th} optimal solution can be written in this form:

$$x_i^* = \lambda_1 x^1 + \lambda_2 x^2 + \cdots + \lambda_i x^i = \sum_{\lambda} \lambda_i x^i \tag{4.17}$$

At each iteration, the master problem will collect all the optimal solutions for each subproblem to generate the full control variable vector while generating a corresponding weighted factor. All of the previous control variable vectors and weighted factors are needed to obtain the current optimal solution as indicated in the equation above. The key information for the master problem in the iterative process can be seen in Table 4-1.

Table 4-1 Iteration information for master problem

Iteration	Weights	Solution returned by subproblems	Current optimal
1	λ_1	x^1	$x_1^* = \lambda_1 x^1$
2	λ_1, λ_2	x^1, x^2	$x_2^* = \lambda_1 x^1 + \lambda_2 x^2$

Table 4-1 Continued

3	$\lambda_1, \lambda_2, \lambda_3$	x^1, x^2, x^3	$x_3^* = \lambda_1 x^1 + \lambda_2 x^2 + \lambda_3 x^3$
4	….	….	….

Therefore by taking into account the complicating constraints, the master problem is defined as [67]:

$$\min_{\lambda} \sum_{\lambda} (\mathrm{P}_{\mathrm{L,i}} + \mathrm{P}_{\mathrm{L,ij}}) \lambda_{\mathrm{p}} \tag{4.18}$$

Subject to

$$\sum \mathrm{L}_{\mathrm{i}} x_i^* \leq \mathrm{b}_0 \tag{4.19}$$

$$\sum_{\lambda} \lambda_{\mathrm{i}} = 1 \tag{4.20}$$

$$\lambda_{\mathrm{i}} \geq 0 \tag{4.21}$$

Where $\mathrm{P}_{\mathrm{L,i}}$ is the objective of the ith subproblem, and $\mathrm{P}_{\mathrm{L,ij}}$ is the mismatch between subarea i and j.

Since the control variable variation information is passed to the master problem from each subproblem and is already a constant vector, the unknowns with which we need to deal are the weights. Substitute the equation in the first equality constraint to get the following form:

$$\sum_{\lambda} L_i x^i * \lambda_i \leq b_0 \tag{4.22}$$

where the answers of the subproblems are considered to be fixed parameters, but adjustable according to their weights, λ_i, at each iteration. Therefore, in the master problem, the original control variable is no longer the control variable, but is the constant parameters for the weights. The objective function consists of the estimation of the individual objective plus the import/export mismatch. The first equality constraint ensures the global feasibility of individual sensitivity in the border bus. The second equality constraint is called convexity, or the unified equation, because it ensures the feasibility of the individual sets of answers in the master problem.

The solution procedure of the DW decomposition method is an iterative process between the master problem and the subproblems, as shown in Figure 4-5.

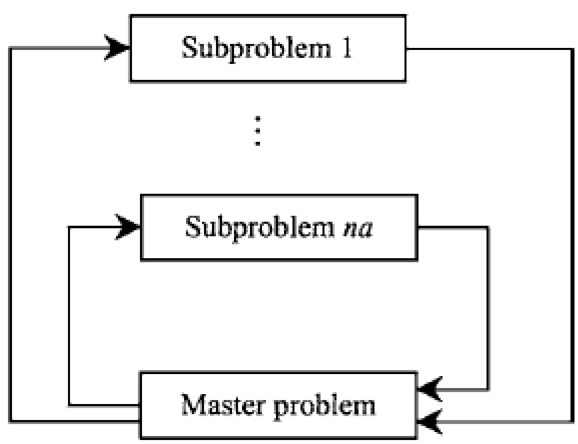

Figure 4-5 Iterative procedure of the Dantzig-Wolfe method [46]

The DW method can reduce, in a very efficient way, the dimensions of the problem by breaking down the original large-scale LP optimization into smaller subproblems. Besides the potential advanced mathematics including the pre-solve techniques, matrix-scaling, pricing, and sparse matrix-handling resulting from applying DW decomposition [68], another attractive feature of the partitioned problem is the relatively straightforward potential for a parallel computational version.

4.2.2 Decomposition of VVC Problem Using DW

Before doing any mathematics operations on the original formulation, there are several assumptions to simplifying the optimization process:

1) Bus voltage angles are assumed to remain constant during the optimization process.
2) Voltage varies only with respect to reactive power variation, therefore, the Jacobian matrix is decoupled.
3) The load remains constant during control.

Due to those assumptions, the VVC problem in *P*-*Q* decoupled form is:

$$minP_{loss} = \sum G_{ij} \left[V_i^2 + V_j^2 - 2V_iV_j\cos(\delta_i - \delta_j)\right] \quad (4.23)$$

subject to:

$$\Delta Q_i = Q_i^{sp} - Q_i(x) = 0 \quad (4.24)$$

$$V^{min} \leq V \leq V^{max} \quad (4.25)$$

$$Q_{SST}^{min} \leq Q_{SST} \leq Q_{SST}^{max} \quad (4.26)$$

In the centralized VVC, the original problem is linearized with respect to both state variables and control variables, but in this decoupled formulation, it is only linearized with respect to system voltages. For a distribution system with *n* nodes, the objective function is linearized by calculating the partial derivative of the original problem with respect to voltages at buses i and j for every feeder:

$$\Delta P_{loss} = \left[\frac{\partial P_{loss}}{\partial V_1} \frac{\partial P_{loss}}{\partial V_2} \dots \frac{\partial P_{loss}}{\partial V_n}\right] \begin{bmatrix} \Delta V_1 \\ \Delta V_2 \\ \vdots \\ \Delta V_n \end{bmatrix} = M[\Delta V] \tag{4.27}$$

where

$$\begin{cases} \dfrac{\partial P_{loss}}{\partial V_i} = 2G_{ij}\left[V_i - V_j \cos(\delta_i - \delta_j)\right] \\ \dfrac{\partial P_{loss}}{\partial V_j} = 2G_{ij}\left[V_j - V_i \cos(\delta_i - \delta_j)\right] \end{cases} \tag{4.28}$$

Loss sensitivities are re-evaluated at the current operating state of the system at the end of every iteration in the optimization process. Hence, the real power-loss increment ΔP_L is related to the bus voltages changes.

The control variables of the system are the reactive power generation at the nodes where the SSTs are connected. Generally, variations in reactive power injections are represented as a function of voltage fluctuations at the same bus. So, sensitivities with respect to the control variables are calculated. Then, the relationship between the voltage variation and changes of reactive power injections are written as follows:

$$\Delta Q = \left[\frac{dQ}{dV}\right]\Delta V = J\Delta V \tag{4.29}$$

Then, the linearized Volt/Var optimization problem in general form is as follows:

$$min \Delta P_L = M\Delta V \tag{4.30}$$

subject to:

$$\Delta Q^{min} \le \Delta Q = J\Delta V \le \Delta Q^{max} \tag{4.31}$$

$$\Delta V^{min} \le \Delta V \le \Delta V^{max} \tag{4.32}$$

Where ΔQ^{min} and ΔQ^{max} are the lower and upper limitation of the step change of reactive power injection at each iteration. ΔV^{min} and ΔV^{max} are the lower and upper limitations, respectively, of voltage variation at each iteration. The control variables for this optimization are the reactive power injection from the SSTs. The inequality constraints are for the nodes where the SSTs are connected. Note that not all nodes in the power distribution system are connected with loads and SSTs; thus, not all nodes are capable in reactive power injections. Therefore, at the nodes where no SSTs are available, the lower and upper limitation of the reactive power variation should be set to a very small value so that they can be ignored.

In order to apply DW decomposition to the inequality constraint, equation (4.31) is modified to the following form:

$$\begin{bmatrix} \dfrac{dQ}{dV} \\ -\dfrac{dQ}{dV} \end{bmatrix} \Delta V \le \begin{bmatrix} \Delta Q^{max} \\ -\Delta Q^{min} \end{bmatrix} \tag{4.33}$$

In the DW decomposition method, system equations have to be decomposed according to the relationships among control areas in the system. DW partitions the system-wide goal into small subproblems based on a linearized formulation. The constraints that represent the links between bus voltages within a specific area will form a subproblem. Any bus within an area that has a link to buses outside that area forms a linking constraint (LC). Then, the solution procedure is based on the decomposition of system equations according to the available number of areas in the power system [46].

Given the inherent characteristics of a power distribution network, the radial topology can be naturally partitioned into different control areas by grouping the nodes on the same feeder. As shown in Figure 4-6, the main feeder can form a sub-area, while all the laterals themselves can be viewed as coupled with the main feeder at the common coupling node. Therefore, the linearized LP problem can be easily turned into a form to which the DW decomposition technique can be applied.

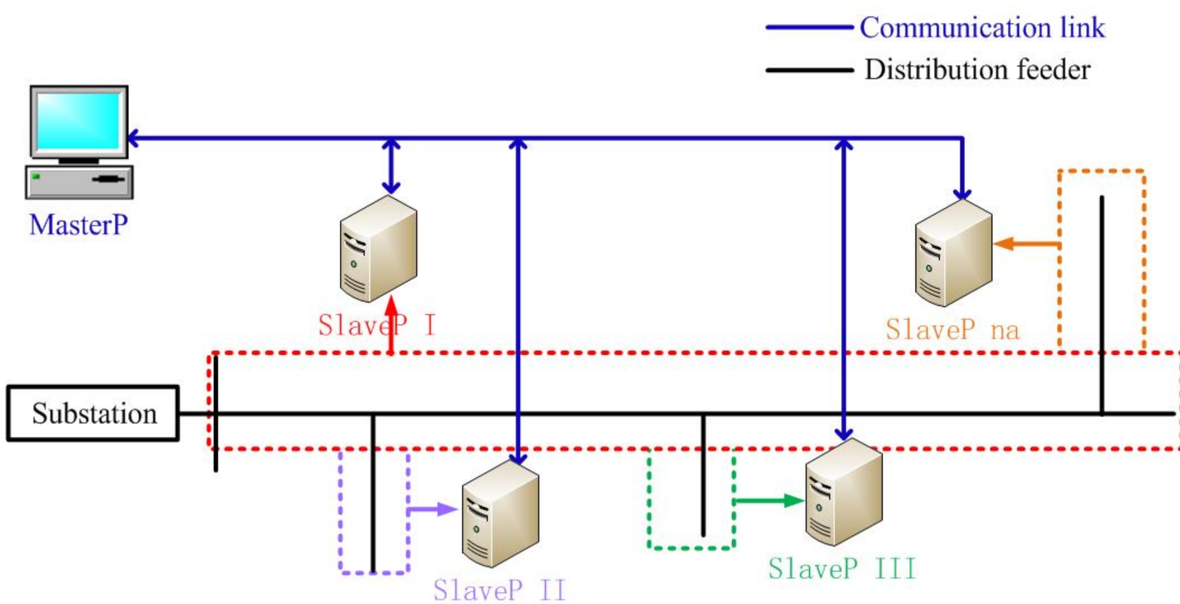

Figure 4-6 Real-life implementation of VVC in a parallel fashion

Given an n node system, suppose there are na control areas. Each area has its own control center, which is responsible for finding the optimal operating point of that area. For area number i, let I_i represent the number of internal buses and C_i represent the number of coupling buses with the other areas.

$$min \frac{\partial P_L}{\partial V_1} \Delta V_1 + \frac{\partial P_L}{\partial V_2} \Delta V_2 + \cdots + \frac{\partial P_L}{\partial V_{na}} \Delta V_{na} \tag{4.34}$$

subject to:

$$L_1 \Delta V_1 + L_2 \Delta V_2 + \cdots + L_{na} \Delta V_{na} \leq b_0 \tag{4.35}$$

$$\begin{bmatrix} A_1 & & & \\ & A_2 & & \\ & & \cdots & \\ & & & A_{na} \end{bmatrix} \begin{bmatrix} \Delta V_1 \\ \Delta V_2 \\ \vdots \\ \Delta V_{na} \end{bmatrix} \leq \begin{bmatrix} b_1 \\ b_2 \\ \vdots \\ b_{na} \end{bmatrix} \tag{4.36}$$

$$\Delta V_i^{min} \leq \Delta V_i \leq \Delta V_i^{max}, i = 1, \ldots, na \tag{4.37}$$

where L_i is the coefficient matrix that corresponds to linking constraints of area i and A_i is a coefficient matrix that corresponds to the subproblem i of area i.

The left-hand side ratio matrix of equality constraints is now in block angular form. The DW decomposition scheme can then be applied to the equality constraints to partition the original large-scale LP into multiple smaller ones that are coordinated by a set of coupling constraints. Following the general DW decomposition technique, the subproblems can be written in the following form:

$$min (M_i - \omega_i L_i) \Delta V_i \tag{4.38}$$

subject to:

$$A_i \Delta V_i \leq b_i \tag{4.39}$$

$$\Delta V_i^{min} \leq \Delta V_i \leq \Delta V_i^{max}, i = 1, \ldots, na \tag{4.40}$$

And the master problem is then in the following form:

$$\min_{\lambda} \sum_{\lambda} (P_{L,i} + P_{L,ij}) \lambda_i \tag{4.41}$$

subject to:

$$\sum L_i \Delta V_i^* \leq b_0 \tag{4.42}$$

$$\sum_{\lambda} \lambda_i = 1 \tag{4.43}$$

$$\lambda_i \geq 0 \tag{4.44}$$

4.2.3 Decentralized VVC Scheme

After DW decomposition, the new formation of the problem can be solved in an iterative process where at each step the subproblems are solved separately. The master problem, which contains the coupling constraints, will be solved by the revised simplex method.

Given an initial feasible state and targeted voltage regulation range ($\pm 5\%$ derivation from rated value), the upper and lower bounds of voltage variation can be easily determined using the following set of equations.

$$\begin{cases} \Delta V_i^{max} = 1.05 - V_i \\ \Delta V_i^{min} = 0.95 - V_i \end{cases} \tag{4.45}$$

At any steady-state operating point, the sensitivity Jacobian matrix of reactive power with respect to system voltage can be calculated:

$$\Delta Q = J \Delta V \tag{4.46}$$

where:

$$\begin{cases} \dfrac{\partial \Delta Q_i}{\partial V_j} = V_i (G_{ij} \sin\theta_{ij} - B_{ij} \cos\theta_{ij}) \\ \dfrac{\partial \Delta Q_i}{\partial V_i} = -2V_i G_{ii} + \sum_{j \neq i} V_j (G_{ij} \sin\theta_{ij} - B_{ij} \cos\theta_{ij}) \end{cases} \tag{4.47}$$

At each iteration, there is a certain range to limit the step change of reactive power injection for each SST:

$$\Delta Q^{min} \leq \Delta Q = J\Delta V \leq \Delta Q^{max} \tag{4.48}$$

This can also be written in the following form:

$$\begin{bmatrix} J \\ -J \end{bmatrix} \Delta V \leq \begin{bmatrix} \Delta Q^{max} \\ -\Delta Q^{min} \end{bmatrix} \tag{4.49}$$

By identifying the coupling constraints and inner constraints for each subproblem, the Jacobian matrix can then be modified to be block angular form; therefore, all the information needed for each subproblem is now available. The subproblems can then be solved individually. If the initial optimal solution for the i^{th} subproblem is represented by ΔV_i^0, then the initial optimal solution for the primal problem is:

$$\Delta V^0 = [\Delta V_1^0, \Delta V_2^0 \ldots \Delta V_{na}^0] \tag{4.50}$$

Substitute the optimal solution in the following equation to get the reduced cost for the current iteration:

$$\text{Redcost}^i = M^i \Delta V^i - \alpha_i \tag{4.51}$$

where $\alpha_0 = 0$ at the first iteration and will be updated in the simplex tableau for the following iterations.

Convergence check to see whether the reduced cost is small enough:

$$\mathrm{Redcost}^0 < \varepsilon \tag{4.52}$$

If the criteria is satisfied, the current solution found is the optimal. Otherwise, it means the current solution is not optimal. In order to find the optimal solution, the revised simplex method is used to solve the master problem by forming the simplex tableau to determine which column will exit the basis and which one will enter.

Assume L is a matrix of size $m \times n$, which means there are m linking constraints in the n node system. The right-hand side (RHS) of linking constraints, b_0, is an $m \times 1$ vector. Similar to the simplex method, introduce slack variables into each linking constraint to convert the inequality constraints to equality and calculate a starting basis. The corresponding basis of the master linking constraints is an identity matrix of size $m \times m$.

$$S_0 = I_{m\times m} = \begin{bmatrix} 1 & \cdots & \\ \vdots & \ddots & \vdots \\ 0 & \cdots & 1 \end{bmatrix} \tag{4.53}$$

Since the unified equation is already equality-constrained, there is no need to introduce a slack variable. At the first iteration, there is only one weighted factor, λ_1. By considering the ratios for weight factors at the initial point, the starting basis of the master problem is an identity matrix of size $(m+1) \times (m+1)$.

$$B_0 = \begin{bmatrix} S & 0 \\ 0 & \lambda_1 \end{bmatrix} = \begin{bmatrix} 1 & \cdots & 0 \\ \vdots & \ddots & \vdots \\ 0 & \cdots & 1 \end{bmatrix} \tag{4.54}$$

By considering the unified equality constraint, the structure of coupling constraints for the master problem is shown in Figure 4-7.

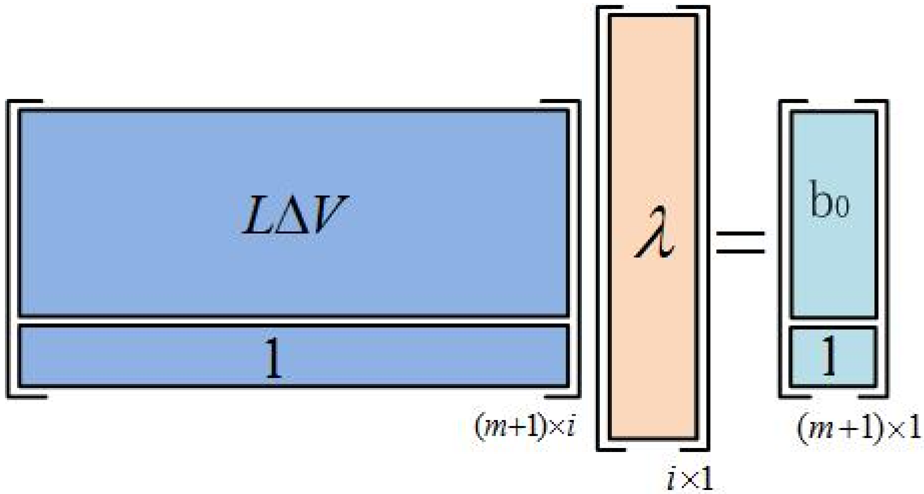

Figure 4-7 Matrix illustration of coupling constraints

Then, the column that is going to enter the basis, named entering column (EC), can be generated using the following equation:

$$EC = \begin{bmatrix} L\Delta V^0 \\ 1 \end{bmatrix} \tag{4.55}$$

where EC is an $(m + 1) \times 1$ vector.

For the initial point, the ratio vector is simply a $1 \times (m + 1)$ zero vector. Then, the formation of a simplex tableau is shown in Figure 4-8.

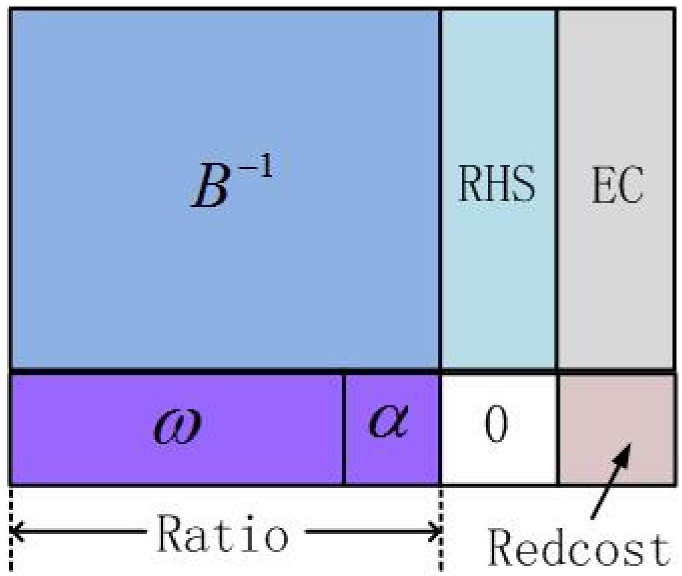

Figure 4-8 Structure of simplex tableau

where B^{-1} is the inverse of the current basis, RHS is the right-hand side of the relaxed equality constraint, and EC is the entering column calculated using the equations.

The ratio vector is initialized as a zero vector and will be updated in the simplex tableau for the iterations that ensue. The reduced cost is calculated using the equation in (4.51).

Since the current optimal doesn't satisfy the convergence criteria, the column that is going to the exit basis needs to be determined. In order to find the pivot element, another parameter is needed:

$$\theta = \mathrm{RHS}/\mathrm{EC} \tag{4.56}$$

where θ is an $(m+1) \times 1$ vector and each element is calculated by dividing the element's RHS by the corresponding one in the EC.

The rule to pick up the pivot element is to find the smallest positive element in θ. After pivoting the chosen element, the corresponding EC element will become 1 and all the other elements in the EC will be 0. At the same time, a new weight is generated at the corresponding RHS, and the ratio vector is updated, too. At this point, a security check is necessary to make sure that the unified equation is satisfied:

$$\sum_{\lambda} \lambda_i = 1 \tag{4.57}$$

In order to better illustrate the pivot process, a fake example is used here. For an optimization problem with three linking constraints, the B^{-1} of the initial table will be a 4×4 matrix where the first three columns correspond to the linking constraints and the fourth column corresponds to the unified equation with respect to λ_i. For the first iteration, since there is only one weight, the RHS of the weight is 1. Then, with the given RHS vector and EC, θ can be easily calculated using the equation. As a result, the smallest positive element in θ can be determined. The corresponding element in EC will be the pivot element, which is also the column for the exit basis. The decision-making process is illustrated in Figure 4-9(a).

Once the pivot element is found, the simplex tableau needs to be pivoted with respect to the exit column by adopting the Gaussian Elimination method. After the pivot, the pivot element in EC will be 1 and all the other elements in the EC will be 0, where the corresponding row in the matrix B^{-1} is now named λ_2. Following the security check $\lambda_1 = 0.9$ and $\lambda_2 = 0.1$, so the equation is satisfied. At the same time, the ratio vector is updated where the information of ω and α are now available to update the subproblem.

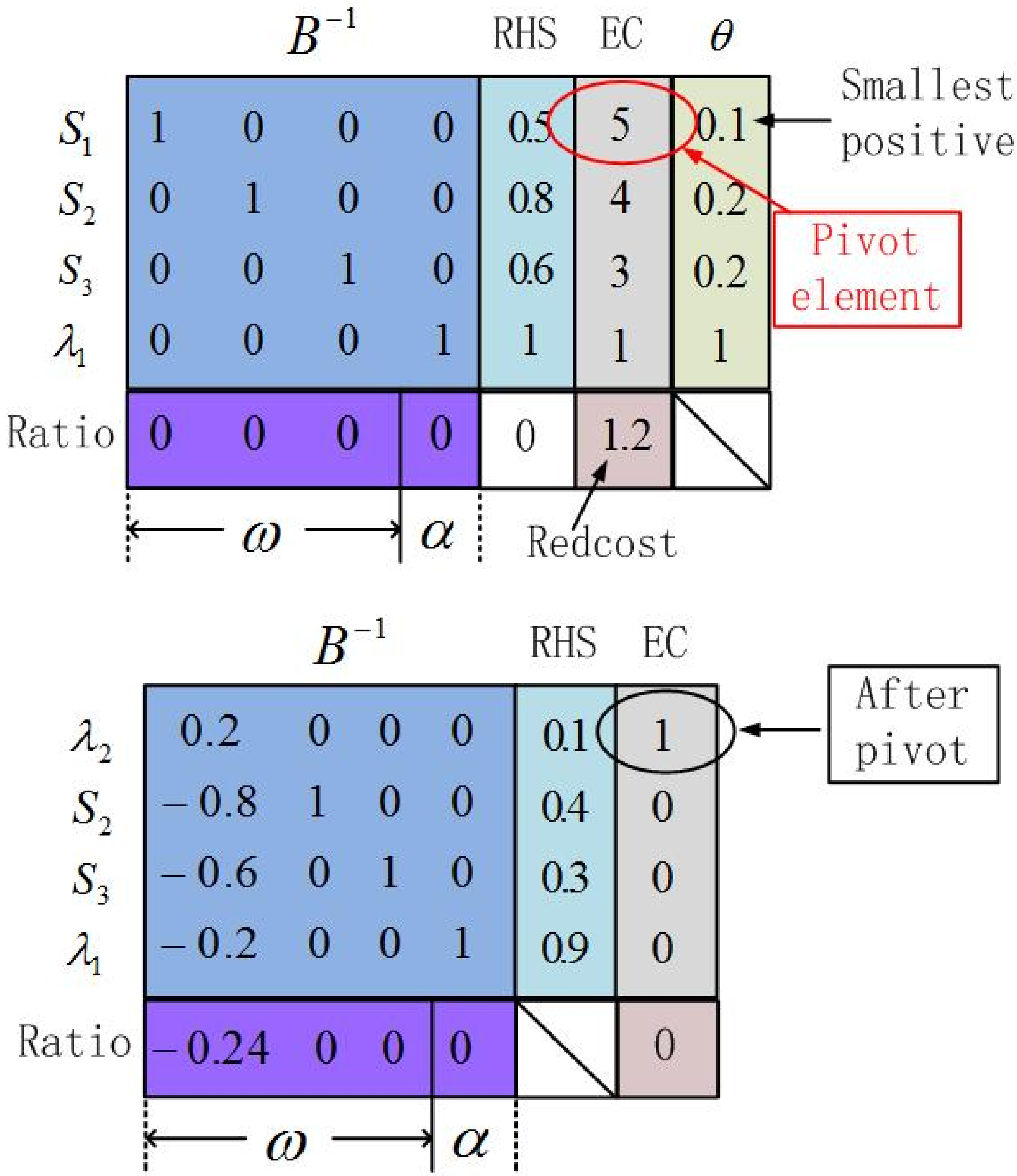

Figure 4-9 Pivot process illustration: (a) original simplex tableau, and (b) simplex tableau after pivot

If the equality constraint is satisfied, we can process the following step. Otherwise, there must be something wrong in the iterative process. In the following, the objective function of the master problem needs to be updated with ω and α, the new objective is defined as:

$$min(M - \omega L)\, \Delta V - \alpha \tag{4.58}$$

which means that the ratio of the objective function is updated using the following equation:

$$M^{new} = M^{old} - \omega L \tag{4.59}$$

Then, the objective for each subproblem can be determined accordingly using the new master objective function and returns to the iterative process where the optimal for each subproblem needs to be found.

The flowchart of the DW optimization is:

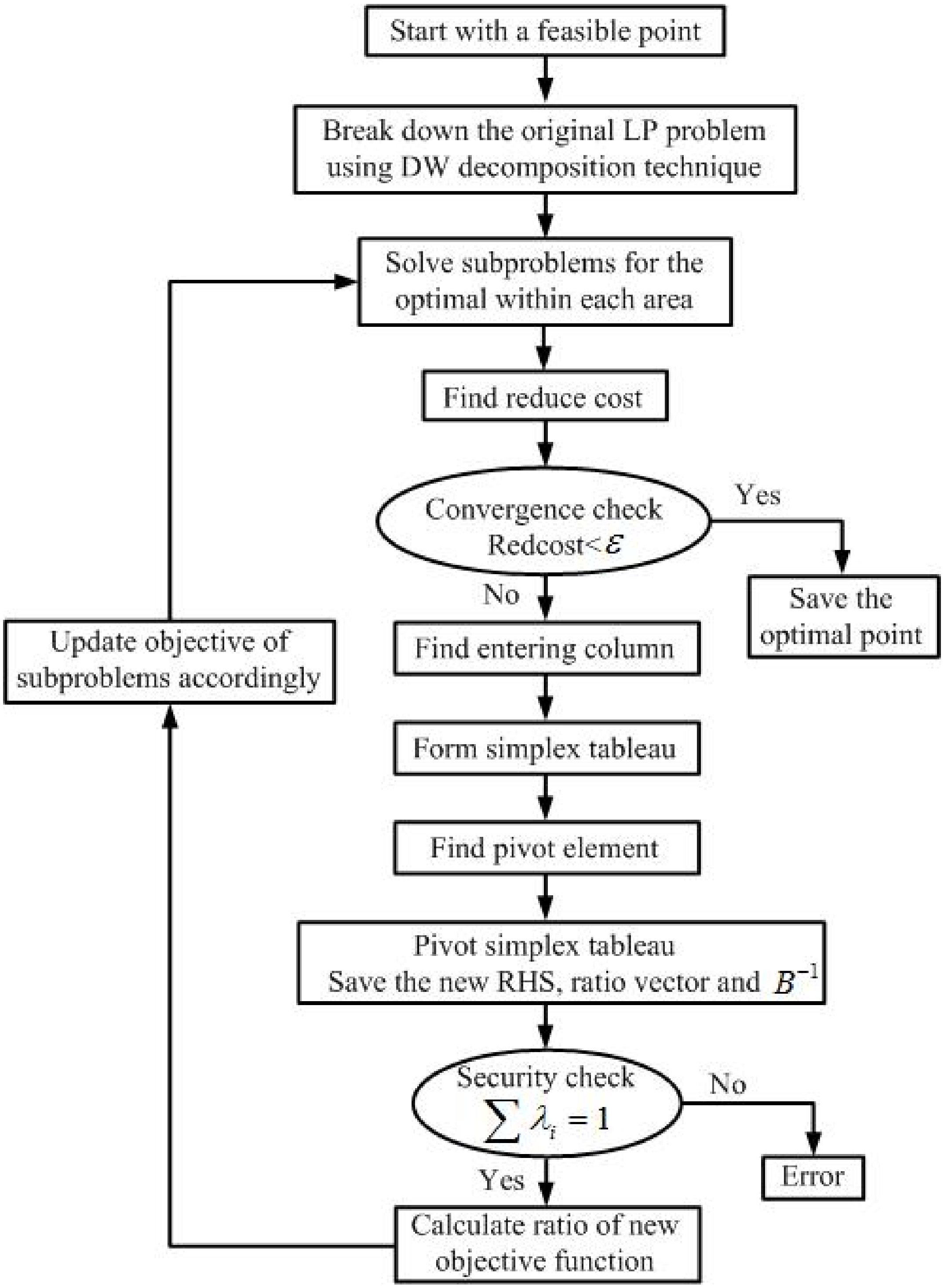

Figure 4-10 Flowchart of the DW optimization

After applying the DW technique to solve the originally large-scale LP in a decomposed and parallel fashion, the expected variations of voltage in order to minimize system power loss are returned. Therefore, the corresponding reactive power injection change can be calculated using the following equation:

$$\Delta Q = J\Delta V \tag{4.60}$$

Note that the voltage variation vector contains the voltage of every node in the power distribution system. Therefore, the calculated reactive power variation vector also contains the step-change information for all the nodes. But not all nodes are connected to SSTs; thus, some of them cannot inject reactive power, so ΔQ also contains information with respect to those non-SST nodes. So, the SST nodes need to be identified from ΔQ:

$$\Delta Q = [\Delta Q_{SST}, \Delta Q_{noSST}] \tag{4.61}$$

Then the current reactive power injection at the node where the SSTs are connected can be updated using the following equation:

$$Q_{SST}^{new} = Q_{SST}^{old} + \Delta Q_{SST} \tag{4.62}$$

The new reactive power information at each node will be updated and result in a new system operating point. A convergence check needs to be done to minimize power loss. If the criteria are satisfied, save the current settings as the optimal point where the lowest power loss can be achieved within the feasible voltage range. Otherwise, go back to the DW optimization solver to find a new optimal until the criteria are satisfied. The full version of the DW decomposition-based VVC optimization process is shown in Figure 4-11.

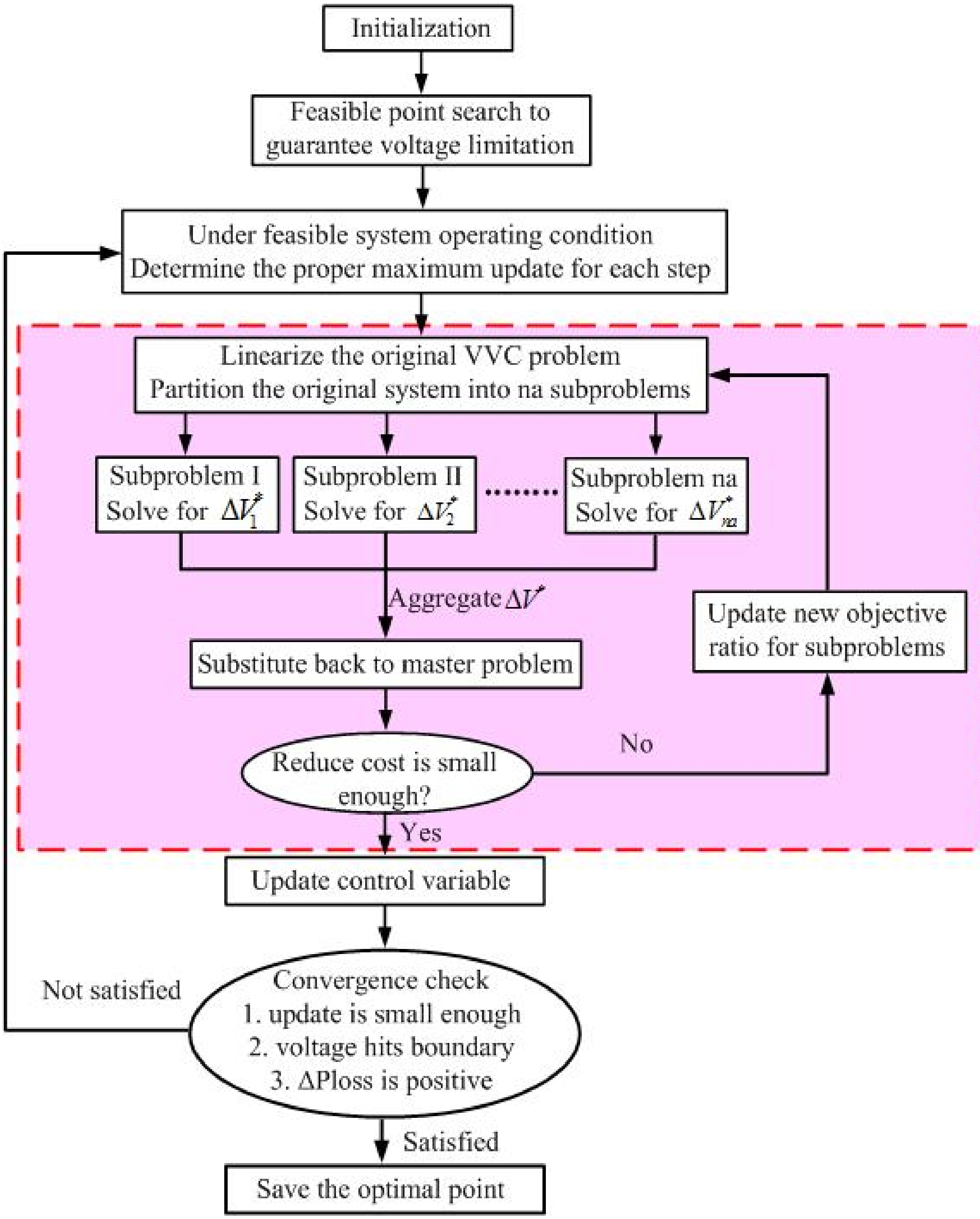

Figure 4-11 The DW decomposition-based VVC optimization

As shown in Figure 4-11, a parallel computation of subproblems is now possible given the fact that the original large-scale optimization problem is now partitioned into smaller subproblems using the DW decomposition technique. Under the guidance of a master problem, the subproblems will work on regulating voltages within their own areas while achieving the system-wide optimization goal. The parallel computation process based on DW decomposition is highlighted in Figure 4-11. In real-life implementation, the master processor would sit at the substation to perform as a part of the distribution automation system. While slave processors can sit at their own control areas and monitor the instant system state variables and save to local disk. In a control cycle, slave processors will first find a temporary optimal with respect to the current subproblem objective. Those temporary optimals will then be passed to the master processor to determine whether the system-wide goal can be achieved. In case a boundary mismatch occurs, the master processor will find new objective ratios for each sub-area and send them back to the slave processors. The whole process is shown in Figure 4-6, in which the black solid line represents the power grid and the blue solid line represents the communications link between the master processor and the slave processors. Slave processors are responsible for collecting system information, such as node voltages and the real and reactive power at each node. After determining its own optimal, the information sent by each slave processor to the master processor is voltage variations. When the new objective ratio is established, the master processor will send the new ratio back to each slave processor. Therefore, the communications infrastructure here should be able to provide two-way information flow. Figure 4-12 is provided here in order to illustrate the information exchange better.

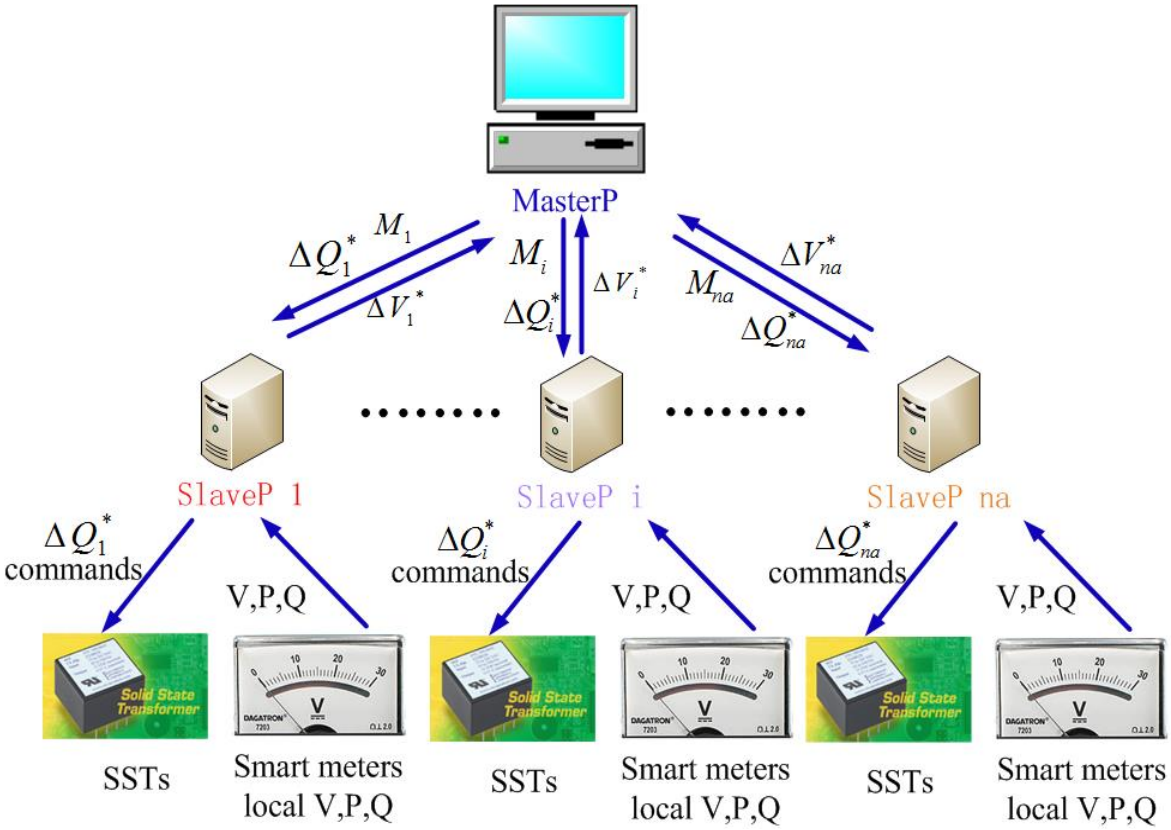

Figure 4-12 Information exchange of the real-life implementation

As shown in Figure 4-12, once the system-wide optimization goal is reached, the master processor will send the optimal reactive power injection settings for each subproblem back to each local controller. Then, the reactive power command will be received by all the SSTs throughout the system to regulate the voltage within acceptable limits while minimizing the system's power loss.

4.3 Decentralized VVC Test Results and Analysis

In order to show the effectiveness of the DW-based decentralized VVC optimization, the FREEDM IEEE 34 Node test feeder and the Residential Notional System are used. Given the different characteristics of those two test systems, the different control effect will be demonstrated later.

Assume that the dispatch time interval for the VVC application is t_{cont_int}. Each time the VVC application receives a new set of measurements, the decentralized VVC will work on regulating the voltage profile and minimizing system losses. Let t_{vvc_resp} represent the response time for the VVC application to finish finding the optimal point and send back the control commands. The system operating condition within t_{vvc_resp} is assumed to be the same. Therefore, the VVC performs as a deterministic control scheme every time it's called.

As shown in Figure 4-13, the two series loading scenarios are considered in the following:

1) Case 1: Heavy load conditions. Using the same load condition as in the centralized VVC, which is the given default peak load of the IEEE 34 Node system.
2) Case 2: A 10% load increase. Assume that the next system status measured results from a 10% load increase, compared to the previous system operating condition.

In the following study, the initial status of the SSTs in the heavy load condition is set to the default value, where the primary side measurements of the SSTs are the unit power factor. As shown in the centralized VVC, a heavy load with no reactive power injection from the SSTs will result in an extremely low voltage in the FREEDM IEEE 34 node system. After voltage regulation and power-loss minimization of the VVC application, the first test case will provide a baseline for the next operation. Therefore, in the following test case, although the real power load increases by about 10%, the measured voltage profile will not drop below the targeted voltage limitation. Details about the test results will be provided and discussed in the rest of the chapter.

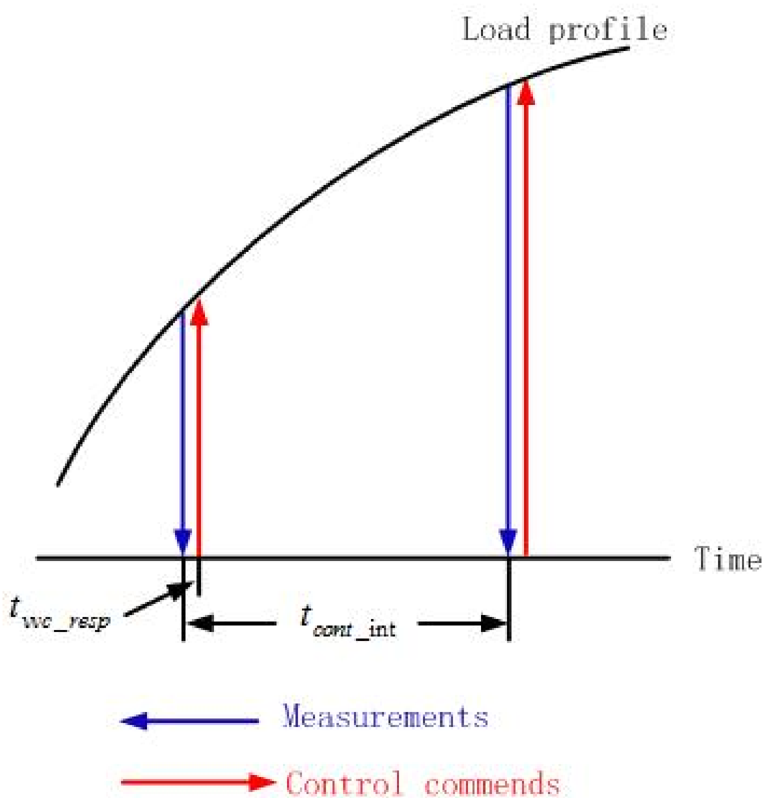

Figure 4-13 Illustration of the control dispatch scheme

4.3.1 Test on the FREEDM IEEE 34 Node System

In the following, the DW decomposition method is applied to the VVC optimization of the FREEDM-type IEEE 34 system, where the constraints need to be formed in block angular form. The system is decomposed according to the properties of the designated areas in the power network. Buses that are controlled by the same control center are said to be within the same area. Constraints that represent links between bus voltages within a specific area will form a subproblem. Any bus within an area that has a link to buses outside the area will form the linking constraints.

Take Phase A of the IEEE 34 system as an example. There are one main feeder and five lateral feeders, which will result in six subsystems. The initial partition of the system is illustrated in Figure 4-14. Then, each control area has one control center, which is responsible for the Volt/Var optimization and control of that area.

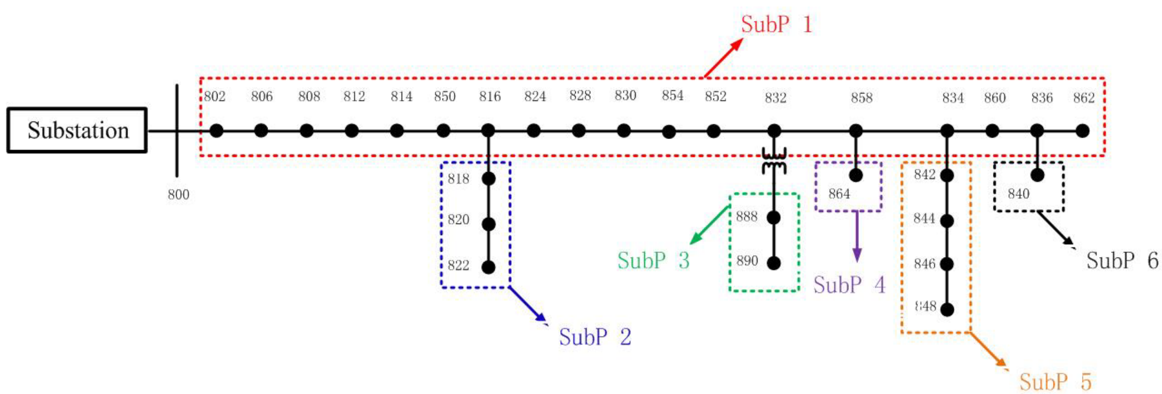

Figure 4-14 Partition of Phase A of IEEE 34

For area i, let N_i resend the total number of buses, where B_i buses are not connected to other areas, and let C_i represent the number of buses linking with other areas. Based on the system structure above, the following bus data can be easily obtained:

Table 4-2 Bus information after Area partition of Phase A of the IEEE 34 system

Area #	N_i	B_i	C_i
1	18	13	5
2	3	2	1
3	2	1	1
4	1	0	1
5	4	3	1
6	1	0	1

In order to organize the constraints in block angular form, first put the linking buses at the beginning and then put the buses within each area as a sequence [69], [70]. The new sequence is better illustrated in Figure 4-15. Note that there is only one node in both area 4 and area 6. Therefore, the only node is a linking node and can be moved to the top of the matrix as a linking constraint. For areas 4 and 6, there is no inner node for their own areas. The method to deal with those areas will be described later.

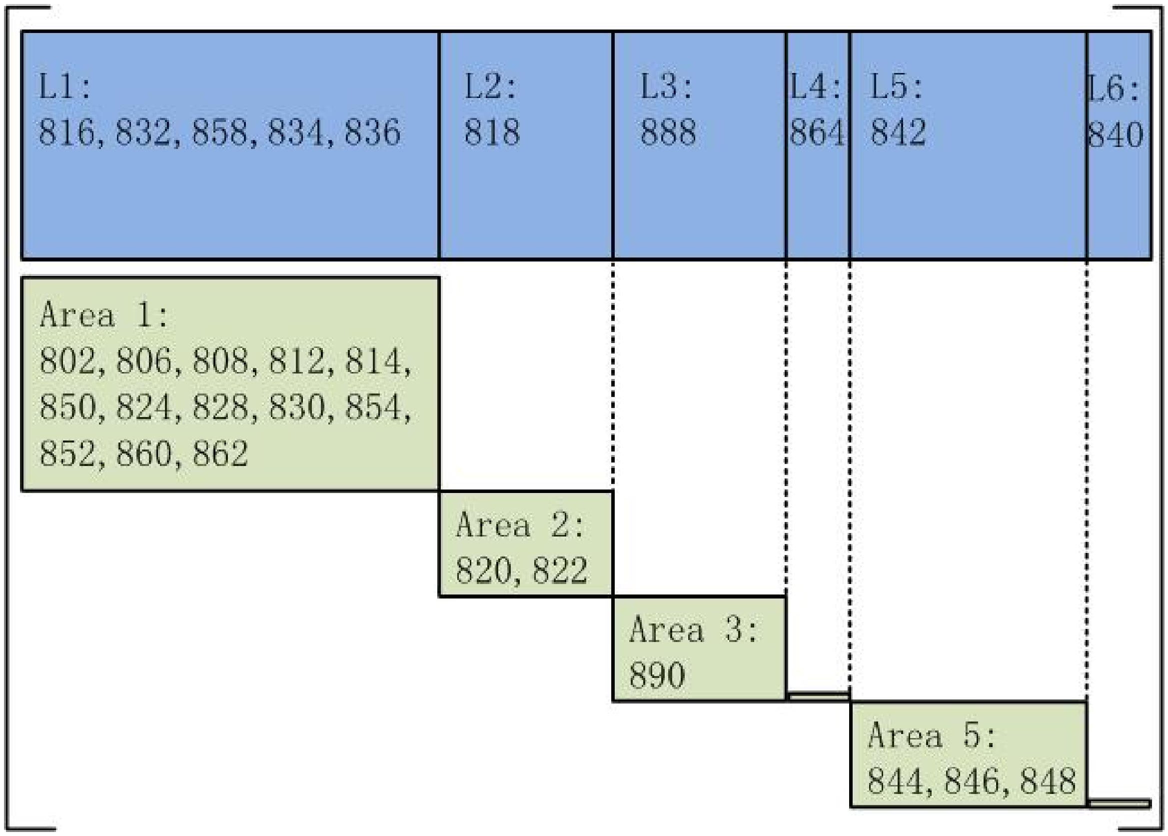

Figure 4-15 Phase A of the IEEE 34 system in block angular form

Based on the area partition, the VVC optimization that aims at minimizing system loss while regulating voltages can be written in a more explicit fashion, as shown in Figure 4-16. According to the problem formulation in equation (4.30), the following equation can be reached:

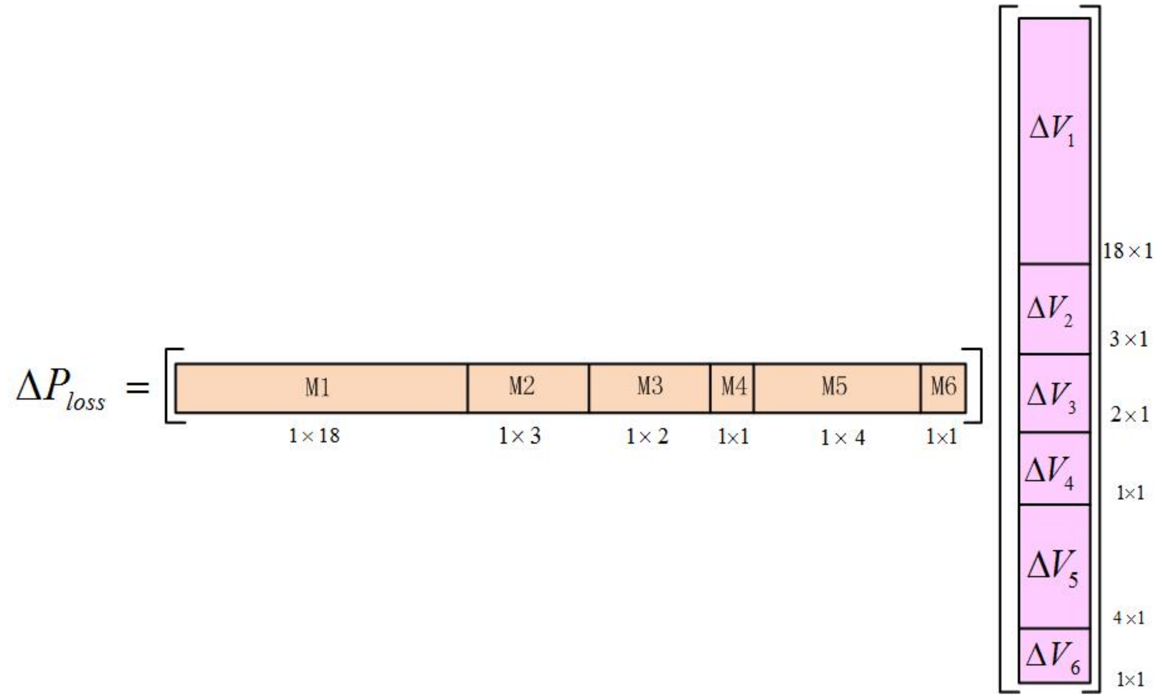

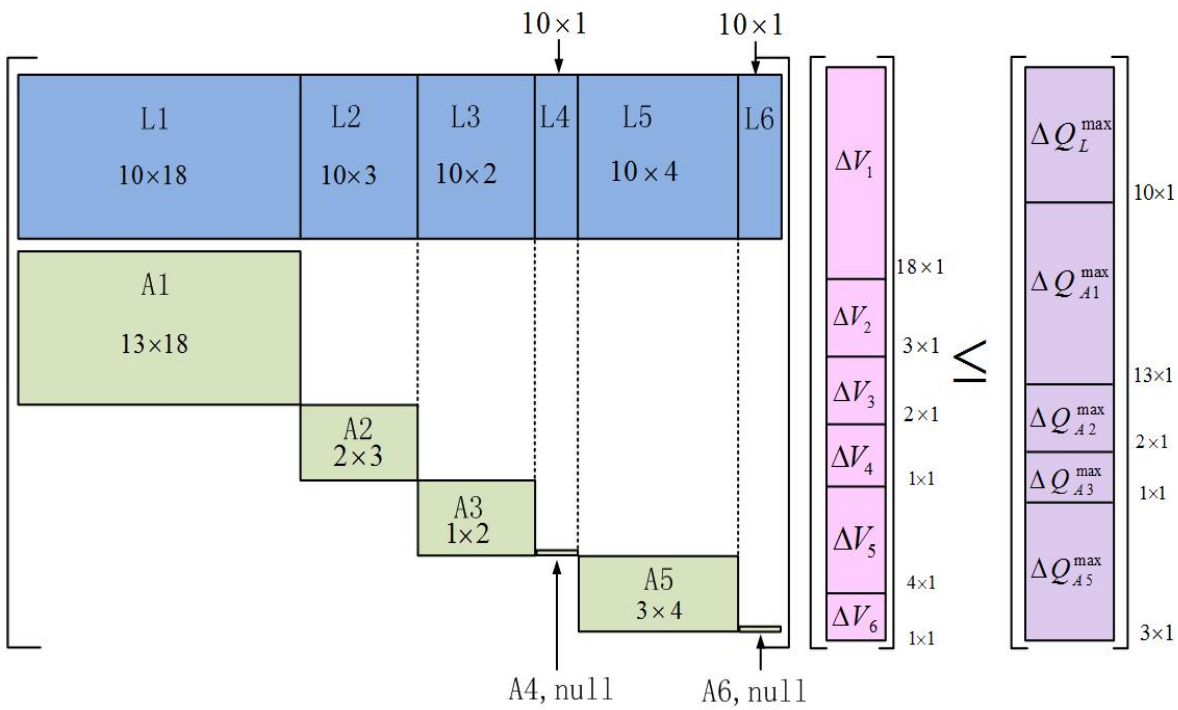

Figure 4-16 The IEEE 34 explicit matrix expression: (a) objective, and (b) constraints

As shown in Figure 4-16 (a), the partition of the objective is based on area, where the sizes of the objective vectors and the control variable vectors are marked in the figure. Both of those vectors are in the size of N_i. When looking at the constraint matrix, since there are 10 linking nodes, the set of linking constraints are in the size of 10×29, where 29 is the total number of buses in the whole system. The size of the inner constraint of the i^{th} area is in the form of $B_i \times N_i$. As a result of the row movement on the left-hand side of the inequality constraint, the sequence of the right-hand side needs to be adjusted accordingly. As a result, the reactive power step change limits correspond to those linking constraints is moved upwards to the top of the matrix and is of the size 10×1. The right-hand side of the i^{th} area is in the form of $B_i \times 1$. Note that both the constraint matrix and right-hand side of those areas that have only one node are null.

As indicated in equation (4.48), in order to consider the upper and lower limits of the reactive power step change for each iteration, the original inequality constraint of:

$$\Delta Q^{min} \le J\Delta V \le \Delta Q^{max}$$

can be written as:

$$\begin{bmatrix} J \\ -J \end{bmatrix} \Delta V \le \begin{bmatrix} \Delta Q^{max} \\ -\Delta Q^{min} \end{bmatrix}$$

Similarly as before, the constraints related to the linking nodes will be moved upwards, and the inner constraints within each area need to be grouped together to put the left-hand side matrix in block angular form. As a result, the number of both linking constraints and inner constraints will be double those of the original.

Note that subproblems 4 and 6 don't have inner inequality constraints. Therefore, the only constraint that needs to be considered for those two areas is voltage limitation, which shows them in the following form:

$$min\Delta P_{Li} = (M_i - \omega_i L_i)\Delta V_i$$

subject to:

$$\Delta V_i^{min} \le \Delta V_i \le \Delta V_i^{max}$$

where i corresponds to the areas that only have a linking node. All other areas remain in the same formulation as the equation.

4.3.1.1 Case 1: Simulation and Result Analysis of Peak-Loading Condition

As indicated in Chapter 3, given a limitation on the step size of the LP update, in order for the LP solver to convergence and meet all the limitations on the control variables, the initial starting point of the iteration should be a feasible operating point. Therefore, similar to the centralized VVC, a feasibility search needs to be finished, first to guarantee that the decentralized VVC starts at a feasible solution, and the ΔQ limitation search is also necessary to make sure that the linearization is still accurate after a certain update is applied to the control variables.

Because of the approximation of linearization, the actual system response may differ from the linearized estimation. Therefore, it is necessary to check the mismatch between the actual DPF result and the estimated linearization result. A similar study in the centralized VVC is explained in detail in Figure 3-5. In the decentralized VVC, the result returned by the DW solver is compared with the MATLAB embedded LP solver result in every iteration to check the performance of the DW decomposition approach. The comparison of the $\Delta \mathrm{Q}_{\mathrm{update}}$

of phase A in the first iteration is given in Table 4-3. Besides, the first iteration with an adjusted reactive power limitation ($\Delta \mathrm{Q}^{\mathrm{limit}} = 0.4\mathrm{kVar}$) in the LPOPF is also provided. As ex-explained earlier, the update of the reactive power injection is calculated using $\Delta \mathrm{Q} = \mathrm{J}\Delta \mathrm{V}$ in the decentralized VVC. Therefore, all the nodes have a corresponding $\Delta \mathrm{Q}$ although some of them may not have SSTs and may not be capable of injecting reactive power. On the other side, $\Delta \mathrm{Q}$ is directly given as part of the optimal solution in centralized VVC only for the SST nodes. This is why the no-load node $\Delta \mathrm{Q}$ is not available in centralized VVC.

As indicated in the table, the step-change limitation of the first iteration is $\Delta Q^{limit} = 0.4kVar$. Therefore, the upper and lower limitations for ΔQ_{sst} are 1.2×10^{-4} p.u. and -1.2×10^{-4} p.u., respectively. The scheme used to limit the effect of a no-load node divides the ΔQ_{sst}^{limit} by a large ratio, and the ratio used here is 100. As a result, the upper and lower limitations for the no-load node are 1.2×10^{-4} p.u. and -1.2×10^{-4} p.u., respectively. In order to distinguish the no-load node from the SST node, the node where the SSTs are available is marked in red. From the results shown in the following table, all the returned results from both the DW and LP solvers satisfy the step-change limitation of the reactive power injection. However, the ΔQ_{update} of two nodes, nodes 830 and 854, are different from each other. This may be caused by the different numerical approaches adopted by the DW and LP solvers. The results from both the DW and LP solvers are considered acceptable.

Table 4-3 Comparison of DW and LP returned ΔQ of phase A in the first iteration

Node #	*dQ_min*	*dQ_max*	*dQ_lp_a*	*dQ_dw_a*	*dQ_LPOPF_a*
802	-1.20E-06	1.20E-06	-1.20E-06	-1.20E-06	N\A
806	-1.20E-06	1.20E-06	-1.20E-06	-1.20E-06	N\A
808	-1.20E-06	1.20E-06	1.20E-06	1.20E-06	N\A
812	-1.20E-06	1.20E-06	1.20E-06	1.20E-06	N\A
814	-1.20E-06	1.20E-06	1.20E-06	1.20E-06	N\A
850	-1.20E-06	1.20E-06	1.20E-06	1.20E-06	N\A
816	-1.20E-06	1.20E-06	1.20E-06	1.20E-06	N\A
824	-1.20E-06	1.20E-06	1.20E-06	1.20E-06	N\A
828	-1.20E-06	1.20E-06	1.20E-06	1.20E-06	N\A
830	-1.20E-04	1.20E-04	1.20E-04	7.05E-05	-1.20E-04
854	-1.20E-06	1.20E-06	1.20E-06	7.05E-07	N\A
852	-1.20E-06	1.20E-06	-1.20E-06	-1.20E-06	N\A
832	-1.20E-06	1.20E-06	-1.20E-06	-1.20E-06	N\A
858	-1.20E-04	1.20E-04	-1.20E-04	-1.20E-04	-1.20E-04
834	-1.20E-04	1.20E-04	-1.20E-04	-1.20E-04	-1.20E-04
860	-1.20E-04	1.20E-04	-1.20E-04	-1.20E-04	-1.20E-04
836	-1.20E-04	1.20E-04	-1.20E-04	-1.20E-04	-1.20E-04
862	-1.20E-06	1.20E-06	-1.20E-06	-1.20E-06	N\A
818	-1.20E-06	1.20E-06	1.20E-06	1.20E-06	N\A
820	-1.20E-04	1.20E-04	-1.20E-04	-1.20E-04	-1.20E-04
822	-1.20E-04	1.20E-04	-1.20E-04	-1.20E-04	-1.20E-04
888	-1.20E-06	1.20E-06	-1.20E-06	-1.20E-06	N\A
890	-1.20E-04	1.20E-04	-1.20E-04	-1.20E-04	-1.20E-04
864	-1.20E-04	1.20E-04	-1.20E-04	1.20E-04	-1.20E-04
842	-1.20E-06	1.20E-06	-1.20E-06	-1.20E-06	N\A
844	-1.20E-04	1.20E-04	-1.20E-04	-1.20E-04	-1.20E-04
846	-1.20E-06	1.20E-06	-1.20E-06	-1.20E-06	N\A
848	-1.20E-04	1.20E-04	-1.20E-04	-1.20E-04	-1.20E-04
840	-1.20E-04	1.20E-04	-1.20E-04	-1.20E-04	-1.20E-04

Based at a feasible starting point and the step-change limitation $\Delta Q^{limit} = 0.4kVar$, the DW-based decentralized power-loss minimization iteration is documented in Figure 4-17. The left-hand axis shows the total system power loss, and the right-hand axis is the minimum voltage in the system. As optimization iteration progresses, both the system power loss and voltage decrease until one of the stopping criteria is satisfied.

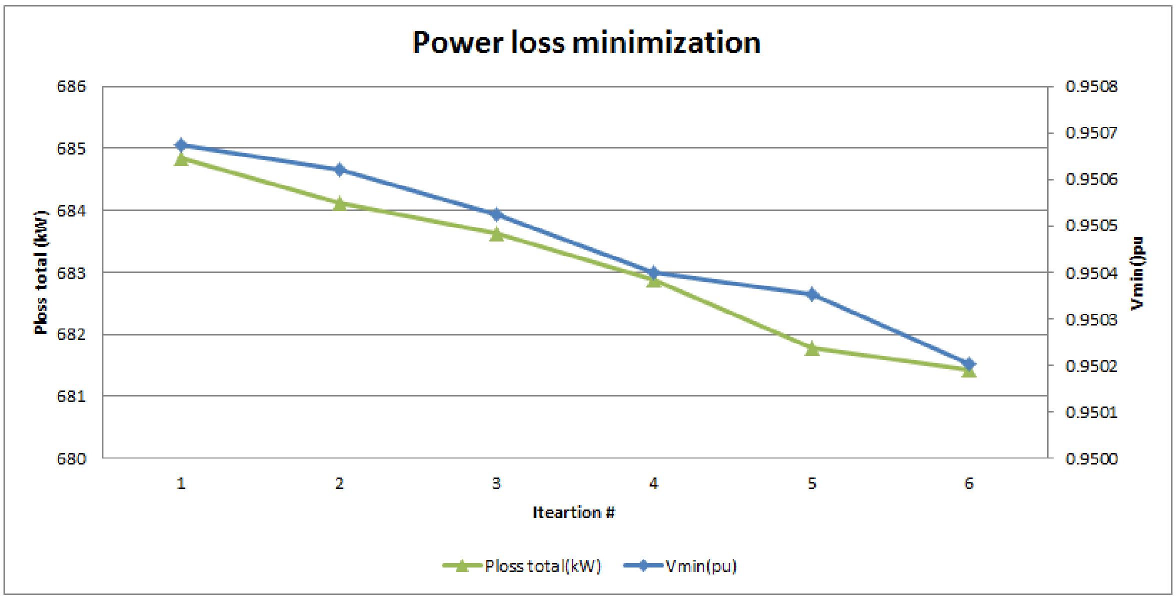

Figure 4-17 Iteration of the DW decentralized power-loss minimization

In order to compare the system voltage profile at the starting feasibility point and after the DW-based decentralized VVC, Figure 4-18 is presented. As shown in the figure, the gradient-based feasibility search brings the voltage back into the feasible region first, where the lowest system voltage has been boosted to 0.9508 p.u. Then, the DW-based decentralized VVC starts to reduce system power loss while maintaining the voltage profile within acceptable limits.

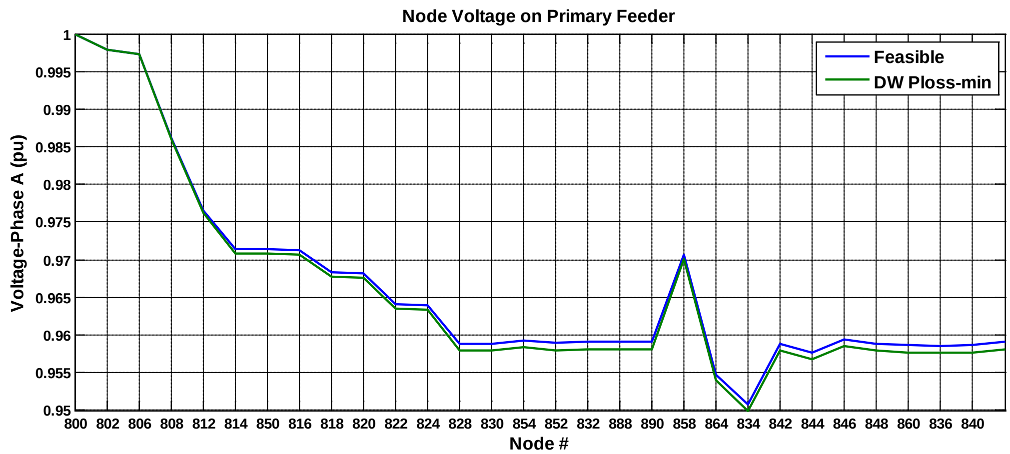

Figure 4-18 Voltage profile comparison of phase A

The reactive power injection at each node to which SSTs are connected is illustrated in Figure 4-19. The blue bar is the reactive power injection needed to boost the voltage back into the feasible region, and the red bar is the reactive power injection at the optimal system operating point.

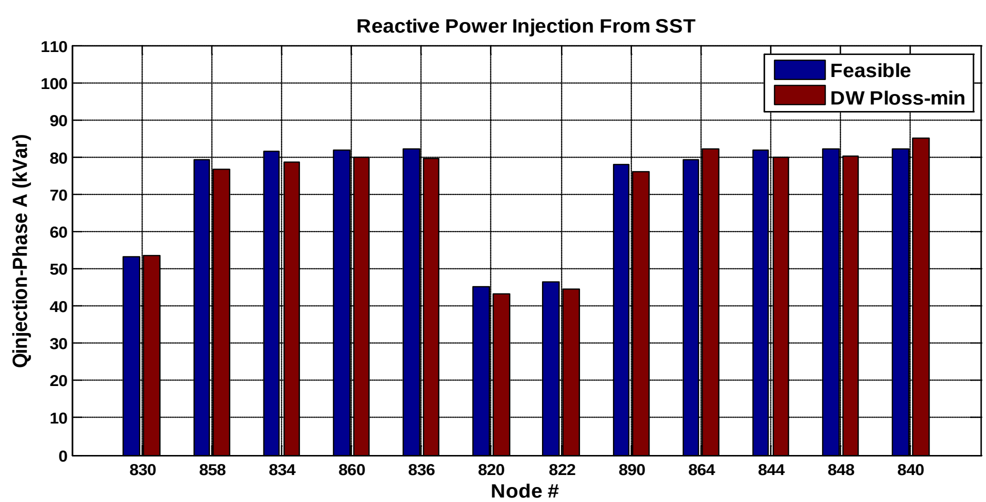

Figure 4-19 Reactive power injection comparison of phase A

Similarly, as in the centralized VVC, the power loss is calculated and documented in all of the optimization stages from the original situation where no VVC is available. As shown in Table 4-4, as well as in the voltage profiles, the power loss is low in the original system condition. Then, a huge reactive power injection is needed to boost the voltage back into the feasible region. At the same time, the system power loss increases dramatically. Then, the DW-based decentralized VVC will work to bring the power loss down.

Table 4-4 Power loss reduction and comparison

Power loss (kW)	*Pa*	*Pb*	*Pc*
Original	92.6352	74.3043	91.1090
After feasibility search	250.5614	191.2031	244.8659
After DW	244.5613	189.8552	242.1170
Reduction	6.0001	1.3479	2.7489
Percentage of reduction	0.023947	0.00705	0.011226

A comparison of the total reactive power injection from the SSTs is also documented in Table 4-5.

Table 4-5 Reactive power injection comparison

Total Reactive Power Injection	*Qa*(kVar)	*Qb*(kVar)	*Qc*(kVar)
After feasibility search	873.7130	790.4567	853.0967
After DW	859.3620	782.3018	845.7590
Reduction	14.3510	8.1549	7.3377
Percentage of reduction	0.0164	0.0103	0.0086

At this point, both the centralized VVC and the decentralized VVC on the IEEE 34 node test feeder have been finished. It is necessary to compare the control effect of these two different approaches. Figure 4-20 and Figure 4-21 are provided here to show the voltage pro-profiles and the reactive power injection along phase A. As shown in Figure 4-20, the voltages in both cases satisfy the "range A" requirement. At some remote nodes, the voltages of the centralized VVC are lower than in the decentralized VVC.

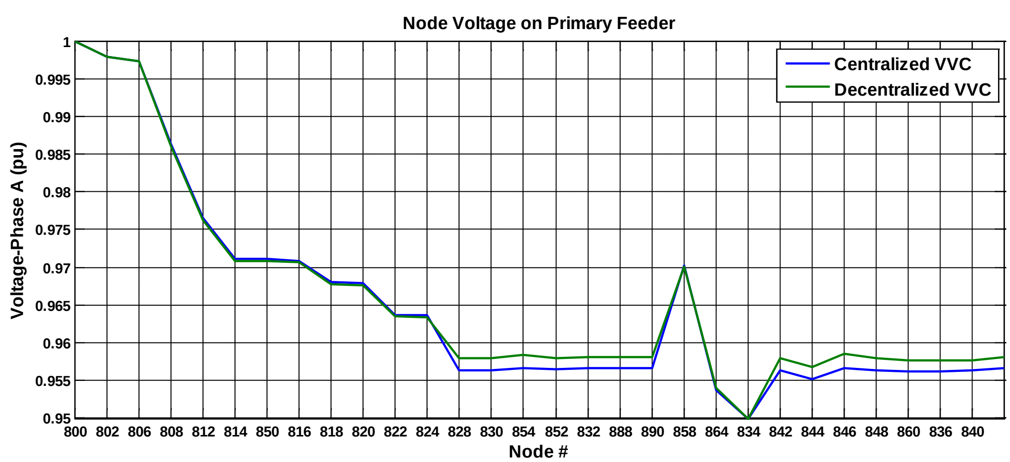

Figure 4-20 Compare the voltage profile of centralized VVC with decentralized VVC

At the same time, the reactive power injection at each SST is also documented in Figure 4-21. The result reflects quite different injection needs at each location. For example, the reactive power injection is about 25kVar more at node 858 in the decentralized case than in the centralized one; but, on the other hand, the reactive power injection is about 15kVar higher at node 848 in the centralized case.

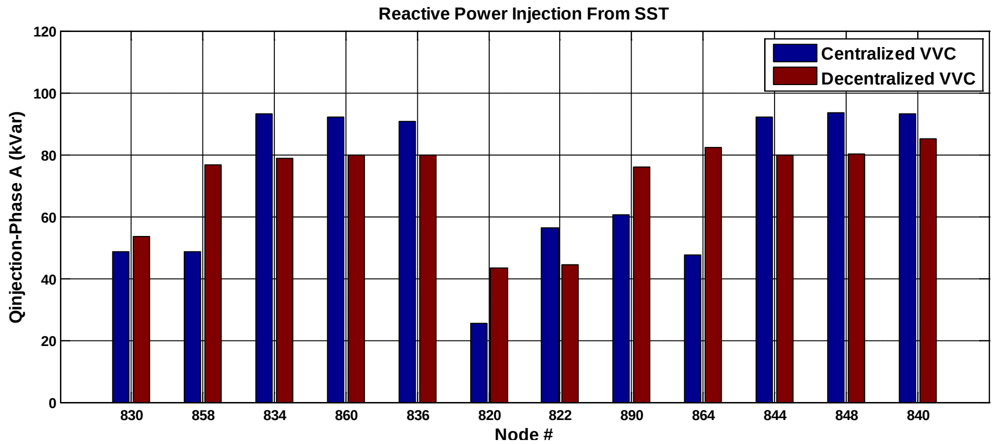

Figure 4-21 Compare the final injection of the centralized VVC with the decentralized VVC

What's more, the power loss and the reactive power injection at each phase are compared in Table 4-6. As shown in the table, the total power loss is about 29kW less in the centralized VVC, and the required reactive power injection is about 84kVar less. Therefore, the control effect of the centralized VVC is better compared to the decentralized approach. The potential reason causing this difference may be: In the centralized VVC, the full Jacobian matrix is used where the effect of the reactive power injection on both voltages and thetas (θ) are considered. But in the decentralized VVC, a decoupled Jacobian matrix is adopted, and, thus, the linearization may lose more accuracy. Therefore, the control effect of the decentralized VVC is not as precise as the centralized VVC.

Table 4-6 Compare power loss and reactive power injection of centralized VVC with decentralized VVC

Power loss (kW)	*Pa*	*Pb*	*Pc*	*Ptotal*
Centralized VVC	235.4325	182.4882	229.1575	647.0782
Decentralized VVC	244.561	189.855	242.117	676.5335

Table 4-6 Continued

Total reactive power injection (kVar)	*Qa*	*Qb*	*Qc*	*Qtotal*
Centralized VVC	841.4245	739.4645	822.2356	2403.1246
Decentralized VVC	859.362	782.302	845.759	2487.4228

4.3.1.2 Case 2: Simulation and Results Analysis in Case of 10% Load Increase

Once the optimal point is found, the deterministic optimization of the VVC is finished. However, the system loading condition varies in daily operations. The VVC application in reality is usually dispatched every 15 minutes to track the new system operating conditions and find a new optimal. The next time the SCADA system monitors system information and sends data to the VVC, assume that the loads increase by about 10% along the feeder. Before the new reactive power injection command is determined and sent to the SSTs, the system voltage with the previous reactive power injection but the new real-power load will result in different values than the previous optimal operating condition, which is shown in Figure 4-22.

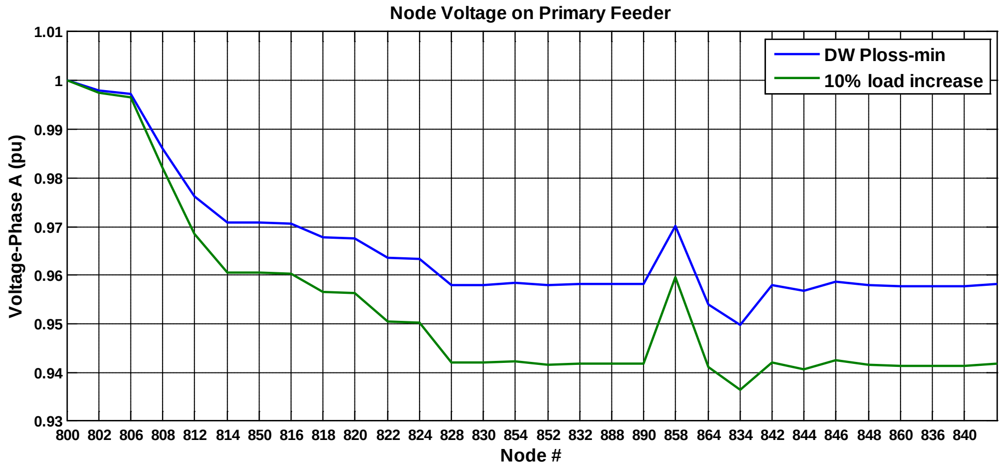

Figure 4-22 Voltage profile comparison of phase A

As shown in the figure, the new system minimum voltage drops to 0.9364 p.u., which is below the lower voltage limitation. Therefore, a new feasibility search procedure is triggered to force the system voltage back, and more reactive power is needed in each node to satisfy the voltage requirements. The new reactive power injection needed for the 10% more loading condition is shown in Figure 4-24. Based on the new feasible point, the DW-based decentralized VVC will work on minimizing the system power loss again to reach a new optimal operating point. The optimization iteration is documented in Figure 4-23. It takes 69 iterations to bring down the power loss while keeping the voltages within limitations.

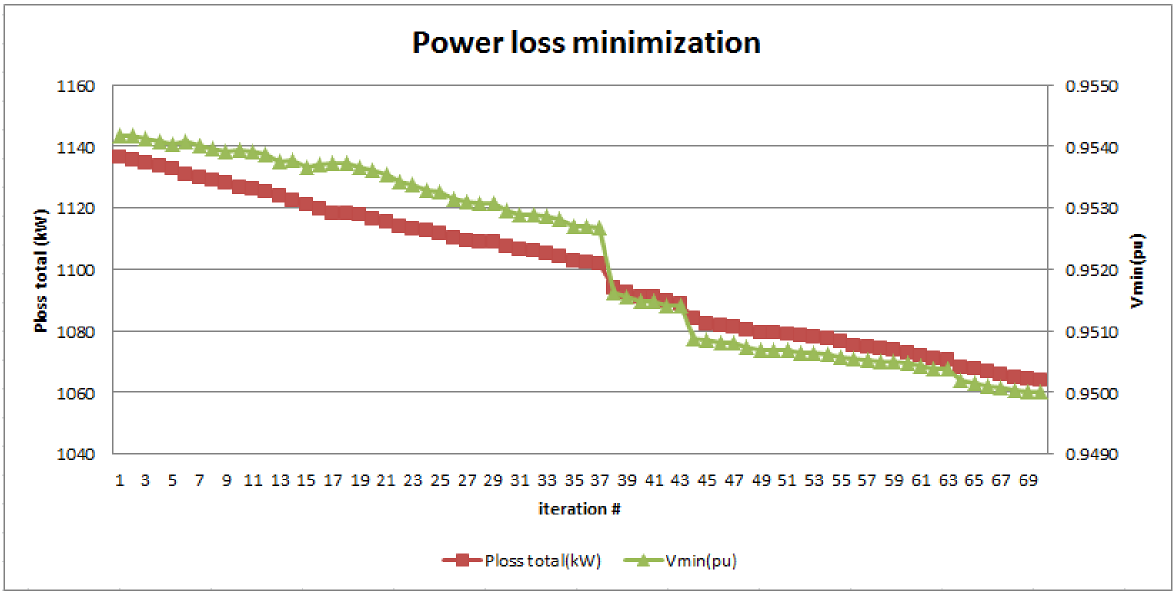

Figure 4-23 Iteration of the DW decentralized power-loss minimization

Then, the new reactive power injection needed for the new optimal operating point is shown in red in Figure 4-24. In order to make a comparison with the initial feasible point, the reactive power injection needed to boost the voltage back into the feasible region is demonstrated in blue in the same figure.

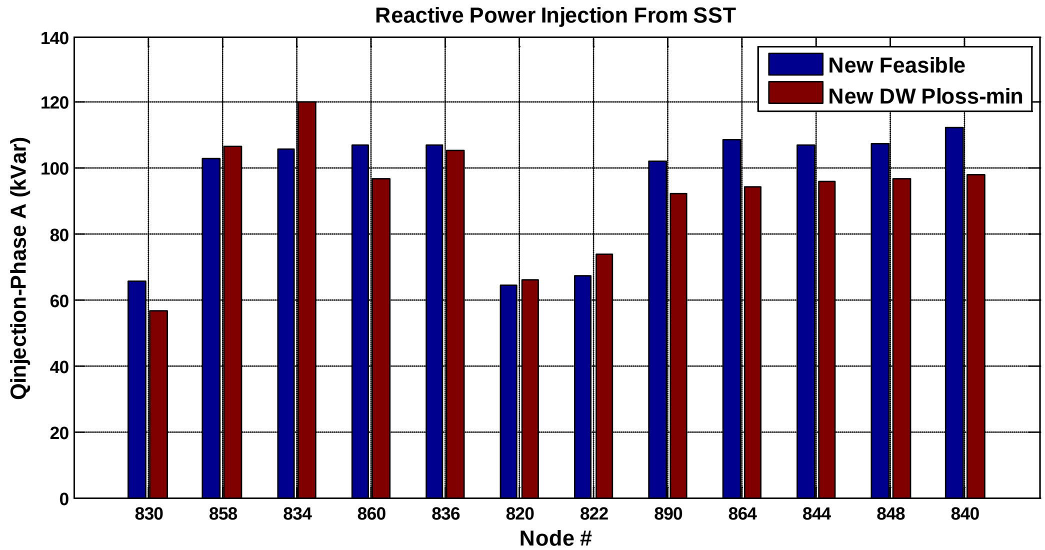

Figure 4-24 Reactive power injection comparison of phase A

The voltage profile is compared for the whole optimization procedure in Figure 4-25. The voltage profile with a 10% real-power load increase but the old reactive power injection from the previous optimization is shown in blue as a base line. The green line is the new feasible operating point after the voltages are boosted back into the feasible region. Starting with the new feasible point, the DW-based decentralized VVC brings down the system power loss as much as possible while guaranteeing that the voltage is still within acceptable limits. A new optimal operating point will be reached finally.

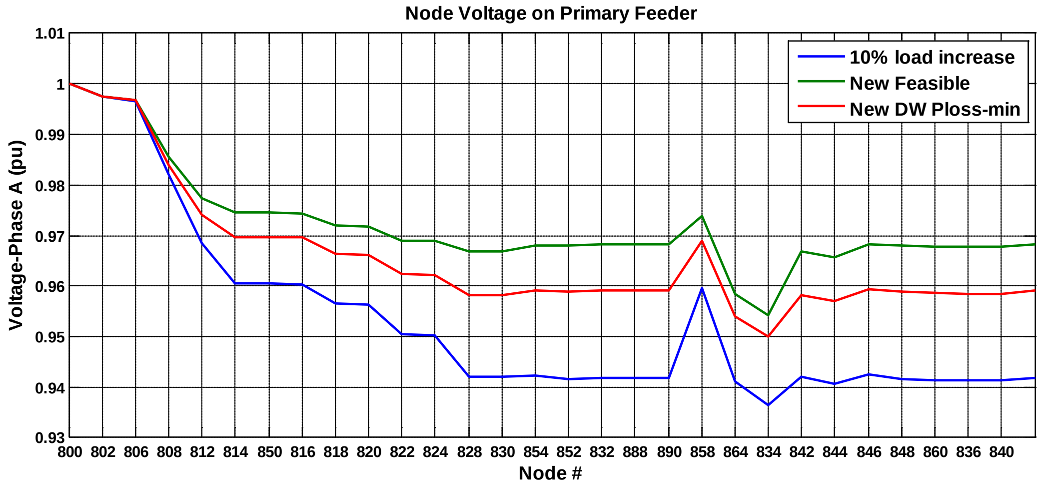

Figure 4-25 The voltage profile comparison of phase A

Power losses for all three phases are documented in Table 4-7. And the comparison of the total reactive power injection from the SSTs is shown in Table 4-8. As expected, a load increase will require more reactive power to maintain system voltages. As a result, the system power loss is also higher than with lighter loading.

Table 4-7 Power loss reduction and comparison

Power loss (kW)	*Pa*	*Pb*	*Pc*
10% load increase	269.5252	208.2977	271.1598
After feasibility search	382.0260	313.9724	440.5504
After DW	364.6112	302.6420	396.4498
Reduction	17.4148	11.3304	44.1006
Percentage of reduction	0.0456	0.0361	0.1001

Table 4-8 Reactive power injection comparison

Total reactive power injection	*Qa*(kVar)	*Qb*(kVar)	*Qc*(kVar)
After feasibility search	1158.2191	1051.1969	1236.9508
After DW	1102.7262	1046.3535	1141.7862
Reduction	55.4929	4.8434	95.1646
Percentage of reduction	0.0479	0.0046	0.0769

For centralized VVC, there is only one central processor that is responsible for collecting all the information throughout the whole system and making decisions based on the system-wide information. Due to the heavy burden, a high-performance computer is usually adopted at the central control station. At the same time, all the measurements should be able to be passed to the central processor, which requires a communications network that can cover the whole power grid. The instant measurements of the system state variables will be sent to the central processor each time the VVC is dispatched. Once the control decision is made, the commands will be sent back to each SST. Therefore, in one control action, there is only a one-round information exchange.

Considering both the computation and communications burdens, the decentralized VVC breaks the original large-scale problem down into smaller ones and processes them in parallel at local processors while the master processor is only responsible for coordinating and eliminating mismatches. Therefore, the computational effort that is required at each processor is much lighter than in the centralized VVC. Each time the VVC is dispatched, a slave processor is responsible for collecting instant measures and sending back control commands to the local controllers. The procedure is similar for the centralized VVC; it is just accomplished by slave processors within their own control areas. However, because of the coordination needs, information exchanges between the master processor and the slave processors may take place multiple times. Although the information exchanged between master processor and slave processors is only ratios, the multiple communications needed is also an extra burden compared with the centralized VVC. An in-depth study needs to be conducted in case real communications links are available.

4.3.2 Test on the FREEDM Notional System

In order to show the general applicability of the DW-based decentralized VVC, an additional test is going to be implemented on the FREEDM Residential Notional System. In order to illustrate the system structure clearly, a general figure can be drawn. As indicated in Figure 4-26, there are two main feeders connected to the substation. Since the substation node is assumed to be a slack bus, those two feeders can be deal with separately. In another words, they can be viewed as two different systems.

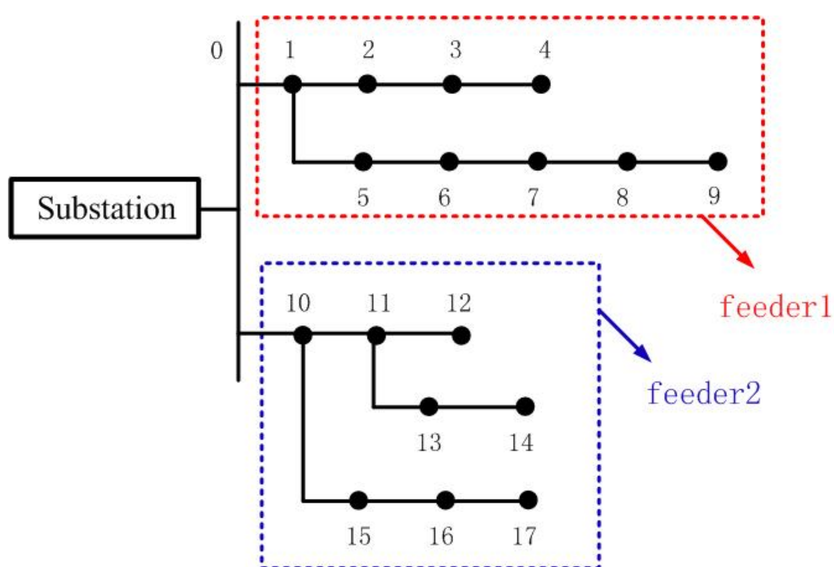

Figure 4-26 The Residential Notional System structure

Given the positive and zero sequence resistance and inductance, it is important to decide the line model that is going to be used in the distribution power flow. According to Dr. Kersting's line model suggestion [71], two models are used here to present both a full-line model and a decoupled-line model.

1) Full-line model for power system simulation:

$$Z_{seq} = \frac{1}{3}\begin{bmatrix} 2Z_1 + Z_0 & Z_0 - Z_1 & Z_0 - Z_1 \\ Z_0 - Z_1 & 2Z_1 + Z_0 & Z_0 - Z_1 \\ Z_0 - Z_1 & Z_0 - Z_1 & 2Z_1 + Z_0 \end{bmatrix} \quad (4.63)$$

2) Decoupled model for decentralized VVC

$$Z_{pos} = \begin{bmatrix} Z_1 & 0 & 0 \\ 0 & Z_1 & 0 \\ 0 & 0 & Z_1 \end{bmatrix} \quad (4.64)$$

With different line models, the distribution power flow of the peak load condition gives totally different state variables, as shown in Table 4-9. In case the full-line model is used, the voltage at phases A and C decreases along the feeder, but the voltage at phase B rises approaching the end of the feeder. When mutual impedance is neglected in the decoupled line model, the voltage drop occurs from the substation toward the remote customers.

Table 4-9 State variables resulting from two different line models (a)Z_{seq} and (b)Z_{pos}

$\mathbf{Z_{seq}}$						
Node #	*Va*	*Theta_a*	*Vb*	*Theta_b*	*Vc*	*Theta_c*
0	1	0	1	-120	1	120
1	0.9830	-2.8652	1.0014	-121.7865	0.9855	118.6190
2	0.9804	-2.9681	1.0001	-122.1924	0.9870	118.5358
3	0.9803	-2.9400	0.9994	-122.2520	0.9874	118.4922
4	0.9805	-2.9425	0.9993	-122.2424	0.9872	118.4635
5	0.9784	-4.3988	1.0052	-122.1403	0.9749	117.9969

Table 4-9 Continued

6	0.9771	-5.5831	1.0052	-122.4701	0.9657	117.0769
7	0.9770	-6.2256	1.0023	-122.8624	0.9609	116.2245
8	0.9769	-6.2721	1.0021	-122.8945	0.9606	116.1689
9	0.9766	-6.3473	1.0019	-122.9654	0.9603	116.0989

Z_{pos}						
Node #	*Va*	*Theta_a*	*Vb*	*Theta_b*	*Vc*	*Theta_c*
0	1	0	1	-120	1	120
1	0.9881	-2.3475	0.9912	-121.8465	0.9908	118.1742
2	0.9873	-2.5227	0.9900	-122.1259	0.9903	118.0357
3	0.9873	-2.5283	0.9898	-122.1680	0.9901	118.0078
4	0.9873	-2.5321	0.9898	-122.1699	0.9901	117.9919
5	0.9831	-3.4330	0.9884	-122.4477	0.9870	117.3662
6	0.9790	-4.3597	0.9858	-123.0556	0.9831	116.4816
7	0.9764	-4.9750	0.9835	-123.6031	0.9801	115.7652
8	0.9762	-5.0196	0.9833	-123.6435	0.9799	115.7162
9	0.9760	-5.0928	0.9830	-123.7151	0.9796	115.6455

Also, power flow information is extracted for both cases and listed in Table 4-10. Due to the heavy coupling between phases in the full-line model case, not only the voltage raise in phase B, but also the power loss of that phase decrease. Besides the phase difference, the total power loss in the full-line model case is about 126.7kW, while it is only about 100kW in the decoupled case.

Given the difference between the results of these two line models, assumptions are made:

1) The full-line model's distributed power flow is used to represent the actual system status.
2) The decoupled line model VVC is used to determine the control signal.

Table 4-10 Real power resulting from different line models

Z_{seq}	A	B	C
P_{total} (kW)	3083.851	2433.54	2405.48
P_{sub} (kW)	3140.093	2427.414	2482.068
P_{loss} (kW)	56.2426	-6.1256	76.5884
Z_{pos}	A	B	C
P_{total} (kW)	3083.851	2433.54	2405.48
P_{sub} (kW)	3137.291	2444.152	2442.248
P_{loss} (kW)	53.4396	10.612	36.7677

In reality, the VVC application performs as an open loop control. At the beginning of a deterministic control, system information will be measured and sent to the VVC center. Then, after the control decision is made, the control command will be sent back to the local control devices. There is no feedback as to how the system performs after the adjustment, according to the VVC control command. As an improvement and additional validation, a feedback test will be added in the following scenario. After the control decision is made based on the decoupled line model VVC, the returned control command will be used in the full-line model distributed power flow. A comparison will be made between the expected system status in the VVC and the actual system response. The validation procedure is demonstrated in Figure 4-27.

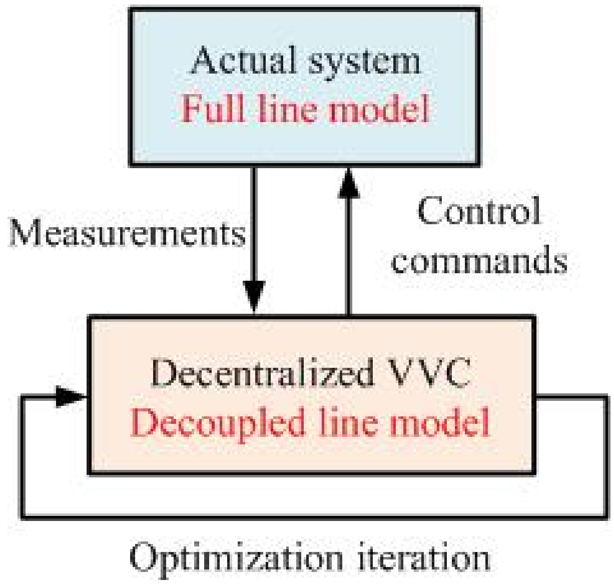

Figure 4-27 Information exchange for close loop control verification

In the following, feeder 1 is used to show the control effect of the decentralized VVC. Similar to the FREEDM IEEE 34 system, the systems themselves are naturally partitioned into different groups, which make the DW decomposition possible. There are two subgroups in feeder 1, as shown in Figure 4-28.

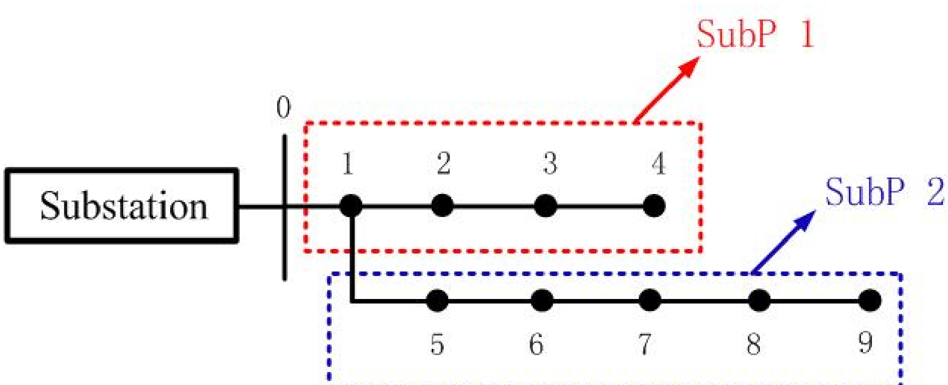

Figure 4-28 Partition feeder 1 into sub-areas

Take feeder 1 as an example and apply DW-based decentralized VVC. The total node number in each sub-area, the number of inner nodes, and the number of coupling nodes is shown in Table 4-11.

Table 4-11 Bus information after area partition of phase A of feeder 1

Area #	N_i	B_i	C_i
1	4	3	1
2	5	4	1

Put the linking buses at the beginning and then the inner buses for each sub-area; the constraints can be organized in block angular form as shown in Figure 4-29.

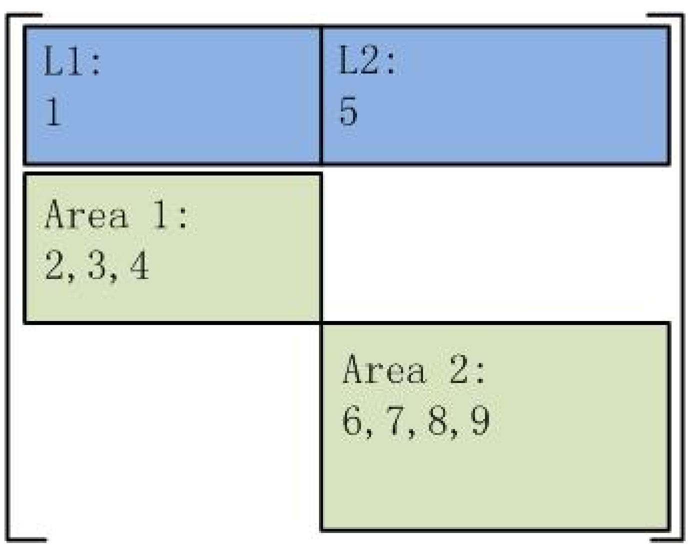

Figure 4-29 Phase A of the Residential Notional System in block angular form

In the following, the same manipulation is performed on the inequality constraint to transfer the upper and lower bounds of the inequality constraint to be upper bound only. The DW-based decentralized VVC is applied similarly.

4.3.2.1 Case 1: Simulation and Result Analysis of Peak Loading Condition

Different from the FREEDM IEEE 34 system, the line length of the FREEDM Residential Notional System is short and the load is comparably light. Given the default peak load condition, the voltage profile of the original system's operating condition without the VVC is already within acceptable limits. In this case, there is no need to do a feasibility search and the application automatically goes to power loss minimization. Similarly, the voltage profile of the initial status is optimized after the VVC is compared and is shown in Figure 4-30. Although the original voltage profile is already quite good, the VVC can still improve the voltage by boosting it by about 0.005 p.u.

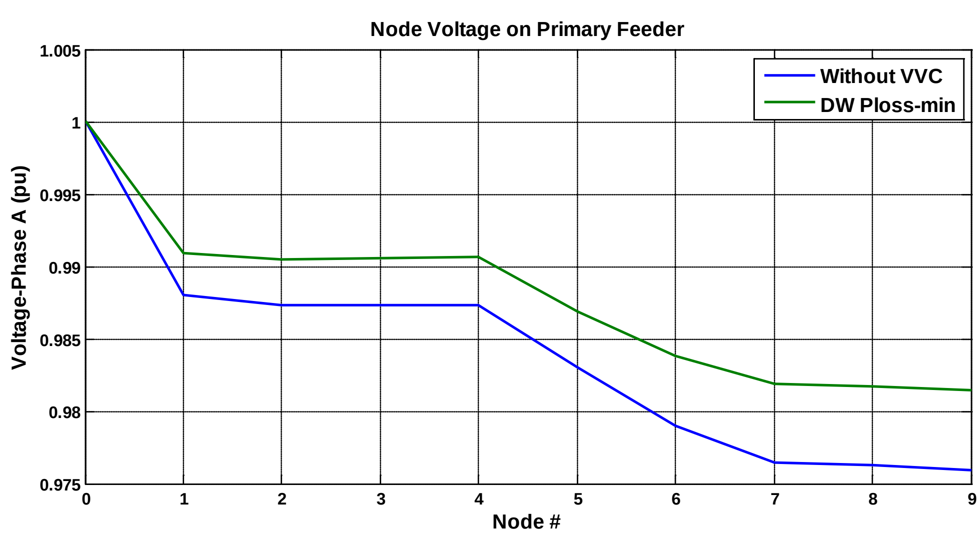

Figure 4-30 Voltage profile comparison of phase A

Based on the already feasible point, the DW-based decentralized power loss minimization iteration is documented in Figure 4-31. The left-hand axis shows the total system power loss, and the right-hand axis is the minimum voltage in the system. As the optimization iteration progresses, the system power loss decreases and the voltage increases until the optimal point is found.

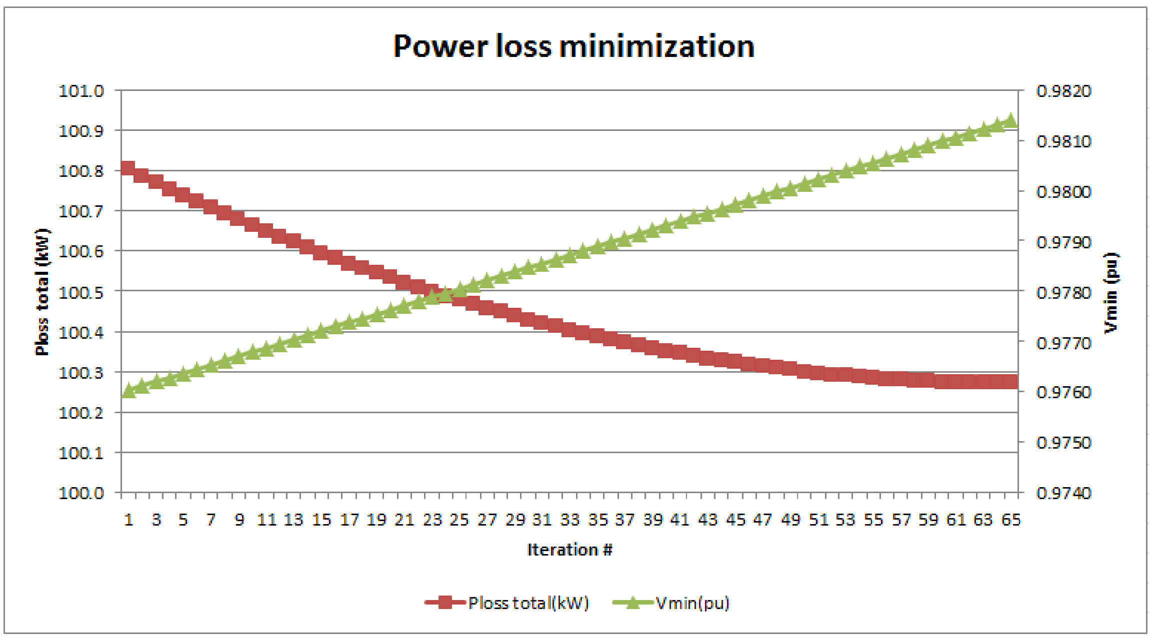

Figure 4-31 Iteration of the DW-decentralized power loss minimization

The reactive power injection needed for the optimal operating point is shown in Figure 4-32.

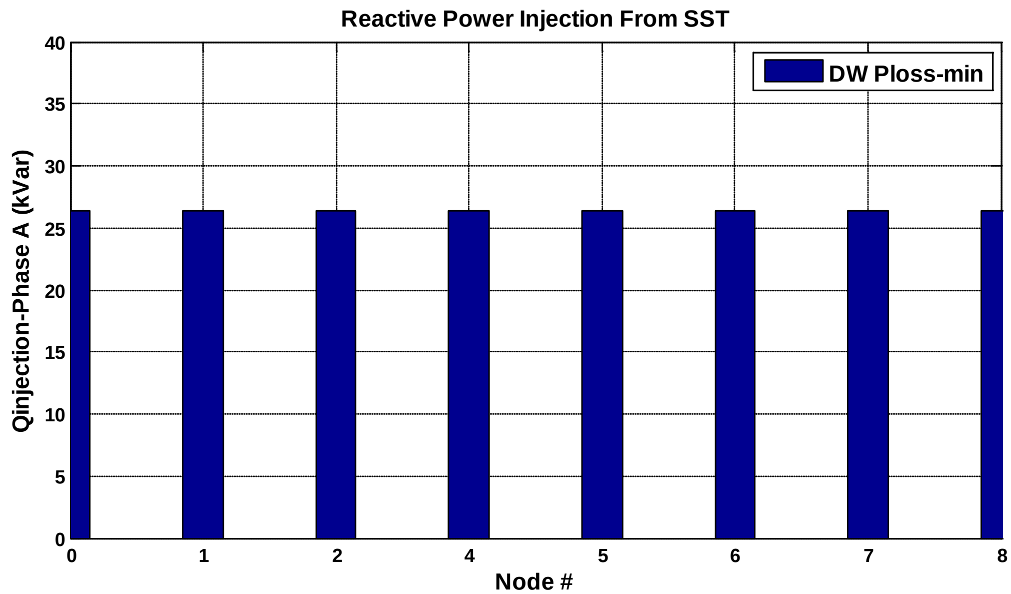

Figure 4-32 Reactive power injection after DW

The power loss in the original system operating condition and the optimal point are documented and shown in Table 4-12. The total reactive power injection needed for all three phases is also mentioned in the table.

Table 4-12 Power loss reduction and reactive power injection

Power loss (kW)	*Pa*	*Pb*	*Pc*
Original	53.4396	10.6120	36.7677
After DW	53.1212	10.5708	36.5801
Reduction	0.3184	0.0412	0.1876
Percentage of reduction	0.005958	0.0038824	0.0051023
Total reactive power injection	*Qa*(kVar)	*Qb*(kVar)	*Qc*(kVar)
After DW	211.2000	237.6000	237.6000

As explained earlier, in order to do additional validations and check on how the actual system responds after being adjusted according to the expected VVC reactive power injection commands, the returned reactive power injection setting is now passed to the full line model distribution power flow simulation and the new state variables are documented in Table 4-13. As expected, the voltage profiles for all three phases rise with the reactive power injection.

Table 4-13 Full-line model power flow result with decoupled VVC returned reactive power injection

Node #	*Va*	*Theta_a*	*Vb*	*Theta_b*	*Vc*	*Theta_c*
0	1	0	1	-120	1	120
1	0.9855	-2.8927	1.0046	-121.8421	0.9890	118.5961
2	0.9830	-2.9966	1.0037	-122.2595	0.9910	118.5134
3	0.9830	-2.9680	1.0033	-122.3296	0.9918	118.4716
4	0.9833	-2.9717	1.0033	-122.3213	0.9917	118.4421
5	0.9819	-4.4321	1.0094	-122.2057	0.9794	117.9660
6	0.9815	-5.6208	1.0103	-122.5438	0.9711	117.0432
7	0.9820	-6.2669	1.0080	-122.9401	0.9670	116.1921
8	0.9820	-6.3136	1.0079	-122.9724	0.9668	116.1367
9	0.9817	-6.3889	1.0077	-123.0431	0.9665	116.0667

What’s more, the power losses are also compared between the full-line model distributed power flow and the decoupled line model VVC results. As indicated in Table 4-14, the expected power loss reduction resulted from the VVC is about 0.6kW. However, the returned result from the distributed power flow with the full-line model is with a 5.25kW increase. The result indicates that there may be mismatches between the actual system response and the VVC expected improvement. Therefore, it is necessary to make sure that the simulation model is as accurate as possible.

Table 4-14 Power loss comparison for full and decoupled line cases with the same reactive power injection

	P_{loss} (kW)	A	B	C	P_{total}
Z_{seq}	Initial status	56.2426	-6.1256	76.5884	126.7054
	With Q_{inj} from Z_{pos} based VVC	60.5374	-1.5477	72.9644	131.9541
Z_{pos}	Initial status	53.4396	10.6120	36.7677	100.8193
	After VVC	53.1212	10.5708	36.5801	100.2721

4.3.2.2 Case 2: Simulation and Result Analysis in Case of 10% Load Increase

A similar loading condition change is also considered for the FREEDM Residential Notional System, assuming that the load measured after 15 minute increases is about 10%. The new system operating point and the decentralized VVC response is documented in Figure 4-33. As the results indicate, with the previous optimal reactive power injection and the new loading condition, the system voltage decreases but is still within acceptable limits. Based on the new starting point, another power loss minimization is applied and the new DW result is also shown in the figure.

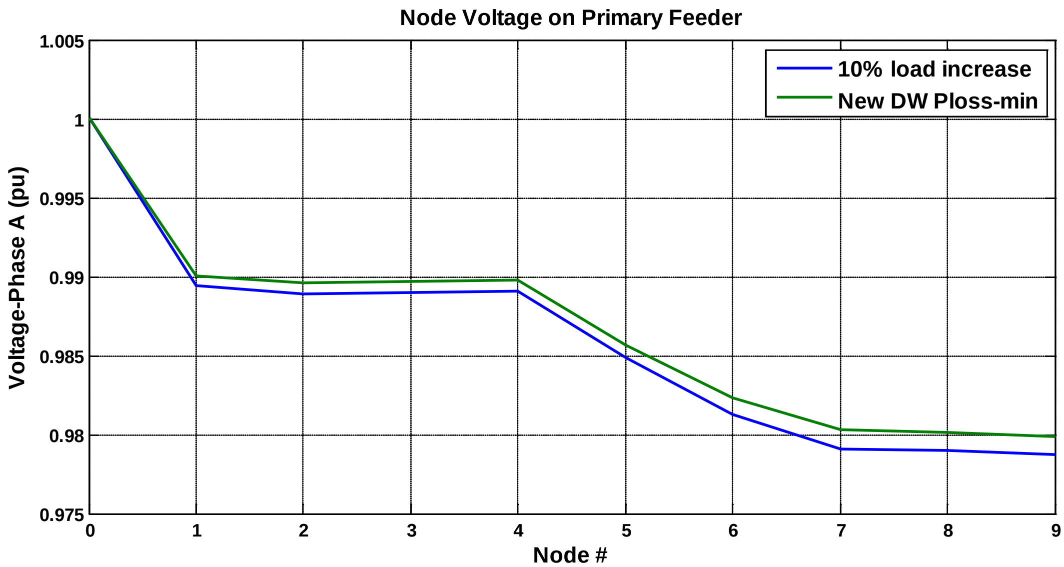

Figure 4-33 Voltage profile comparison of phase A

The power loss minimization iteration is documented in Figure 4-34. As the power loss decreases, the minimum system voltage increases. The result shows that the decentralized VVC can help improve system voltage, as well as reduce power loss.

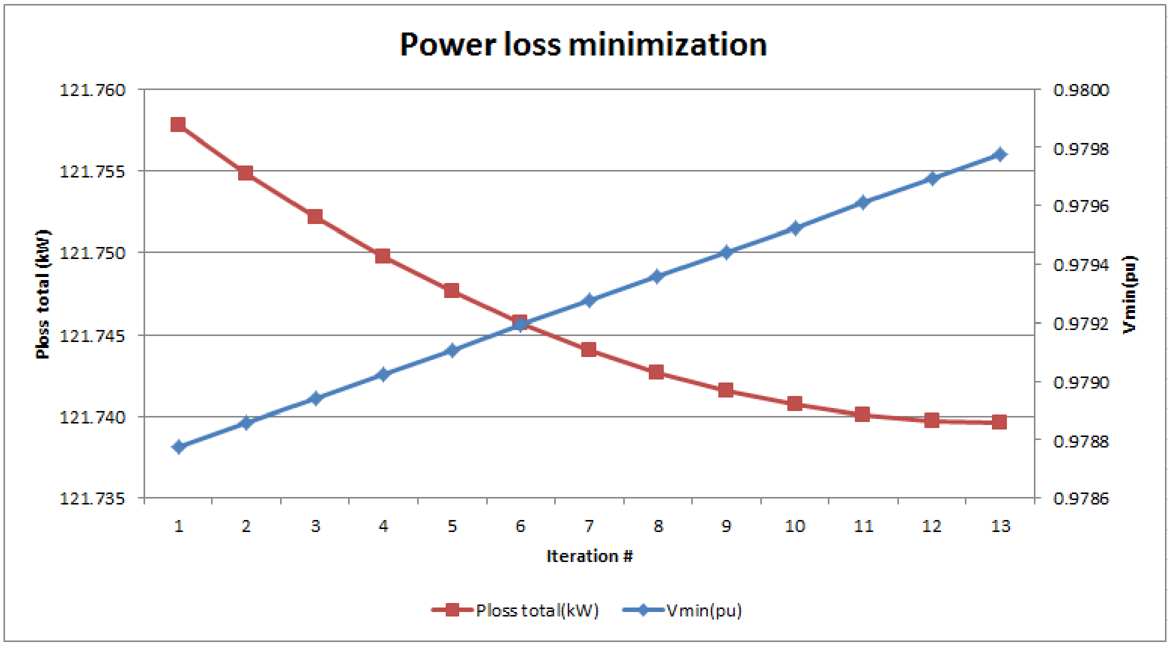

Figure 4-34 Iteration of DW decentralized power loss minimization

A comparison of the different reactive power injections needed for different loading conditions is shown in Figure 4-35. Then, the new reactive power injection needed for the new optimal operating point is shown in red and the previous reactive power injection is shown in blue.

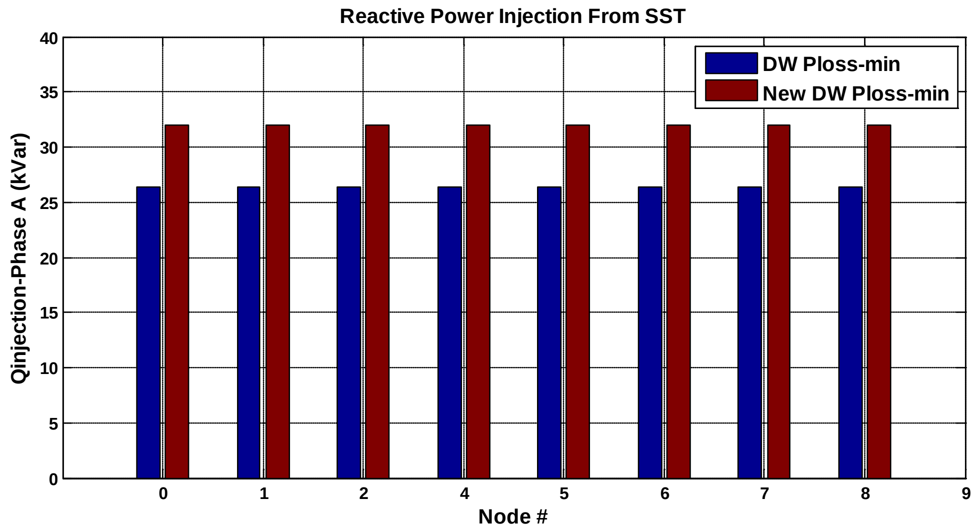

Figure 4-35 Reactive power injection comparison of phase A

The power loss for the 10% load increase and the new optimal point is documented and shown in Table 4-15. The total reactive power injection needed for all three phases is also mentioned in the table.

Table 4-15 Power loss reduction and reactive power injection

Power loss (kW)	*Pa*	*Pb*	*Pc*
10% load increase	64.5459	12.8197	44.3954
After DW	64.5107	12.8262	44.4029
Reduction	0.0352	-0.0065	-0.0075
Percentage of reduction	0.000545	-0.00051	-0.00017
Total reactive power injection	Qa(kVar)	Qb(kVar)	Qc(kVar)
After DW	256.0000	288.0000	288.0000

4.4 Conclusion

In this chapter, the general concept about centralized, decentralized, and distributed control is presented at the beginning. Compared with the heavy computational burden and dependence on communications infrastructure, decentralized control can achieve a system-wide optimization goal, as well as parallel computations and a weaker requirement for communications. With the appearance of the advanced power electronics devices, it is possible to break down the original centralized control into smaller subproblems and process them at local slave controllers. In this case, the master controller will only work to eliminate boundary mismatches between sub-areas. Under the guideline of a decentralized control concept, a DW-based decentralized VVC scheme is proposed in this chapter.

By adopting the same problem formulation and linearization idea as centralized VVC, DW shows its advantage in partitioning large-scale LP problems into smaller subproblems. By rearranging the sequence of inequality constraints, the original Jacobian matrix can be put into a "block angular" form, which can be handled by the DW-decomposition scheme. After DW decomposition, the new formation of the problem can be solved in an iterative process where at each step, the subproblems are solved separately. The master problem, which contains the coupling constraints, will be solved by the revised simplex method.

In order to check the effectiveness of the proposed decentralized control scheme, two test feeders are used here: the FREEDM IEEE 34 node test feeder and the FREEDM Notional System. An accuracy check is also conducted within the DW solve iteration to make sure that the DW returned result is close enough to the LP solver's result. By comparing the centralized and decentralized VVC control effect on the FREEDM IEEE 34 node system, it is clear that the decoupled assumption may result in less power loss reduction. Also, the actual system response and the VVC expected improvement are compared for the FREEDM Notional System. The results show that it is necessary to model the VVC in a more accurate way. After all, although the control effect of the DW-based decentralized VVC is not as good as centralized VVC, it can still help to regulate system voltages, as well as to minimize power losses.

CHAPTER 5. Conclusion and Future Work

5.1 Conclusion

With the appearance of DRER in the conventional power distribution network, the original system operation and control schemes are facing new challenges that have never been raised before. In order to investigate the potential issues for accommodating high-penetration renewables, two testbeds are modeled in the FREEDM system center. By connecting load and PV via the SSTs to the primal distribution feeder, conventional voltage regulation devices can also be removed since the SST itself can perform as a continuous-type reactive power resource. Under the new circumstance, there is an urgent need to find new VVC schemes that can deal with both renewables and the SSTs that spread everywhere in the distributed network.

The main contributions of this work include:

1) Impact studies of high-penetration residential-level PV are conducted. Daily operational conditions, including the heavy load condition and the reverse power flow condition, are considered thoroughly under the guidance of 1547.7. Besides, the cloud-passage scenario is also studied. Given the daily voltage variation of the testbed, it is necessary to develop new VVC strategies that can deal with the new enabling devices.
2) The objective of the VVC is formulated as minimizing system power loss while regulating the voltage profile within acceptable limits. In the following, a two-phase centralized VVC scheme is proposed. Phase I control is then targeted at regulating

voltages when a voltage violation exists. The feasibility search is based on the gradient method to find the steepest recent update direction. Then, based on a feasible operating condition, the phase II optimization is aiming at minimizing the power loss within the feasible region. Improvements have been made to make sure the linearization is accurate. The optimality check is also conducted to demonstrate different VVC performances with different initial feasible points.

3) As a continuous study, a DW-based decentralized VVC scheme is proposed by adopting the same problem formulation and linearization idea as centralized VVC. The DW decomposition scheme can effectively reduce the size of the optimization problem by partitioning large-scale LP problems into smaller subproblems. The effectiveness of the proposed decentralized control scheme is tested on two test feeders.

5.2 Future work

The proposed decentralized VVC scheme is only applied to the power loss minimization stage (Phase II) of VVC optimization. Given the inherent nature of the radial-type distribution feeder, it is also possible to break down the gradient-based feasibility search (Phase I) of the VVC optimization.

From an application perspective, the centralized VVC program, realized in MATLAB, is already embedded in the PSCAD simulation platform. An online control scenario has already been implemented and demonstrated in the FREEDM annual site visit. Similarly, the decentralized VVC will also need to be implemented in the same way. Figuring out how to realize parallel computations and distribute the subproblems to different servers requires in-depth hands-on experience.

As indicated in the VVC problem formulation, the loading balance becomes an important factor in reducing the power loss as more DRERs appear in the already unbalanced distribution network. Therefore, in the future, the elimination of imbalance should be considered as another objective of the VVC optimization problem. Unlike the traditional network reconfiguration method, which is achieved by changing the status of the sectionalizing switches, the control variables will still be the reactive power that can be dispatched from each SST.

REFERENCES

[1] H. Gharavi and R. Ghafurian, “Smart Grid : The Electric Energy System of the Future,” *Proc. IEEE*, vol. 99, no. 6, pp. 917–921, 2011.

[2] A. R. Khattak, S. A. Mahmud, and G. M. Khan, “The power to deliver: Trends in smart grid solutions,” *Power Energy …*, no. July, 2012.

[3] H. Brown and S. Suryanarayanan, “A survey seeking a definition of a smart distribution system,” *North Am. Power …*, vol. 80401, pp. 1–7, 2009.

[4] R. H. Lasseter, “Smart Distribution: Coupled Microgrids,” *Proc. IEEE*, vol. 99, no. 6, pp. 1074–1082, Jun. 2011.

[5] A. Q. Huang, M. L. Crow, G. T. Heydt, J. P. Zheng, and S. J. Date, “The future renewable electric energy delivery and management (FREEDM) system: the energy internet,” *Proc. …*, 2011.

[6] T. Zhao, J. Zeng, S. Bhattacharya, M. Baran, and A. Q. Huang, “An average model of solid state transformer for dynamic system simulation,” *Power Energy Soc. Gen. Meet.*, pp. 1–8, 2009.

[7] M. Delghavi and A. Yazdani, “Islanded-mode control of electronically coupled distributed-resource units under unbalanced and nonlinear load conditions,” *IEEE Trans. Power Deliv.*, vol. 26, no. 2, pp. 661–673, 2011.

[8] Colorado, “PV Module Simulink models Simulink models of PV modules,” *http://ecee.colorado.edu/~ecen2060/materials/simulink/PV/PV_module_model.pdf*, 2008.

[9] A. Huang, “FREEDM system - a vision for the future grid,” *IEEE PES Gen. Meet.*, pp. 1–4, Jul. 2010.

[10] A. Q. Huang and J. Baliga, “FREEDM System: Role of power electronics and power semiconductors in developing an energy internet,” *2009 21st Int. Symp. Power Semicond. Devices IC’s*, pp. 9–12, Jun. 2009.

[11] M. Baran, “Smart Distribution System Research and Education,” *IEEE PES Gen. Meet.*, pp. 1–3, 2011.

[12] W. H. Kersting, “Radial distribution test feeders,” *IEEE Trans. Power Syst.*, vol. 6, no. 3, pp. 975–985, 1991.

[13] IEEE PES Distribution System Analysis Subcommittee's Distribution Test Feeder Working Group, "IEEE 34 Node Test Feeder." .

[14] P. Kundur, *Power system stability and control*, vol. 20073061. 1994.

[15] T. Gonen, "Electric Power Distribution System Engineering.pdf." McGraw-Hill, 2008.

[16] R. Yan and T. Saha, "Investigation of voltage stability for residential customers due to high photovoltaic penetrations," *IEEE Trans. Power Syst.*, vol. 27, no. 2, pp. 651–662, 2012.

[17] T. Ackermann and V. Knyazkin, "Interaction between distributed generation and the distribution network: operation aspects," *PES Transm. Distrib. Conf, Asia Pacific*, vol. 2, pp. 1357–1362, 2002.

[18] K. Katiraei and J. Aguero, "Solar PV integration challenges," *IEEE Power Energy Mag.*, pp. 62–71, 2011.

[19] Y. Liu, B. Bebic, J. Bedout, and W. Ren, "Distribution system voltage performance analysis for high-penetration PV," *IEEE ENERGY 2030 Conf*, no. November, 2008.

[20] "IEEE P1547.7^{TM}/D4.0, Draft Guide to Conducting Distribution Impact Studies for Distributed Resource Interconnection." .

[21] "American National Standard For Electric Power Systems and Equipment — Voltage Ratings (60 Hertz)," *Am. Natl. Stand. Inst. Inc*, 2006.

[22] E. Kern, E. Gulachenski, and G. Kern, "Cloud effects on distributed photovoltaic generation: Slow transients at the Gardner, Massachusetts photovoltaic experiment," *IEEE Trans. Energy Convers.*, vol. 4, no. 2, pp. 184–190, 1989.

[23] T. Tomson, "Fast dynamic processes of solar radiation," *Sol. Energy*, vol. 84, no. 2, pp. 318–323, Feb. 2010.

[24] J. Grainger and S. Civanlar, "Volt-Var control on Distribution Systems with Lateral Branches Using Switched Capacitors and Voltage Regulators, Part III : The Volt / Var Control," *IEEE Trans. Power Appar. Syst.*, no. November, p. 3291, 1985.

[25] J. Grainger and S. Civanlar, "Volt-Var control on Distribution Systems with Lateral Branches Using Switched Capacitors and Voltage Regulators, Part I: The Overall Problem," *IEEE Trans. Power Appar. Syst.*, no. November, p. 3278, 1985.

[26] J. Grainger and S. Civanlar, “Volt-Var control on Distribution Systems with Lateral Branches Using Switched Capacitors and Voltage Regulators, Part II: The solution Method,” *IEEE Trans. Power Appar. Syst.*, vol. 4, no. 11, pp. 3284–3290, 1985.

[27] V. Borozan, M. E. Baran, and D. Bivisel, “Integrated Volt/Var Control in Distribution Systems,” *IEEE Power Eng. Soc. Winter Meet.*, no. C, pp. 1485–1490, 2001.

[28] J. Dixon, L. Moran, and J. Rodriguez, “Reactive power compensation technologies: state-of-the-art review,” *Proc. IEEE*, vol. 93, no. 12, 2005.

[29] M. Lin, R. K. Rayudu, and S. Samarasinghe, “A review of voltage/Var control,” *Australas. Univ. Power Eng. Conf.*, pp. 1–5, 2003.

[30] “http://www.cooperindustries.com/content/public/en/power_systems/solutions/ivvc.html.” .

[31] ABB, “Volt-VAr Management Software (V VMS) for smart grid distribution automation applications,” *http://www05.abb.com/global/scot/scot245.nsf/veritydisplay/cb20417bfa9255d6c12578ef0052d2b6/$file/vvms_2guz5015_2-22-11.pdf*.

[32] M. E. Baran and F. F. Wu, “Network Reconfiguration in Distribution Systems for Loss Reduction and Load Balancing,” *IEEE Trans. Power Deliv.*, vol. 9, no. 4, pp. 101–102, 1989.

[33] M. W. Siti, D. V. Nicolae, A. a. Jimoh, and A. Ukil, “Reconfiguration and Load Balancing in the LV and MV Distribution Networks for Optimal Performance,” *IEEE Trans. Power Deliv.*, vol. 22, no. 4, pp. 2534–2540, Oct. 2007.

[34] C. Chen, S. Member, C. Tsai, C. Lin, and W. Hsieh, “Loading Balance of Distribution Feeders With Loop Power Controllers Considering Photovoltaic Generation,” *IEEE Trans. Power Syst.*, vol. 26, no. 3, pp. 1762–1768, 2011.

[35] R. A. Hooshmand and S. Soltani, “Fuzzy Optimal Phase Balancing of Radial and Meshed Distribution Networks Using BF-PSO Algorithm,” *IEEE Trans. Power Syst.*, vol. 27, no. 1, pp. 47–57, Feb. 2012.

[36] R. Baldick, *Applied Optimization: Formulation and Algorithms for Engineering Systems*. Cambridge University Press, 2006.

[37] J. Zhu, *Optimization of Power System Operation*. John Wiley & Sons, 2009.

[38] P. Gill, W. Murray, and M. Wright, *Practical optimization*. Academic Press, 1981.

[39] D. Sun, B. Ashley, B. Brewer, A. Hughes, and W. F. Tinney, “Optimal power flow by Newton approach,” *IEEE Trans. Power Appar. Syst.*, no. 10, pp. 2864–2880, 1984.

[40] A. Wood and B. Wollenberg, “Power Generation, Operation and Control (2nd Edition).” John Wiley & Sons, 1996.

[41] J. Lavei, A. Rantzer, and S. Low, “Power flow optimization using positive quadratic programming ⋆,” in *18th IFAC World Congress Conference*, 2011.

[42] J. Lavaei and S. H. Low, “Zero Duality Gap in Optimal Power Flow Problem,” *IEEE Trans. Power Syst.*, vol. 27, no. 1, pp. 92–107, Feb. 2012.

[43] M. Potkonjak and J. Rabaey, “Algorithm Selection: A quantitative computation-intensive optimization approach,” *IEEE Trans. Comput. Des. Integr. Circuits Syst.*, pp. 90–95, 1999.

[44] B. Stott, O. Alsac, and A. J. Monticelli, “Security Analysis and Optimization,” *Proc. IEEE*, vol. 75, no. 12, pp. 1623–1644, 1987.

[45] M. U. Tariq, S. Grijalva, and M. Wolf, “Towards a Distributed, Service-Oriented Control Infrastructure for Smart Grid,” *2011 IEEE/ACM Second Int. Conf. Cyber-Physical Syst.*, pp. 35–44, Apr. 2011.

[46] S. Mohammad and W. Yaoyu, *Communication and Control in Electric Power Systems*. .

[47] Z. Zhang, X. Ying, and M. Chow, “Decentralizing the economic dispatch problem using a two-level incremental cost consensus algorithm in a smart grid environment,” *2011 North Am. Power Symp.*, pp. 1–7, Aug. 2011.

[48] Yong-Hua Song, *Modem Optimisation Techniques in Power Systems*. Kluwer Academic Publishers.

[49] D. Bertsekas and J. Tsitsiklis, *Parallel and distributed computation*. Prentice-Hall Inc, 1989.

[50] X. Hu and R. Eberhart, “Solving constrained nonlinear optimization problems with particle swarm optimization,” *Proc. sixth world multiconference …*, pp. 2–5, 2002.

[51] R. Poli, J. Kennedy, and T. Blackwell, “Particle swarm optimization: An Overview,” *Proc. ICNN’95 - Int. Conf. Neural Networks*, vol. 4, pp. 1942–1948, 2010.

[52] Z. Michalewicz and M. Schoenauer, “Evolutionary algorithms for constrained parameter optimization problems,” *Evol. Comput.*, 1996.

[53] M. E. Baran and I. M. El-Markabi, “A Multiagent-Based Dispatching Scheme for Distributed Generators for Voltage Support on Distribution Feeders,” *IEEE Trans. Power Syst.*, vol. 22, no. 1, pp. 52–59, Feb. 2007.

[54] H. Farag, E. El-Saadany, and R. Seethapathy, “A two ways communication-based distributed control for voltage regulation in smart distribution feeders,” *IEEE Trans. Smart Grid*, vol. 3, no. 1, pp. 271–281, 2012.

[55] K. Rogers, R. Klump, H. Khurana, A. A. Aquino-Lugo, and T. J. Oyerbye, “An authenticated control framework for distributed voltage support on the smart grid,” *IEEE Trans. Smart Grid*, vol. 1, no. 1, pp. 40–47, 2010.

[56] H. Yoshida, Y. Fukuyama, S. Takayama, and Y. Nakanishi, “A particle swarm optimization for reactive power and voltage control in electric power systems considering voltage security assessment,” *IEEE SMC’99 Conf. Proceedings. 1999 IEEE Int. Conf. Syst. Man, Cybern. (Cat. No.99CH37028)*, vol. 6, pp. 497–502.

[57] N. K. Sharma, D. S. Babu, and S. C. Choube, “Application of Particle Swarm Optimization Technique for Reactive Power Optimization,” in *IEEE- International Conference On Advances In Engineering, Science And Management (ICAESM -2012)*, 2012.

[58] K. K. Swarnkar, S. Wadhwani, and a. K. Wadhwani, “Optimal Power Flow of large distribution system solution for Combined Economic Emission Dispatch Problem using Partical Swarm Optimization,” *2009 Int. Conf. Power Syst.*, no. 3, pp. 1–5, 2009.

[59] M. Kleinberg and K. Miu, “A study of distributed capacitor control for electric power distribution systems,” *2011 North Am. Power Symp.*, pp. 1–6, Aug. 2011.

[60] G. B. Dantzig and P. Wolfe, “Decomposition Principle for Linear Programs.pdf,” *Oper. Res.*, vol. 8, no. 1, p. p101, 1960.

[61] G. B. Dantzig and P. Wolfe, “The Decomposition Principle for Linear Programs,” *Econom. Soc.*, vol. 29, no. 4, 1961.

[62] J. Enamorado, A. Ramos, and T. Gomez, “Multi-area decentralized optimal hydro-thermal coordination by the Dantzig-Wolfe decomposition method,” *IEEE Power Eng. Soc. Summer Meet.*, vol. 00, no. c, 2000.

[63] R. Romano, V. Quintana, R. Lopez, and V. Valadez, “Constrained economic dispatch of multi-area systems using the Dantzig-Wolfe decomposition principle,” *IEEE Trans. Power Appar. Syst.*, vol. PAS-100, no. 4, 1981.

[64] J. López, M. Granada, and J. Mantovani, "Multi-area decentralized optimal VAr planning using the Dantzig-Wolfe decomposition principle," *IEEE/PES Transm. Distrib. Conf. Expo. Lat. Am.*, pp. 92–98, 2010.

[65] M. Aganagic and S. Mokhtari, "Security constrained economic dispatch using nonlinear Dantzig-Wolfe decomposition," *IEEE Trans. Power Syst.*, vol. 12, no. 1, pp. 105–112, 1997.

[66] R. Cheng, J. Forbes, and W. Yip, "Dantzig-Wolfe decomposition and large-scale constrained MPC problems," *Symp. Dyn. Control*, 2004.

[67] D. Luenberger and Y. Ye, *Linear and nonlinear programming*, 3rd ed. Springer, 2003.

[68] J. Tebboth, "A computational study of Dantzig-Wolfe decomposition," University of Buckingham, 2001.

[69] N. I. Deeb and S. M. Shahidehpour, "Decomposition approach for minimising real power losses in power systems," *IEEE Proc. C Gener. Transm. Distrib.*, vol. 138, no. 1, p. 27, 1991.

[70] N. Deeb and S. Shahidehpour, "Linear reactive power optimization in a large power network using the decomposition approach," *IEEE Trans. Power Syst.*, vol. 5, no. 2, 1990.

[71] W. Kersting and W. Phillips, "Distribution feeder line models," *IEEE Trans. Ind. Appl.*, vol. 31, no. 4, 1995.

APPENDICES

Appendix A Residential Notional System Datasheet

Table A-1 Base value for Residential Notional System

	3-phase	per-phase
Vbase(kV)	12	6.9282
Sbase(MVA)		10
Zbase		4.8

Table A-2 Load data for Residential Notional System

load #	PL A(kW)	IQL A (kVAR)	PL B(kW)	IQL B (kVAR)	PL C(kW)	IQL C (kVAR)
Ld1	57.75	81.62	165.55	110.11	112.42	66.99
Ld2	532.07	273.35	734.83	364.99	338.8	173.25
Ld3	0	0	141	68	14.63	7.7
Ld4	20.02	10.01	10.01	1.54	85.47	43.12
Ld5	651.42	332.64	171.71	80.08	100.1	56.98
Ld6	544.39	278.74	56.98	29.26	254.1	120.12
Ld7	145.53	74.69	112.42	57.75	245.63	120.12
Ld8	597.52	304.92	510.51	253.33	733.81	386.54
Ld9	535.15	272.58	530.53	261.8	520.52	264.88
Ld10	32.725	28.028	25.564	26.334	50.743	34.804
Ld11	455.84	189.651	715.176	325.094	841.841	353.661
Ld12	235.081	112.959	207.438	98.945	196.119	93.709
Ld13	319.396	145.222	317.856	141.603	95.326	39.578
Ld14	15.862	8.701	0	0	0	0
Ld15	357.665	168.553	207.207	105.798	59.598	35.266
Ld16	499.576	232.617	424.424	187.957	846.461	364.133
Ld17	168.938	55.363	608.839	271.887	227.227	87.549

Table A-3 Line data for Residential Notional System

Line	R1 (ohm)	R0 (ohm)	L1 (H)	L0 (H)	C1 (F)	C0 (F)	Length (km)
1	0.1502	0.8004	0.0017	0.0067	1E-15	1E-15	7.141
2	0.0618	0.3294	0.0007	0.0027	1E-15	1E-15	2.939
3	0.0546	0.2910	0.0006	0.0024	1E-15	1E-15	2.596
4	0.0366	0.1949	0.0004	0.0016	1E-15	1E-15	1.739
5	0.0851	0.4536	0.0009	0.0038	1E-15	1E-15	4.047
6	0.0978	0.5209	0.0011	0.0043	1E-15	1E-15	4.647
7	0.0919	0.4898	0.0010	0.0041	1E-15	1E-15	4.37
8	0.0075	0.0399	0.0001	0.0003	1E-15	1E-15	0.356
9	0.0261	0.1389	0.0003	0.0012	1E-15	1E-15	1.239
10	0.0711	0.3786	0.0008	0.0032	1E-15	1E-15	3.378
11	0.0476	0.2534	0.0005	0.0021	1E-15	1E-15	2.261

Table A-3 Continued

12	0.0050	0.0268	0.0001	0.0002	1E-15	1E-15	0.239
13	0.0439	0.2342	0.0005	0.0019	1E-15	1E-15	2.089
14	0.1197	0.6379	0.0013	0.0053	1E-15	1E-15	5.6913
15	0.0593	0.3160	0.0007	0.0026	1E-15	1E-15	2.819
16	0.0186	0.0990	0.0002	0.0008	1E-15	1E-15	0.883
17	0.0667	0.3553	0.0007	0.0030	1E-15	1E-15	3.17

Table A-4 Line type parameter for Residential Notional System

R1 (ohm/km)	R0 (ohm/km)	L1 (H/km)	L0 (H/km)
0.021035	0.112089	0.000234	0.000933

Table A-5 Substation transformer information for Residential Notional System

substation voltage	69kV/12kV
transformer capacity	30MVA
transformer winding type	delta/wye
transformer impedance	0.19
neutral reactor	0.315 Ω

Table A-6 Capacitor data for Residential Notional System

Cap #	Connected to	IQL A(kVAR)	IQL B (kVAR)	IQL C (kVAR)
C1	5	400	400	400
C2	8	200	200	200
C3	12	400	400	400
C4	17	400	400	400

Appendix B IEEE 34 Node System Datasheet

Table A-7 Base values for IEEE 34 System

	3-phase	per-phase
Vbase(kV)	24.9	14.3760217
Sbase(MVA)		10
Zbase		20.667

Table A-8 Load data for IEEE 34 System

#	connected to	P_a	Q_a	P_b	Q_b	P_c	Q_c
1	860	36	24	40	26	130	71
2	840	27	16	31	18	9	7

Table A-8 Continued

3	844	144	110	135	105	135	105
4	848	20	16	43	27	20	16
5	890	150	75	150	75	150	75
6	830	17	8	10	5	25	10
7	806	0	0	30	15	25	14
8	810	0	0	16	8	0	0
9	820	34	17	0	0	0	0
10	822	135	70	0	0	0	0
11	824	0	0	5	2	0	0
12	826	0	0	40	20	0	0
13	828	0	0	0	0	4	2
14	856	0	0	4	2	0	0
15	858	7	3	2	1	6	3
16	864	2	1	0	0	0	0
17	834	4	2	15	8	13	7
18	836	30	15	10	6	42	22
19	838	0	0	28	14	0	0
20	846	0	0	25	12	20	11

Table A-9 Line type for IEEE 34 System

300			
Z=	1.3238+ 1.357i	0.2109 + 0.5965i	0.2051 + 0.4616i
	0.2109 + 0.5965i	1.3385+ 1.3313i	0.2124 + 0.5026i
	0.2051 + 0.4616i	0.2124 + 0.5026i	1.3266 + 1.3521i
B=	5.0983	-1.5211	-0.6242
	-1.5211	5.3492	-0.9921
	-0.6242	-0.9921	4.8714

301			
Z=	1.9157 + 1.4282i	0.2336 + 0.6431i	0.2273 + 0.5256i
	0.2336 + 0.6431i	1.9318 + 1.4094i	0.2352 + 0.5699i
	0.2273 + 0.5256i	0.2352 + 0.5699i	1.9188 + 1.4246i
B=	4.906	-1.4267	-0.5975
	-1.4267	5.1337	-0.3799
	-0.5975	-0.3799	4.7005

Table A-9 Continued

301			
Z=	1.9157 + 1.4282i	0.2336 + 0.6431i	0.2273 + 0.5256i
	0.2336 + 0.6431i	1.9318 + 1.4094i	0.2352 + 0.5699i
	0.2273 + 0.5256i	0.2352 + 0.5699i	1.9188 + 1.4246i
B=	4.906	-1.4267	-0.5975
	-1.4267	5.1337	-0.3799
	-0.5975	-0.3799	4.7005

303			
Z=	0+ 0i	0+ 0i	0+ 0i
	0+ 0i	2.7799 + 1.4804i	0+ 0i
	0+ 0i	0+ 0i	0+ 0i
B=	0	0	0
	0	4.2463	0
	0	0	0

304			
Z=	0+ 0i	0+ 0i	0+ 0i
	0+ 0i	1.9216 + 1.4213i	0+ 0i
	0+ 0i	0+ 0i	0+ 0i
B=	0	0	0
	0	4.3692	0
	0	0	0

200			
Z=	0.0369 + 0.0378i	0.0058 + 0.0166i	0.0057 + 0.0128i
	0.0058 + 0.0166i	0.0373 + 0.0371i	0.0059+ 0.0140i
	0.0057 + 0.01288i	0.0059 + 0.0140i	0.0370+ 0.0377i
B=	182.6574625	-54.49664912	-22.36329523
	-54.49664912	191.6464897	-35.54409677
	-22.36329523	-35.54409677	174.5282865

Table A-10 Line parameters for IEEE 34 System

#	From	To	Length	Type	#	From	To	Length	Type
1	800	802	2580	300	17	834	860	2020	301
2	802	806	1730	300	18	834	842	280	301
3	806	808	32230	300	19	836	840	860	301
4	808	810	5804	303	20	836	862	280	301
5	808	812	37500	300	21	842	844	1350	301
6	812	814	29730	300	22	844	846	3640	301
7	814	850	1	VR	23	846	848	530	301
8	816	818	1710	302	24	850	816	310	301
9	816	824	10210	301	25	852	832	1	VR
10	818	820	48150	302	26	854	856	23330	303
11	820	822	13740	302	27	854	852	36830	301
12	824	826	3030	303	28	858	864	1620	303
13	824	828	840	301	29	858	834	5830	301
14	828	830	20440	301	30	860	836	2680	301
15	830	854	520	301	31	862	838	4860	304
16	832	858	4900	301	32	888	890	10560	200

Table A-11 Voltage regulator parameter for IEEE 34 System

814 - 850	Ph-A	Ph-B	Ph-C
R - Setting	2.7	2.7	2.7
X - Setting	1.6	1.6	1.6
852 - 832	Ph-A	Ph-B	Ph-C
R - Setting	2.5	2.5	2.5
X - Setting	1.5	1.5	1.5

Table A-12 Transformer parameters for IEEE 34 System (a) substation trans (b) distribution trans

Z=	2.48+19.84i	0+ 0i	0+ 0i
	0.00	2.48+19.84i	0+ 0i
	0+ 0i	0+ 0i	2.48+19.84i

Z=	0.057+ 0.1224i	0+ 0i	0+ 0i
	0+ 0i	0.057+ 0.1224i	0+ 0i
	0+ 0i	0+ 0i	0.057+ 0.1224i

Table A-13 Capacitor data for IEEE 34 System

Cap #	Connected to	IQL A(kVAR)	IQL B (kVAR)	IQL C (kVAR)
1	844	100	100	100
2	848	150	150	150